UNIVERSITY OF CALIFORNIA, MERCED

SCHOOL OF ENGINEERING

BIOLOGICAL ENGINEERING AND SMALL SCALE TECHNOLOGY

IMPACTS OF ENGINEERING NANOPARTICLES ON DISSOLVED ORGANIC MATTER ASSEMBLY

By

CHI-SHUO CHEN

A dissertation submitted in partial fulfillment of the requirements for the degree of Doctor of Philosophy at the University of California, Merced

Spring Semester, 2012

Chapter 1 Introduction

Dissolved organic mater and carbon cycle

The ocean serves as one of the largest bioactive carbon reservoirs on Earth. Composed of approximately 700 Pg (1Pg=1 petagram = 1billion tones = 10^{15} grams) carbon residences, the dissolved organic matter (DOM) pool in the ocean is comparable to the carbon stock in the atmosphere. Surface ocean microorganisms play critical roles in the distribution and cycling of marine organic carbon. More than 50% of global photosynthesis takes place in the surface ocean, and this "invisible forest" transports ~ 5-10 Pg carbon from the atmosphere into the ocean (Emerson and Hedges, 2008; Falkowski, 2002; Najjar, 2009). Marine phytoplankton captures and converts inorganic carbon from the atmosphere into organic carbon. The carbon fixed by marine phytoplankton, stored as living biomass, is ~ 35 Pg. However, the carbon stored as biomass is only short-term. Dead phytoplankton and organic debris sink through the water column, transporting with them organic carbon down to the deep ocean. This "biological pump" sequesters carbon from the atmosphere and depletes the dissolved inorganic carbon from the ocean surface. Organic carbon can be transported to the deep ocean as sinking particles known as particulate organic matter (POM). Traditionally, the division of marine DOM and POM is an operational: Organic matter retained on the membrane (filter pore size usually range from 0.2 to 1 μm) is considered POM, whereas the filterable organic matter is considered DOM.

Marine POM serves as an important nutrition source driving the microbial loop in ocean. Below the euphotic zone, microbes attached to sinking organic particles (POM) utilize part of the sinking organic carbon by remineralization processes. Rich dissolved organic matter (DOM) is released from sinking POM to support free-living bacteria. Part of organic carbon is converted back into gaseous CO_2 and returns to the atmosphere through microbial remineralizaiton, when, for instance, some of its biomass is consumed by protists and zooplankton; here it enters higher trophic levels. The remaining carbon is transferred into the small organic molecules as the nonliving, dissolved organic mater

(DOM) (Ducklow, 2001). DOM in the deep sea (below 500 m) is mainly composed of biological refractory compounds with the average ages ranging from 3,000 to 6,000 years. Studies report the DOM-POM assembly/ remineralization process is one of key elements in global carbon cycle (Azam, 1998; Cermeno et al., 2008; del Giorgio and Duarte, 2002; Hansell and Carlson, 2003; Hopkinson and Vallino, 2005; Kiorboe and Jackson, 2001; Sunda, 2010; Vergugo, 2012)

Chemical composition

The DOM exported from ocean surface represent ~20% of total organic carbon flux to the deep ocean. In the transportation process, due to the biochemical interactions, the C: N:P stoichiometry of the DOM pool changes dynamically (Hopkinson and Vallino, 2005). Due to its natural variation and the difficulty to isolate sufficient DOM for representative analysis, the chemical characteristics of marine DOM are still largely unknown. For instance, the compositions of DOM collected at three different depth in the North Pacific Ocean were analyzed with tangential-flow ultrafiltration and ^{13}C nuclear magnetic resonance (Benner et al., 1992). DOM molecules can be divided into colloid pool and true solutes, or into a high molecular weight (HMW) and a low molecular (LMW) fraction. The DOM (> 1000 daltons) collected by ultrafiltration can represented 22 to 33 percent of the total DOM and included all colloidal material in the water column. Data indicated the relative abundance of polysaccharides is in the surface water DOM (~2-6% , <100 m) and decreases to ~0.3-0.9% of DOM in deep waters (>1000 m). The relative abundance of aromatic or olefinic carbon in surface DOM was threefold lower than DOM from deeper waters (Hansell and Carlson, 2003). Gel permeation chromatography has been also applied to characterize the molecular size distribution, polarity, charge and aromaticity of DOC (Dittmar and Kattner, 2003). A group of small molecules (~600 $g.mol^{-1}$) with hydrophobic functional groups were found in the deep sea, which may contribute to the refractory DOM pool in the ocean.

Marine microgels

The detailed mechanisms and pathways of DOM/POM transitions are complex and still not fully explored (Verdugo et al., 2004). This study mainly focuses on the gel properties

of marine DOM and the self-assembly of DOM. The concept of reversible DOM/POM transition was first raised in 1963, where nonliving particulate organic matter in micron-size ranges were suggested to play significant roles in marine ecosystem (Gordon, 1963). The experimental foundation of the ubiquitous assembly/dispersion of organic matter in water column was not established until 1998. In addition, the DOM self-assembly in ocean was explained by a simple polymer model (Chin et al., 1998). Though more field studies are need to precisely estimate the carbon budget of self-assembly DOM, from available data, it is widely recognized ~ 70 Gt per carbon flux per year is transported from the DOM pool into POM pool through this abiotic DOM-POM gel transition (Verdugo et al., 2006).

Gel, as a three dimension matrix, is composed of polymer chains with physical and/or chemical interactions. High binding energy (100~ 400 kJ $mole^{-1}$) is required for forming new chemical bonds between polymer chains in chemical-type assembly. In physical gels, polymers interconnect by tangles and/or low-energy physical bonds. In contrast to the high binding energy requirements, the binding energy of physical assembly is much lower (<50 kJ $mole^{-1}$) and assembly/dispersion equilibrium highly depends on polymer properties and surrounding environments. Various functional groups distribute on polyelectrolyte chains, and charges exposed on chain surfaces serve as binding sites. Electrostatic interactions contribute to stabilize the polyelectrolyte chains within gel matrices. For amphiphilic polymer chains, hydrophobic domains can act as the binding sites to promote polymer matrix (gel) formations.

Though the precise chemical composition and molecular conformation of DOM are still largely unknown, it has been shown the electrostatic force and hydrophobic interactions serve important roles in marine gel assembly. Due the negative charge of functional groups located on DOM polymers, the divalent ion Ca^{2+} surrounding the DOM polymer serve as cross-linkers to hold polymer chain together (Chin et al., 1998; Verdugo et al., 2004). It was also demonstrated the low concentration (100 nM) hydrophobic EPS can induce the DOM assembly (Ding et al., 2008; Vergugo, 2012). From nuclear magnetic resonance data, the abundance of aromatic functional groups in DOM collected from the

deep ocean suggests the hydrophobic interaction may serve important role in DOM assembly in the deep ocean.

From the viewpoint of analytical chemistry, the properties of DOM are complex, though considered relatively inert. However, the polymer properties of marine DOM, such as assembly kinetics, are active and may be altered by environmental changes.

Climate changes and carbon cycle

Environmental factors such as ocean pH, temperature, pressure, and current circulation can influence the temporal and spatial distribution of DOM in the ocean. For instance, sunlight may influence the fate of marine DOM as well. Seawater samples collected at 3800 m depth were exposed to broad-band ultraviolet/visible light (~170 Whm^{-2}), which correspond to solar noon irradiation at the sea surface. This study showed biological refractory DOM can be degraded by sunlight (solar ultraviolet-B radiation) through photochemical reactive, and suggested sunlight plays an important role to degrade refractory DOM into biological labile compounds (Mopper et al., 1991). In this study, we are interested in the impact of anthropogenic activities on DOM/POM assembly—emphasiszing the influence of engineering nanoparticles, ocean acidification and surface ocean warming.

In the last few decades, in part from increasing anthropogenic CO_2 emission, the ocean environment has changed. Since Industrial Revolution, ~500 Pg carbon was released into the environment from human activities, and the partial pressure of CO_2 in the atmosphere has raise form 280 ppm in 1750 to 387 ppm in 2009. For 55% of anthropogenic carbon emission were absorbed by land and ocean sink, the change of atmosphere CO_2 concentration is lower than predicted. Several climate models and field studies have investigated the carbon flux from atmosphere into ocean inertia through the air-sea interface (Caldeira and Wickett, 2003; Le Quere et al., 2009). It is widely recognized that the global ocean inventory of anthropogenic carbon was around 120 Pg C in the mid-1900, increasing about 2.2 Pg C per year (Sabine and Tanhua, 2010). The ocean absorbs much of the excessive carbon in the atmosphere, staving off a substantially

worse global warming scenario, with little known changes to the global carbon cycle. However, excessive carbon entering into the water column affects ocean environments. Ocean reserves carbon through the interaction between CO_2 (gas) and seawater; CO_2 diffuse into the oceans to form carbonic acid (H_2CO_3) and its dissociation product is bicarbonate (HCO_3^-) and carbonate (CO_3^-) ions. The average pH of surface ocean has fallen by 0.1 unit since preindustrial times years (Doney et al., 2009). According to climate prediction model, ocean pH may decrease from current value (~8.2) to 7.4 at 2100 (Caldeira and Wickett, 2003; Doney et al., 2009; Orr et al., 2005). Ocean acidification not only affects calcifying organisms, but also influences the interactions between metals complex and phytoplankton in the water column (Karl, 2002). In addition to ocean acidification, rising CO_2 in the atmosphere causes the earth surface temperature to increase. Studies centered over the tropical ocean indicate the mean surface temperature increased 0.1˚C/decade over the past 30 year (Solomon and (eds.), 2007). By the year 2100, the tropical mean sea surface temperature is projected to increase 3˚C, relative to the 1961-1990 mean (Johnson and Xie, 2010).

The development of nanotechnology

In addition to anthropogenic CO_2 resulting from fossil fuel burning, the environmental impacts of industrialized nanomaterials have drawn recent attention (Biswas and Wu, 2005; Leppard, 2008). Engineered Nanoparticles (ENs), which range in size from 1 to 100 nm, are widely used in our daily life—added to the paints and plastics and cosmetics we consume—the environment impacts of nonmaterial are highly understudied. Compared to bulk material of identical chemical composition, nanomaterials display different chemical/physical characteristics. Nanomaterials, based on the material compositions, can be categorized into five classes: 1) carbon nanotubes and related products, 2) metal containing particles (e.g., metal oxides), 3) quantum dots (QDs, e.g., CdSe/ZnS and InGaP/ZnS), 4) zero-valent metal products (e.g., zero-valent iron), and 5) dendrimers (Klaine et al., 2008; Leppard, 2008) . Owing to the material size and sample-collecting limitations, the concentration of nanomaterial released into the environment is difficult to evaluate. Based on the model, there are 1-10 μg $liter^{-1}$ nanoparticles in the environment (Boxall, 2007). However, the impacts of nanomaterial on marine ecosystem

are largely unexplored. For the unique hydrophobic properties, nanopolymers were used as the study model in our study.

The goal of this study is to apply the principle of polymer physics to study the influences of anthropogenic activities, including nanomaterial pollutions, ocean surface warming and acidification, on the critical DOM-POM shunt—microgel formation. The outcomes of this study will facilitate the establishing of regulations for nanotechnology and timely carbon emission strategies.

Reference

Azam, F., 1998. Microbial control of oceanic carbon flux: The plot thickens. Science 280, 694-696.

Benner, R., Pakulski, J.D., McCarthy, M., Hedges, J.I., Hatcher, P.G., 1992. Bulk Chemical Characteristics of Dissolved Organic-Matter in the Ocean. Science 255, 1561-1564.

Biswas, P., Wu, C.Y., 2005. 2005 Critical Review: Nanoparticles and the environment. Journal of the Air & Waste Management Association 55, 708-746.

Boxall, A.C., Q; Sinclair, C; Jones, A; Aitken, R; Jefferson, B; Watts, C 2007. Current and future predicted environmental exposure to engineered nanoparticles.

Caldeira, K., Wickett, M.E., 2003. Oceanography: anthropogenic carbon and ocean pH. Nature 425, 365.

Cermeno, P., Dutkiewicz, S., Harris, R.P., Follows, M., Schofield, O., Falkowski, P.G., 2008. The role of nutricline depth in regulating the ocean carbon cycle. Proc Natl Acad Sci U S A 105, 20344-20349.

Chin, W.C., Orellana, M.V., Verdugo, P., 1998. Spontaneous assembly of marine dissolved organic matter into polymer gels. Nature 391, 568-572.

del Giorgio, P.A., Duarte, C.M., 2002. Respiration in the open ocean. Nature 420, 379-384.

Ding, Y.-X., Chin, W.-C., Rodriguez, A., Hung, C.-C., Santschi, P.H., Verdugo, P., 2008. Amphiphilic exopolymers from Sagittula stellata induce DOM self-assembly and formation of marine microgels. Marine Chemistry 112, 11-19.

Dittmar, T., Kattner, G., 2003. Recalcitrant dissolved organic matter in the ocean: major contribution of small amphiphilics. Marine Chemistry 82, 115-123.

Doney, S.C., Fabry, V.J., Feely, R.A., Kleypas, J.A., 2009. Ocean Acidification: The Other CO(2) Problem. Annual Review of Marine Science. Annual Reviews, Palo Alto, pp. 169-192.

Ducklow, H.W.S., D. K. Buesseler, K. O, 2001. Upper Ocean Carbon Export And The Biological Pump. OCEANOGRAPHY 14, 50-58.

Emerson, S.R., Hedges, J.I., 2008. Chemical Oceanography and the Marine Carbon Cycle. Cambridge University Press.

Falkowski, P.G., 2002. The ocean's invisible forest - Marine phytoplankton play a critical role in regulating the earth's climate. Could they also be used to combat global warming. Scientific American 287, 54-61.

Gordon, A.R., 1963. Organic Aggregates in Seawater and the Dynamics of Their Formation and Utilization. Limnology and Oceanography 8, 372-381.

Hansell, D., Carlson, C., 2003. Biogeochemistry of Marine Dissolved Organic Matter Academic Press.

Hopkinson, C.S., Vallino, J.J., 2005. Efficient export of carbon to the deep ocean through dissolved organic matter. Nature 433, 142-145.

Johnson, N.C., Xie, S.P., 2010. Changes in the sea surface temperature threshold for tropical convection. Nature Geoscience 3, 842-845.

Karl, D., 2002. Nutrient dynamics in the deep blue sea. Trends in Microbiology 10, 410-418.

Kiorboe, T., Jackson, G.A., 2001. Marine snow, organic solute plumes, and optimal chemosensory behavior of bacteria. Limnology and Oceanography 46, 1309-1318.
Klaine, S.J., Alvarez, P.J., Batley, G.E., Fernandes, T.F., Handy, R.D., Lyon, D.Y., Mahendra, S., McLaughlin, M.J., Lead, J.R., 2008. Nanomaterials in the environment: behavior, fate, bioavailability, and effects. Environmental toxicology and chemistry / SETAC 27, 1825-1851.
Le Quere, C., Raupach, M.R., Canadell, J.G., Marland, G., et al., 2009. Trends in the sources and sinks of carbon dioxide. Nature Geosci 2, 831-836.
Leppard, G.G., 2008. Nanoparticles in the environment as revealed by transmission electron microscopy: Detection, characterisation and activities. Current Nanoscience 4, 278-301.
Mopper, K., Zhou, X.L., Kieber, R.J., Kieber, D.J., Sikorski, R.J., Jones, R.D., 1991. Photochemical Degradation of Dissolved Organic-Carbon and Its Impact on the Oceanic Carbon-Cycle. Nature 353, 60-62.
Najjar, R., 2009. OCEANOGRAPHY The dark side of marine carbon. Nature Geoscience 2, 603-604.
Orr, J.C., Fabry, V.J., Aumont, O., Bopp, L., Doney, S.C., Feely, R.A., Gnanadesikan, A., Gruber, N., Ishida, A., Joos, F., Key, R.M., Lindsay, K., Maier-Reimer, E., Matear, R., Monfray, P., Mouchet, A., Najjar, R.G., Plattner, G.K., Rodgers, K.B., Sabine, C.L., Sarmiento, J.L., Schlitzer, R., Slater, R.D., Totterdell, I.J., Weirig, M.F., Yamanaka, Y., Yool, A., 2005. Anthropogenic ocean acidification over the twenty-first century and its impact on calcifying organisms. Nature 437, 681-686.
Sabine, C.L., Tanhua, T., 2010. Estimation of Anthropogenic CO(2) Inventories in the Ocean. Annual Review of Marine Science, pp. 175-198.
Solomon, S., D. Qin, M. Manning, Z. Chen, M. Marquis, K.B. Averyt, M. Tignor and, (eds.), H.L.M., 2007. Climate Change 2007: The Physical Science Basis. Contribution of Working Group I to the Fourth Assessment Report of the Intergovernmental Panel on Climate Change. Cambridge Univ Press, Cambridge, UK.
Sunda, W.G., 2010. Oceans. Iron and the carbon pump. Science 327, 654-655.
Verdugo, P., Alldredge, A.L., Azam, F., Kirchman, D.L., Passow, U., Santschi, P.H., 2004. The oceanic gel phase: a bridge in the DOMâ€“POM continuum. Marine Chemistry 92, 67-85.
Vergugo, P., 2012. Marine microgels. Annual Review of Marine Science 4, 1-25.

Chapter 2 The impact of nanoparticles on marine dissolved organic matter assembly

Abstract

Nanoparticles are widely used in our daily life—finding applications in cosmetics and sunscreens, in surface coating and industrial paints (Maynard et al., 2006). The fate of these artificial materials, ultimately, is their release into the natural aquatic environment. Intensive nanomaterial studies thus far have focused on cytotoxicity, but ecological impacts of engineering nanoparticles (ENs) remain under-explored. Marine dissolved organic mater (DOM), as one of the major carbon pool on earth, influences the global carbon balance. The spontaneous assembly of DOM into POM (particulate organic matter) can significantly impact critical processes—such as colloidal pump and microbial loops—and nutrition availability for phytoplankton photosynthesis within the euphotic zone. Here, we report that ENs (polystyrene, 25 nm, 10 μg/L) can double the rate of the kinetic assembly of DOM into POM. Dynamic laser scattering (DLS) was used to monitor DOM assembly. The unanticipated disturbance of the largest marine carbon pool induced by ENs warrants particular caution, given current EN usage and disposal. Moreover, this unexpected ENs-induced carbon flow from DOM to POM raises the possibility of utilizing ENs to mitigate the greenhouse effects caused by excess CO_2 emission.

2.1 Marine dissolved organic matter and nanoparticles

The largest active carbon sink on the Earth, the ocean, has uptaked around one third of anthropogenic CO_2 emission over the industrial era (Le Quere et al., 2009; Sabine et al., 2004). The ocean inventory of anthropogenic CO_2 in 2008 was 140 ±25 Pg and the uptake rate was 2.3 ±0.6 Pg C per year (Khatiwala et al., 2009). Unfortunately, possibly due to its higher carbon content in the surface water and excessive fossil fuel consumption, this natural carbon sink has gradually saturated (Khatiwala et al., 2009; Le Quere et al., 2009). As a result, intense researches recently have focused on how to capture CO_2 from the atmosphere and store carbon on long term—the goal being permanent sequestration (Figueroa et al., 2008). For instance, injecting CO_2 hydrate into the deep-sea sediment (< 3,000m depth) was proposed as a means of storing anthropogenic CO_2; at the low temperature and high pressure the deep-sea provides, CO_2 maintains its denser liquid phase, making it able to be sealed below the seafloor (House et al., 2006). Through the reaction between amines and CO_2, various solid amine-based sorbents have been developed to capture excessive CO_2. High surface-ratio metal organic frameworks are applied to absorb CO_2 as well. Nevertheless, most of the proposed technologies raise concerns regarding safety, environmental impacts, practicality and financial cost (Herzog, 2001). One of promising geoengineering solutions, ocean gardening (iron fertilization), utilizes the natural sequestration capacity of marine phytoplankton and has been proposed to sequester CO_2 from the atmosphere into the ocean (Falkowski, 2002). By 2004, nine iron-enrichment experiments were carried out. During one ocean gardening experiment, the IronExII plan, 2 nM of iron was spread in the high-nutrient, low-cholrophy II (NHLC) region to induce the phytoplankton blooms. In euphotic zone, phytoplankton transferred inorganic carbon into primary production through photosynthesis. Satellite data indicated dramatic increase of chlorophyll, a widely used proxy for phytoplankton biomass, was observed in those regions (Behrenfeld et al., 1996). In the center of the iron-fertilized region, the CO_2 fugacity fell from 510 μatm to 420 μatm and the data indicated the transient sequester of carbon in the first 8 days (Cooper et al., 1996). However, a large chlorophyll increase and surface CO_2 decrease may not represent the long-term carbon sequestrations. Some experiments indicate a significant portion of primary products was utilized rapidly by surface

microbes. The influence of microbial respiration seriously comprises the efficiency of ocean gardening (Obernosterer et al.).

Colloidal formation plays essential roles in mediating the marine carbon cycle. Degrading phytoplankton materials collide with other smaller particles, such as DOM or transparent extracellular polysaccharides (TEP), and grow into the organic aggregations (marine snow) (Azam and Malfatti, 2007). Those organic colloids grow over time and may reach several centimeters sizes. The critical sinking process of marine particulate organic carbon (POC), in marine colloidal pump, drains dissolved organic carbon (DOC) from ocean surface into the deep ocean (Ducklow, 2001; Najjar, 2009). Sinking colloidal particles serve as critical vehicles in vertical carbon flux (Verdugo et al., 2004). 80% of current anthropogenic CO_2 is expected to be transferred into ocean on a 1,000 year timescale (Herzog, 2001). As a result, increasing the efficient of colloid sinking is expected to enhance the efficiency of transporting carbon into ocean interior and potentially facilitate carbon sequestration into the ocean.

Engineering Nanoparticles (ENs), whose diameters range from 1 to 100 nm, show many unique properties differing from bulk material with identical chemical composition—an appeal to their numerous applications. ENs are increasingly being developed to improve and innovate industrial and consumer products; for example, they are used to develop new semiconductors, sunscreens and cosmetics and in the pharmaceutical industry as image enhancers and drug delivery vehicles (Nel et al., 2006). The unique interactions between nanoparticle and polymers have been noticed in nanomaterial composites related researches. For example, multilayer polyelectrolyte can be deposited on nanoparticles by controlling the charge properties of nanoparticles; the stability of nanoparticle polyelectrolyte composite also depended on the polyelectrolyte length and ionic strength of the surrounding medium (Gittins and Caruso, 2001). In contrast to the appreciation for the interaction between nanoparticle and synthetic polymers, the study of the relationship between nanoparticles and natural polymers is relatively rare.

Here, we investigate the effect of ENs at low concentrations (in ppb range) on the surface critical colloidal pump. The ENs-induced accelerating downward carbon flow can serve

as an effective complementary approach to the current ocean gardening for efficient carbon sequestration.

2.2 Materials and Methods

Water sampling and filtration

North pacific seawater samples collected at the Puget Sound (WA, USA) near Friday Harbor Marine Laboratories in April 2009. Seawater samples from the Gulf of Mexico were collected at 2 m and 1500 m depth. All samples were filtered through a GF/F fiberglass membrane and a 0.22-μm membrane (prewashed with 0.1 N HCl), treated with 0.02% sodium azide—a microbial biocide—and stored in clean, sealed bottles in dark at 4°C before use.

Particle Sizing

Microgel assembly was monitored with dynamic laser scattering (DLS) as described previously (Chin et al., 1998). Sea water aliquots (10 ml) were refiltered through a 0.22-μm membrane (low-protein binding Durapore®, Millipore) and poured directly into scattering cells. Scattering cells were placed in the goniometer of a Brookhaven laser spectrometer (Brookhaven Instruments, NY) and the scattering fluctuation signals were detected at 45° scattering angle. The autocorrelation function of scattering intensity fluctuations was averaged over a 12-minute sampling time. Hydrodynamic diameters of microgels were analyzed by CONTIN method (Chen et al., 2011; Chin et al., 1998).

Nanoparticle preparation

In order to study the influence of different charges and hydrophobicity of ENs surface on DOM assembly, polystyrene nanoparticles (Bangs Laboratories, IN, USA) were used in our study as model ENs. The primary size and surface area of these non-fluorescence nanoparticles were 25 nm and 2.48×10^{14} $\mu m^2/g$ (certificate provided by vendor). The size of these ENs was independently confirmed by DLS in lab. In order to avoid the undesired nanoparticle aggregations, thorough sonication was applied to nanoparticle stock solutions before experiments, as described in our previous study (Chen et al., 2010) Nanoparticles with different surface modifications (amine functional group and carboxyl functional group) were used in this study to investigate the effect of surface charges on DOM assembly kinetics.

2.3 Results and Discussion

DLS was used to monitor the assembling kinetics of DOM/POM transition by measuring particle size as a function of time. Result showed that DOM in 0.22 μm-filtered seawater can spontaneously assemble, forming polymer gels range from colloidal to micrometer size within ~120 hrs, which consisted with our previous study (Chin et al., 1998) . The data here shows that microgels reach the equilibrium size within ~60 hrs, and indicated 10 ppb ENs can accelerate the assembling kinetic by 200% (Fig-1). We compare different surface modification ENs—positive-charged, negative–charged and with non-charged. Data indicated no significant difference on DOM assembly acceleration and the microgel equilibrium sizes with different surface modifications ENs.

In order to investigate the impact of ENs at different ocean regions and depths, seawater samples collected from Mexico Golf at different sampling depth (ocean surface and 1500 m depth) were investigated (Fig-2; Fig-3). For the Golf surface seawater samples with higher concentration of DOM (~131 μM), results indicated that DOM assembled faster (~96 hrs) than specimens collected form North Pacific Ocean (Guo et al., 1994; Hung et al., 2003). ENs (10 ppb) showed similar accelerating effects on DOM from Mexico Golf. The kinetics of assembly were accelerated and reached equilibrium state within ~ 60 hrs with various surface properties of ENs (Fig-2). The DOM assembly reach plateau after ~ 200 hrs in the seawater sampled from deep ocean, the DOM concentration of which is 50 μM—lower than ocean surface seawater (Guo et al., 1994; Hung et al., 2003). Obvious accelerated assembly was found in these seawater samples with 10 ppb ENs addition (Fig-3).

Due to the complex DOM chemical composition, the mechanisms of DOM assembly may depend on weak electrostatic interactions and hydrophobic interactions (Verdugo et al., 2004). Since ENs with various surface charges did not show obvious differences on DOM accelerations, electrostatic forces may not dominate the interactions between ENs and DOM. Hence, we further explored the role of hydrophobic interactions in ENs-DOM assembly.

In order to evaluate the contribution of hydrophobicity, we studied the thermodynamic equilibrium by adjusting environment temperatures (Ding et al., 2008; Vergugo, 2012), The interactions of hydrophobic domains on polymers are highly temperature-dependent (Qin et al., 2006; Ross and Subramanian, 1981). In this study, we investigated the role of hydrophobicity in ENs-DOM assembly by adjusting the environment temperatures from 22˚C to 40˚C (Fig-4). Microgels assembled were treated with/ or without 100 ppb ENs for 7 days at 22˚C in dark. Before adjusting the experimental temperatures, the equilibrium microgel sizes were measured with DLS. Then, microgels were incubated at different temperatures and the size changes were monitored with DLS. Over 30˚C, microgels without ENs dispersed after ~4 hrs high-temperature incubations (Fig-4). The size of microgels decreased from ~6 μm to less than 2 μm after 24 hrs heat treatment. In contrast to the dispersion of natural microgels, there was no noticeable size changes of microgels contained ENs during 24 hr high temperature incubation (Fig-4). The equilibrium sizes of microgels with different surface modification ENs were measured as well (Fig-5); there is no significant difference between the equilibrium gel size of ENs-DOM at 22˚C and higher temperatures. Results imply the hydrophobic interactions could be the main driving force between ENs and DOM polymers, and ENs can stabilize the gel matrix at high temperature. Our data here agrees with the observation of the acceleration effects on deep ocean DOM (Fig-3-5). In previous study, a higher fraction of hydrophobic aromatic structures was found in the deep ocean DOM than DOM collected form the ocean surface (Hansell and Carlson, 2003). Our results supported the notion that assembly acceleration induced by ENs can potentially be driven by the hydrophobic interactions.

In order to reduce impacts of anthropogenic carbon dioxide emission, capturing CO_2 from atmosphere and storing into deep ocean is one of potential geoengineering approaches (Figueroa et al., 2008). Nevertheless, energy consumption is one of challenging issues in most of current approaches. In our model, no external energy consumption is required to drive the pumping efficiency of natural colloid pump. The sedimentation of the ENs- induced POM is driven by gravity, and naturally increases the downward carbon flux into the seafloor.

Our results indicated that a low level of ENs (25 nm, ~10 ppb) can drastically accelerate the kinetic assembly of DOM into POM pool by 200%, potentially to increase the sinking rate of organic carbon leading to more organic carbon burial on the seafloor. We conclude that ENs in aqueous system can influence assembling kinetics of DOM/POM and can cause potential impacts to the global carbon cycle. This unexpected ENs-induced carbon flow from DOM to POM suggests the feasibility of EN applications to mitigate the greenhouse effects caused by excess CO_2 emission.

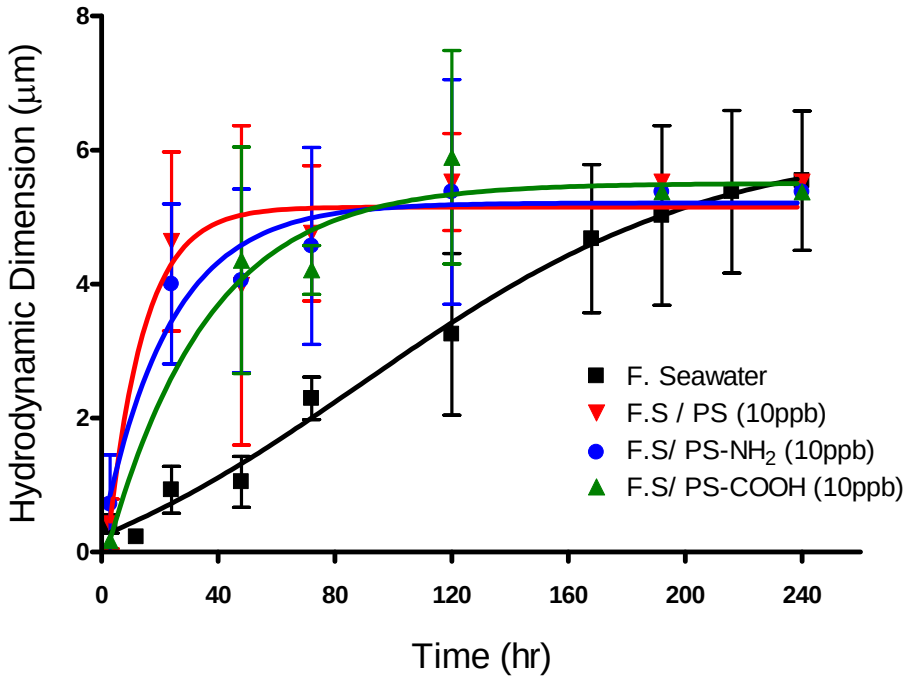

Fig-1 The assembly kinetics of DOM (Friday Harbor, WA) with various non-functional, amine and carboxyl, ENs (10 ppb). The hydrodynamic dimensions of microgels were measured using DSL for 10 days. Data indicated the DOM assembled into ~ 5 μm microgels within 120 hrs, without ENs (F.Seawater/black). Assembly kinentic accelatrion were observed with three types of ENs (polystyrene/red; amine-modified/blue; carboxyl-modified/ green). Each data point represents (mean ± SD) of six measurements made in each of six replicate samples.

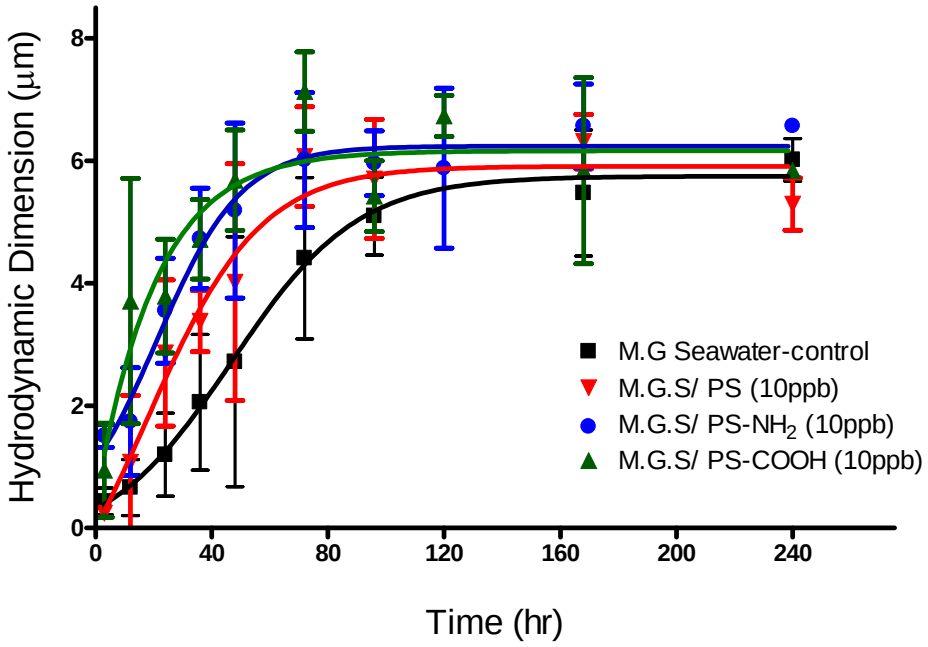

Fig-2 The assembly kinetics of DOM sampled from Gulf of Mexico surface region. The effects of ENs with different surface modifications were investigated. The natural DOM from the gulf assembled within 120 hrs (M.G Seawater/ Black). Data showed ENs (polystyrene/red; amine-modified/blue; carboxyl-modified/ green) can promote the assembly of DOM regardless of the sample origins. Each data point represents (mean ± SD) of six measurements made in each of six replicate samples.

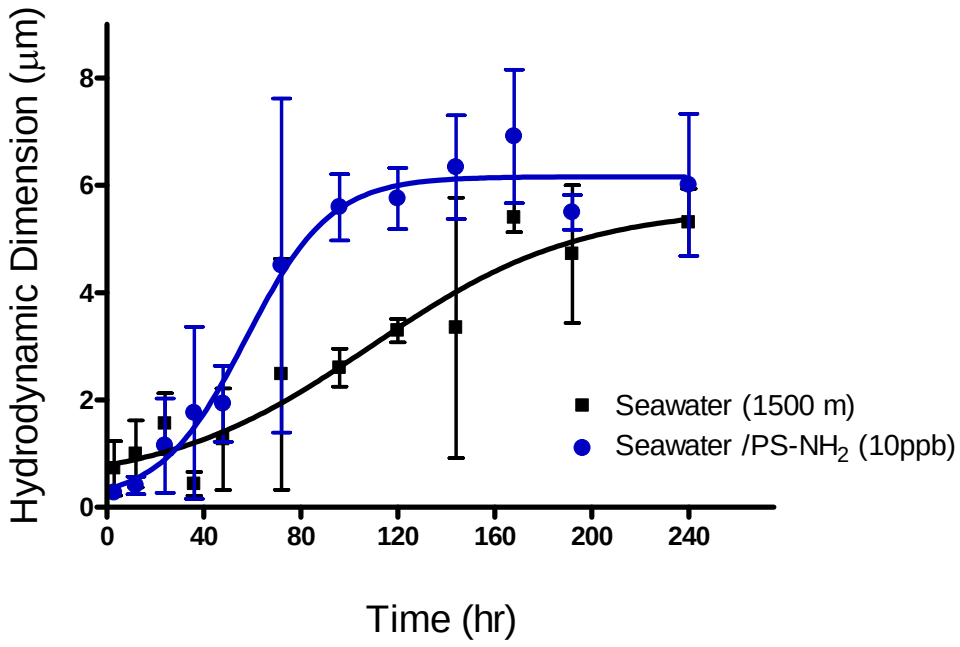

Fig-3 The assembly kinetics of DOM sampled at 1500 m depth. Data shows the assembly of DOM from deeper ocean (seawater/black) is slower than the assembly of DOM sampled from surface region (see Fig-2). The accelerated DOM assembly was observed with 10 ppb ENs (amine- modified/blue). Each data point represents (mean ± SD) of six measurements made in each of six replicate samples.

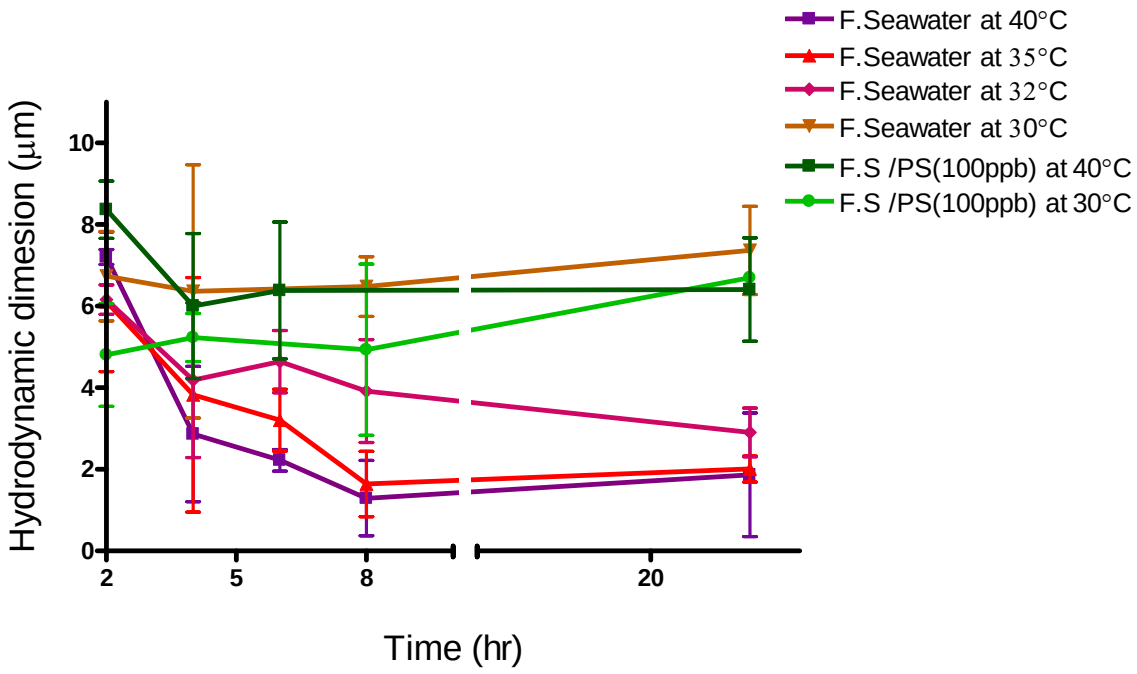

Fig-4 The stability of ENs-microgels at various temperatures. Microgels were formed with/without ENs and were incubated at temperatures 30-40˚C. Without ENs, microgels were dispersed when incubated at temperatures higher than 30 ˚C (30˚C/ brown; 32˚C/ light purple; 35˚C/ red; 40˚C/purple). In contrast, the equilibrium size of ENs-microgels did not change significantly within the temperature range tested (30˚C/light green; 40˚C/ green). Each data point represents (mean ± SD) of six measurements made in each of six replicate samples.

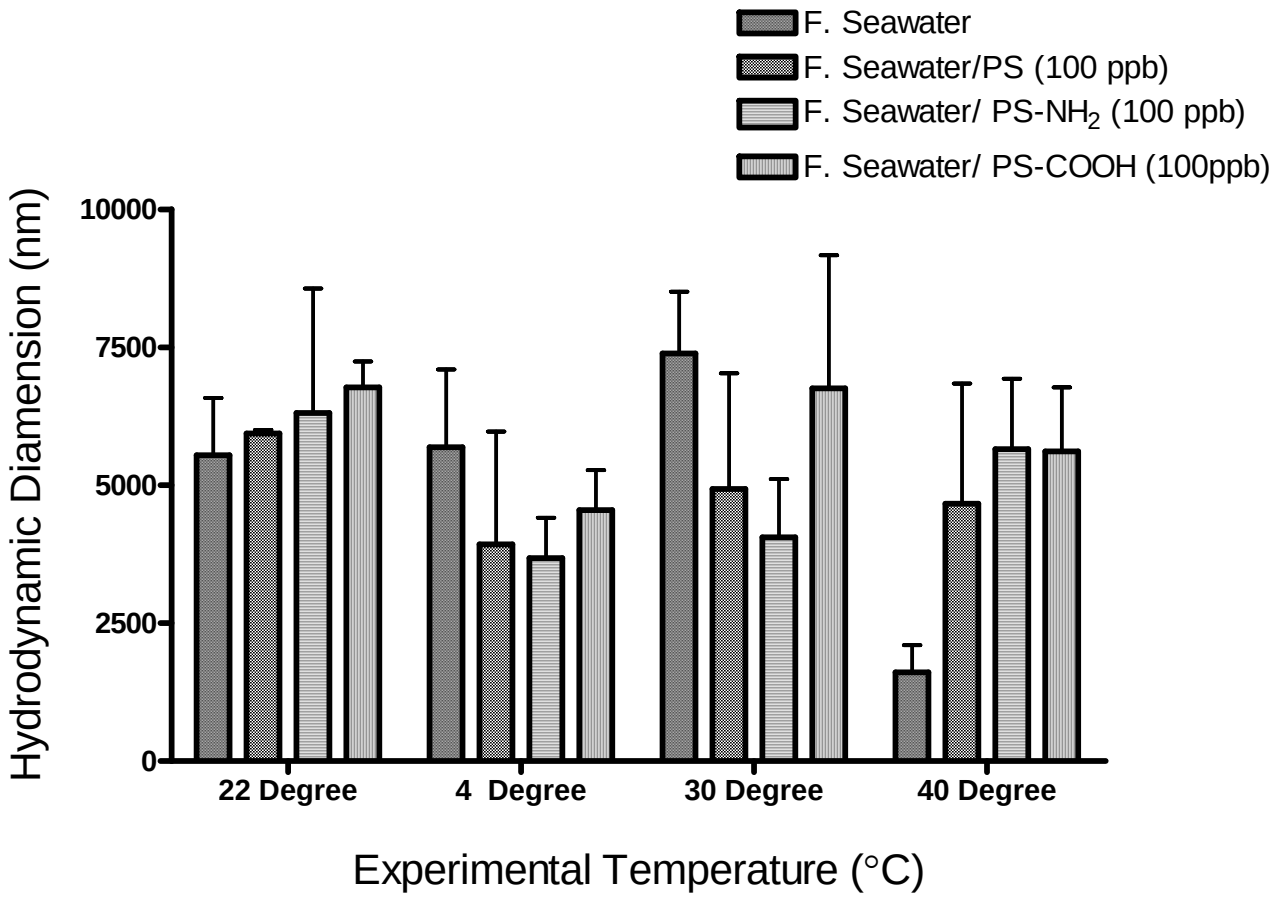

Fig-5 The equilibrium size of microgels at different temperatures. Microgels were assembled with three different types of ENs (100 ppb) and then incubated at various temperatures for 24 hrs. Data indicated a significant size reduction of microgels at 40˚C, but no significant size difference observed on ENs-microgels at higher temperatures.

Reference

Azam, F., Malfatti, F., 2007. Microbial structuring of marine ecosystems. Nat Rev Micro 5, 782-791.

Behrenfeld, M.J., Bale, A.J., Kolber, Z.S., Aiken, J., Falkowski, P.G., 1996. Confirmation of iron limitation of phytoplankton photosynthesis in the equatorial Pacific Ocean. Nature 383, 508-511.

Chen, C.-S., Anaya, J.M., Zhang, S., Spurgin, J., Chuang, C.-Y., Xu, C., Miao, A.-J., Chen, E.Y.T., Schwehr, K.A., Jiang, Y., Quigg, A., Santschi, P.H., Chin, W.-C., 2011. Effects of Engineered Nanoparticles on the Assembly of Exopolymeric Substances from Phytoplankton. PLoS ONE 6, e21865.

Chen, E.Y.T., Wang, Y.-C., Chen, C.-S., Chin, W.-C., 2010. Functionalized Positive Nanoparticles Reduce Mucin Swelling and Dispersion. PLoS ONE 5, e15434.

Chin, W.C., Orellana, M.V., Verdugo, P., 1998. Spontaneous assembly of marine dissolved organic matter into polymer gels. Nature 391, 568-572.

Cooper, D.J., Watson, A.J., Nightingale, P.D., 1996. Large decrease in ocean-surface CO2 fugacity in response to in situ iron fertilization. Nature 383, 511-513.

Ding, Y.-X., Chin, W.-C., Rodriguez, A., Hung, C.-C., Santschi, P.H., Verdugo, P., 2008. Amphiphilic exopolymers from Sagittula stellata induce DOM self-assembly and formation of marine microgels. Marine Chemistry 112, 11-19.

Ducklow, H.W.S., D. K. Buesseler, K. O, 2001. Upper Ocean Carbon Export And The Biological Pump. OCEANOGRAPHY 14, 50-58.

Falkowski, P.G., 2002. The ocean's invisible forest - Marine phytoplankton play a critical role in regulating the earth's climate. Could they also be used to combat global warming. Scientific American 287, 54-61.

Figueroa, J.D., Fout, T., Plasynski, S., McIlvried, H., Srivastava, R.D., 2008. Advances in CO2 capture technologyâ€”The U.S. Department of Energy's Carbon Sequestration Program. International Journal of Greenhouse Gas Control 2, 9-20.

Gittins, D.I., Caruso, F., 2001. Tailoring the Polyelectrolyte Coating of Metal Nanoparticles. The Journal of Physical Chemistry B 105, 6846-6852.

Guo, L., Coleman Jr, C.H., Santschi, P.H., 1994. The distribution of colloidal and dissolved organic carbon in the Gulf of Mexico. Marine Chemistry 45, 105-119.

Hansell, D., Carlson, C., 2003. Biogeochemistry of Marine Dissolved Organic Matter Academic Press.

Herzog, H.J., 2001. Peer Reviewed: What Future for Carbon Capture and Sequestration? Environmental Science & Technology 35, 148A-153A.

House, K.Z., Schrag, D.P., Harvey, C.F., Lackner, K.S., 2006. Permanent carbon dioxide storage in deep-sea sediments. Proceedings of the National Academy of Sciences of the United States of America 103, 12291-12295.

Hung, C.-C., Guo, L., Santschi, P.H., Alvarado-Quiroz, N., Haye, J.M., 2003. Distributions of carbohydrate species in the Gulf of Mexico. Marine Chemistry 81, 119-135.

Khatiwala, S., Primeau, F., Hall, T., 2009. Reconstruction of the history of anthropogenic CO2 concentrations in the ocean. Nature 462, 346-349.

Le Quere, C., Raupach, M.R., Canadell, J.G., Marland, G., et al., 2009. Trends in the sources and sinks of carbon dioxide. Nature Geosci 2, 831-836.

Maynard, A.D., Aitken, R.J., Butz, T., Colvin, V., Donaldson, K., Oberdorster, G., Philbert, M.A., Ryan, J., Seaton, A., Stone, V., Tinkle, S.S., Tran, L., Walker, N.J., Warheit, D.B., 2006. Safe handling of nanotechnology. Nature 444, 267-269.
Najjar, R., 2009. OCEANOGRAPHY The dark side of marine carbon. Nature Geoscience 2, 603-604.
Nel, A., Xia, T., Madler, L., Li, N., 2006. Toxic potential of materials at the nanolevel. Science 311, 622-627.
Obernosterer, I., Christaki, U., LefÃ¨vre, D., Catala, P., Van Wambeke, F., Lebaron, P., Rapid bacterial mineralization of organic carbon produced during a phytoplankton bloom induced by natural iron fertilization in the Southern Ocean. Deep Sea Research Part II: Topical Studies in Oceanography 55, 777-789.
Qin, S., Geng, Y., Discher, D.E., Yang, S., 2006. Temperature-Controlled Assembly and Release from Polymer Vesicles of Poly(ethylene oxide)-block- poly(N-isopropylacrylamide). Advanced Materials 18, 2905-2909.
Ross, P.D., Subramanian, S., 1981. Thermodynamics of Protein Association Reactions - Forces Contributing to Stability. Biochemistry 20, 3096-3102.
Sabine, C.L., Feely, R.A., Gruber, N., Key, R.M., Lee, K., Bullister, J.L., Wanninkhof, R., Wong, C.S., Wallace, D.W.R., Tilbrook, B., Millero, F.J., Peng, T.H., Kozyr, A., Ono, T., Rios, A.F., 2004. The oceanic sink for anthropogenic CO(2). Science 305, 367-371.
Verdugo, P., Alldredge, A.L., Azam, F., Kirchman, D.L., Passow, U., Santschi, P.H., 2004. The oceanic gel phase: a bridge in the DOMâ€“POM continuum. Marine Chemistry 92, 67-85.
Vergugo, P., 2012. Marine microgels. Annual Review of Marine Science 4, 1-25.

Chapter 3 The impact of nanoparticles on dissolved organic matter assembly in a fresh water system

Abstract

The assembly of polymers in the dissolved organic matter (DOM) pool has been shown to play a critical role in the aquatic carbon cycle (Chin et al., 1998; Verdugo et al., 2004a; Verdugo et al., 2008; Wells, 1998). A potential disturbance to the bioavailability between DOM and particulate organic matter (POM) of this critical DOM-POM exchange by engineered nanoparticles (ENs) may impact the global carbon cycling balance (Amon and Benner, 1996b; Kepkay, 1994; Verdugo et al., 2004a). Our previous study investigated the involvement of ENs in marine DOM assembly. Here, we aim to investigate the effects of ENs on DOM assembly kinetics and their mechanisms in a fresh water system. We expect the outcome from this study will provide needed knowledge quantifying ecological impacts of ENs which may inform policy regulating EN usage and disposal.

3.1 Dissolved organic matter in a fresh water system and nanoparticles

Engineered Nanoparticle

Engineering Nanoparticles (ENs), which range in size from 1 to 100 nm, have unique properties that vary from bulk materials of the same chemical compositions. ENs have been used in more than 800 commercial products—spanning sunscreens, computer construction and drug delivery. Based on their compositions and functions, ENs are generally categorized into five classes: 1) carbon nanotubes and related products, 2) metal containing particles (e.g., metal oxides), 3) quantum dots (QDs, e.g., CdSe/ZnS and InGaP/ZnS), 4) zero-valent metal products (e.g., zero-valent iron), and 5) dendrimers, with each class having a huge potential for many different applications (Klaine et al., 2008). Due to the promising commercial value of ENs, funding for the National Nanotechnology Initiative (NNI) in the USA was over $1 billion dollars in 2006. With the rapid development of nanotechnology, it is expected that significant amount of ENs will eventually find their way to aquatic systems.

Dissolved Organic Carbon in Natural Waters

Traditionally the organic carbon in aquatic system has been divided into two major pools: dissolved organic matter (DOM) and particulate organic matter (POM). DOM is operationally defined as the pool of organic substances that pass through a 0.2 μm filter and POM is the organic material retained by the filter. The DOM pool is one of the largest active carbon sinks on the Earth. Half of the global photosynthetic activity takes place in seawater; this activity helps transform the ocean into as a sink of atmospheric CO_2 (Chisholm, 2000; Hartnett et al., 1998; Shaw 2002). Around 700 Pg (1 Pg = 10^{15}g) carbon resides in this marine DOM pool—an amount comparable to the mass of carbon in atmospheric CO_2—and marine DOM carbon stock is only slightly smaller than the amount of carbon in terrestrial biomass and soil humus (Hedges, 1992, Hansell and Carlson 1998, Benner et al., 1992). According to the Committee of carbon flux to the ocean, approximately 116×10^{12} moles of carbon enter the riverine systems every year and around 50% of this carbon is transported into the ocean (Thurman, 1985). In freshwater systems, high concentration (~5-10 mg/l) of organic carbon is stored as DOM. The amounts of carbon in the DOM pool often exceed living organisms and drastically

change with the seasons (Thurman, 1985). In addition to carbon storage, some compositions of DOM—such as free amino acids, proteins and humic substances—provide energy to aquatic microorganisms and organisms in higher trophic levels (Thomas, 1997). In order to characterize the marine/terrestrial DOM, samples collected from different locations were analyzed with fluorescence spectroscopy. Various excitation/emission spectrums indicated varied DOM chemical compositions within water column (Coble, 1996). However, the discovery that there is a shunt between the DOM and POM pools, owing to the self-assembly of DOM polymers into microscopic gels (microgels), has introduced an important new perspective to the complexity of carbon cycling in the natural water (Bhaskar and Bhosle, 2005; Chin et al., 1998; Kerner et al., 2003; Verdugo et al., 2004a; Wells, 1998). In both seawater and freshwater, significant amounts of DOM polymers (up to 25 % in river water and ~10 % in seawater) were found to transform into microgels spontaneously. This abiotic aggregation not only influences the carbon cycle of the largest active reduced carbon pools, but also can affect the aquatic ecosystem.

The spontaneous microgel formation can change the nutrition cycle in microbial loops. Previous studies showed the bioreactivity of organic substrates in the water column decreases drastically with their size (Amon and Benner, 1994; 1996a; Benner et al., 1992; Kepkay, 1994). Since DOM is largely made of small polymers, DOM has been assumed to remain as a refractory pool (i.e., low bioreactivity) (Hartnett et al., 1998; Hedges, 1992; Kepkay, 1994, Hansell and Carlson 1998; Shaw 2002). However, this assumption requires re-evaluation, considering DOM polymers can spontaneously self-assemble to form bioreactive gels that can then be readily colonized by bacteria (Chin et al., 1998; Orellana and Verdugo, 2003; Orellana et al. 2000; Orellana and Verdugo 2000). The formation of microgels increases the possibility for organic carbon to enter directly into higher trophic levels as well (Kerner et al., 2003).

Potential interactions between DOM and ENs

Although concentrations of most ENs in natural waters are estimated by simple box models to be in the order of 1-10 μg/liter (Boxall et al., 2007), their actual distributions in

the environment remain largely unknown (Dunphy Guzman et al., 2006; Oberdorster et al., 2005; EPA White paper, 2007). The transport of ENs is dominated by convection and diffusion, whereas attachment is controlled by the total interaction energy between two objects. The collision frequency (transport) could largely be described by Smoluchovsky's equations while the collision event that results in aggregation/deposition (attachment) mostly follows the DLVO theory (Brant et al., 2005; Derjaguin and Landau, 1993; Kallay and Zalac, 2002; Lecoanet et al., 2004; Lecoanet and Wiesner, 2004; MolinaBolivar et al., 1997; Verwey, 1945, Smoluchowski, 1917). Therefore, EN transport and fate in the environment is dependent not only on physical parameters—such as temperature, ionic strength, pH, particle concentration and size (Dunphy Guzman et al., 2006; Elimelech and Omelia, 1990; Filella and Buffle, 1993; Kretzschmar and Sticher, 1997; Lecoanet et al., 2004)—but also on the relative hydrophobicity of ENs (Pellegrino et al., 2004; Zhang et al., 2007), which is not described by the DLVO theory.

Potential interactions between DOM and ENs

Due to concerns over nanomaterial risks, there has been a dramatic increase in safety research about ENs (Maynard et al., 2006). In most of environment studies, researchers focus on nanomaterial transport, exposure, and toxicity (Klaine et al., 2008; Nel et al., 2006). Aggregation and deposition are two interrelated processes which ultimately determine the EN distribution and fate in the ecosystems; EN deposition/aggregation could be defined as a two-step process of particle transport followed by attachment (Elimelech and Omelia, 1990). The research on EN aggregation and deposition suggests that the principle for colloidal fluid transportation may apply to ENs in many cases. For example, natural organic matter (NOM) can add a level of complexity beyond the scope of the DLVO theory. Although ENs tend to form aggregates in aquatic environments, especially when the ionic strength is high, NOM can either increase their stability by coating the surface of ENs with negative charges by steric repulsion (Santschi et al., 1998; Verdugo et al., 2004a), or decrease EN stability through a variety of mechanisms, including bridging (Buffle et al., 1998) and pearls-on-a-string formation (Santschi et al., 1998). With potential increases in EN stability in natural waters by NOM, more and more ENs may remain suspended in aquatic environments so that their transport—and often

toxic interactions with aquatic organisms—will need to be re-examined (Dubois et al., 2007; Pellegrino et al., 2004; Wang et al., 2003; Yu et al., 2007, Miao et al., 2009a).

Given the rapid development of the nanotechnology, the health and ecological impacts of ENs have not been fully explored. (Maynard et al., 2006). Because the riverine system is on first-line exposure to the urban nanopollution, and DOM is in high concentration in freshwater systems, this study aimed to investigate the environmental impacts of ENs on DOM-POM transition in freshwater (lake water).

3.2 Material and methods

Freshwater sample preparation

Freshwater samples were collected from Lake Yosemite (Merced, CA) in April, 2009. The samples were gravity-filtered through a GF/F fiberglass membrane and a 0.22-μm membrane tandem (prewashed with 0.1 N HCl), stored in clean sealed bottles and treated with 0.02% sodium azide to inhibit microbial activity. The collected samples were stored in the dark at 4°C before use.

EN preparation

Polystyrene nanoparticles (Bangs Laboratories, IN, USA) with two different sizes (25 nm and 100 nm) were used in our study as model ENs. The size of these ENs was independently confirmed by DLS (dynamic laser scattering) in lab. Thorough sonication was applied to nanoparticle solutions to avoid undesired nanoparticle aggregations. Nanoparticles with different surface modifications (amine functional group and carboxyl functional group) were used in this study to investigate the effect of surface charges on DOM assembly kinetics.

DOM microgel assembly

The concentration of most ENs in natural waters has been estimated to be in the order of 1-10 μg/l (Boxall et al., 2007). We used 10 μg/l polystyrene nanoparticles (25 nm and 100 nm) and 0.2 μm-filtered lakewater as our study model. Dynamic laser scattering (DLS) was used to monitor the formation of microgels as described previously (Chin et al., 1998). Lakewater aliquots were refiltered through a 0.22-μm membrane (prewashed with 0.1 N HCl) after thorough shaking and poured directly into scattering vials. The scattering vials were positioned in the goniometer of a Brookhaven laser spectrometer (Brookhaven Instruments, NY). Polymer assembly was monitored for 5 d by analyzing the scattering fluctuations detected at 45° scattering angle. The scattering intensity fluctuations were averaged over a 10 m sampling time. Particle size distribution was calculated by the CONTIN method (Chin et al., 1998; Provencher and Stepanek, 1996).

3.3 Result and Discussion

Interactions between dissolved organic mater (DOM) and ENs

In our study, we found that ENs can accelerate the assembly kinetics of freshwater DOM. In control lake water samples (no ENs), microgel formation reached equilibrium in 48-72 hrs. However, with 10 μg/l ENs, shorter equilibrium time (24-36 hrs) was observed for 25nm and 100 nm diameter ENs (Fig-1).

The size of ENs influences the assembly of DOM

Several previous studies demonstrated that the size of nanomaterial drives their most desirable characteristics. Though chemical compositions remain the same, different sized ENs show varied chemical properties and catalyzing rates (Caruso et al., 1998; Kelly et al., 2003; Mirkin et al., 1996; Murray et al., 2000). In our study, we compared the acceleration effects of polystyrene ENs of two sizes. In this study, 25 nm and 100 nm ENs were added into the specimen at 10 μg/L concentration. We found that ENs-DOM reached equilibrium within 36 hours with 25 nm ENs, and 48 hours for 100 nm ENs (Fig-1). The final hydrodynamic diameter of microgels did not show any correlation to the ENs diameters.

The surface properties of ENs affect the assembly kinetics of DOM assembly

In this set of experiments, we used 25 nm polystyrene nanoparticles with different surface charges as our study model. By measuring the size of DOM microgels by DLS over 5 days, we compared the influences of carboxyl-modified, amine-modified and no surface-modification polystyrene nanoparticles. At low concentration (10 μg/L), ENs with various surface modifications accelerated the DOM assembly (Fig-2). Results showed the DOM-POM transition reaches equilibrium state around 48 hrs with the polystyrene, amine-modified, and carboxyl-modified ENs. At high concentration (10 mg/L) of polystyrene ENs, we found that the DOM-POM transition reached equilibrium sizes within 48 hrs. However, amine-modified ENs accelerated microgel assembly significantly: Within 24 hrs, DOM assembled into ~ 5 μm microgels with amine-modified ENs. The positive-charge distributed on the EN surface may serve a similar

function as divalent ions to hold DOM polymers together (Chin et al., 1998). On the contrary, carboxyl-modified ENs at high concentration (10 mg/L) delayed assembly kinetics more than 24 hrs (Fig-3). Since divalent ions (e.g., Ca^{2+}) are critical for microgel formation, higher concentration of carboxyl modified ENs might chelate divalent ions—such as Ca^{2+}—to reduce the assembly kinetics (Fig-3). Our results here also show that the surface charge properties of ENs change the DOM kinetics, and are not able to change microgel equilibrium size. This observation is consistent with the prediction from de Gennes' tangled polymer gel theory (PG de Gennes, 1979).

In contrast to the changes of lakewater DOM assembly kinetics with different surface charge ENs, our data showed there is no significant difference between the marine assembly kinetics exposed to different ENs (Chapter 2). The difference may be caused by the high concentration of ions (Na^{+}: 400 mM) in seawater. Ions surrounding ENs may shield the charges on the polymer surface. As a result, highly concentration ions may reduce the electrostatic interactions between marine DOM and ENs. The difference of DOM compositions should also be considered. Our observations here are consistent with previous field study results that indicated the abundance of organic acid in lake water DOM—implying electrostatic interactions serve an important role in DOM assembly (Thurman, 1985) (Fig-2 and 3).

Changes of pH influence the assembly of DOM

Based on our previous study (Chin et al., 1998), pH value is one of critical parameters in DOM assembly kinetics. Under low pH conditions, the negative parts of the DOM polymers are neutralized by protons and the DOM assembly rate decreases. We used 0.05 N HCl and 0.05 N NaOH to adjust the pH of filtered surface water and measured the assembly by DLS over 5 days (Fig-4). Though the equilibrium microgel sizes were similar, we observed that the transition slope decreased under pH 6.0. These results also show that the ENs accelerated the kinetics of DOM even under lower pHs by decreasing initial delay time. Additional H^{+} in the aquatic environment may protonate the negative charges distributed on the DOM polymer chains, which would lead to their slower assembly rate. The EN-induced DOM assembly accelerations observed at lower pH

conditions suggested the electrostatic force and hydrophobic interactions may both serve as driving forces for EN-DOM assembly.

ENs Serve as Alternative Crosslinkers for Microgel Assembly

DOM polymer networks can be stabilized by physical or chemical interactions (Verdugo et al., 2004a; Verdugo et al., 2008). Physical interactions include low energy ionic forces, hydrophobic linkages, chemical interactions and covalent linkages. According to one previous report (Chin et al., 1998), Ca^{2+} ions play an important role in the marine DOM assembling process. In order to investigate the effects of Ca^{2+} ions in EN-induced DOM assembly, we added 10 mM EDTA (ethylenediamine-tetra-acetic acid)—a Ca^{2+} chelator—into 0.2 μm- filtered lake water to remove free Ca^{2+} ions. In the absence of Ca^{2+}, there is no obvious microgel assembly after 5 days (Fig-5). This result demonstrated the critical role of Ca^{2+} in DOM assembly. However, we found that 25 nm hydrophobic ENs can induce DOM assembly without Ca^{2+} ions. Compared to our control, ENs increased the rate of DOM assembly, but microgel equilibrium size remained 2-3 μm. The equilibrium size of microgels depends on DOM polymer concentration and the persistence length of polymers (Gennes, 1979). Under the absence of Ca^{2+} condition, the hydrophobic ENs can bind to the hydrophobic domains on the DOM polymers to serve as cross-linkers for the microgel matrices. Our result further confirmed hydrophobic interaction can serve a driving force for microgel formation (Ding et al., 2008; Verdugo et al., 2004b; Vergugo, 2012). However, without Ca^{2+}, the decreasing entangle friction within polymer matrices leaded to smaller equilibrium assembly sizes (Fig-5).

Our result indicate that different size and surface characteristics of ENs can significantly influence their interactions with DOM—and therefore determine the transport and fate of nanowaste disposed in the ecosystem. The data also suggest that diverse ENs could have completely different effects on the ecosystem, which merits further investigation. Since the freshwater aquatic system will be the first encountered water body for most man-made nanowaste, the outcomes from this study provide needed knowledge of nanowaste impact on ecology and serves to inform future policies aimed at regulating EN usage and disposal.

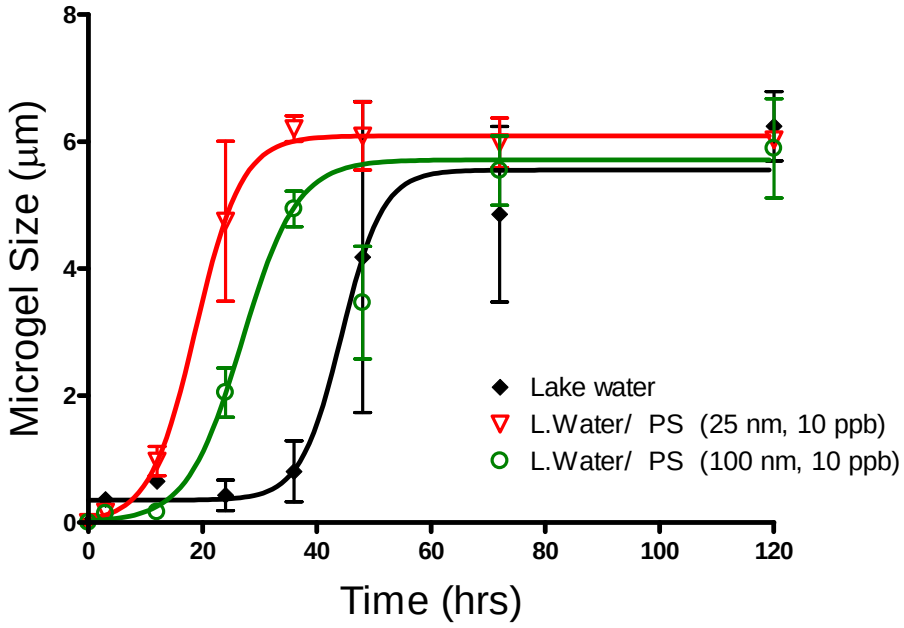

Fig-1. Kinetics of EN-DOM assembly over 120 hrs measurements. ENs with different diameters (25 nm and 100 nm) were added to the filtered river water samples. The kinetics of ENs-DOM assembly was monitored with DLS. Data showed that EN-DOM assembly reached equilibrium sizes within 36 hours with 25 nm ENs, and 48 hours for 100 nm ENs, ENs and DOM polymers formed microgels with 4~6 μm hydrodynamic diameter for both sizes of ENs (25 nm/ red; 100 nm/green).

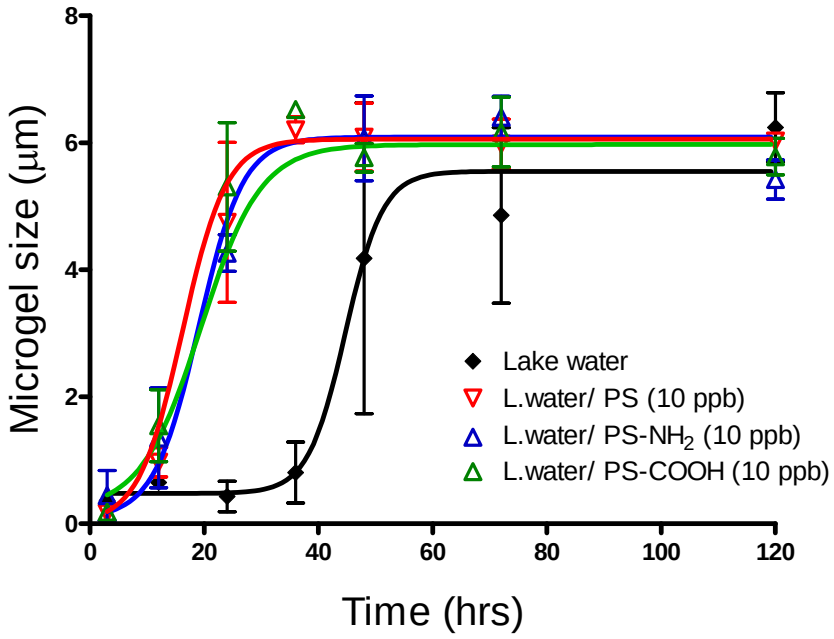

Fig – 2. Assembly kinetics for ENs and DOM in 0.2μm- filtered river water monitored by DLS. Addition of 10 μg L^{-1} ENs resulted in accelerated DOM assembly that reached equilibrium size in ~48 hours, yielding microgels of 5-6 μm hydrodynamic diameter. ENs with different surface modification were tested (hydrophobic/ red; amine- modification/ blue; carboxyl-modification/green). All three surface modifications on ENs show similar assembly kinetics.

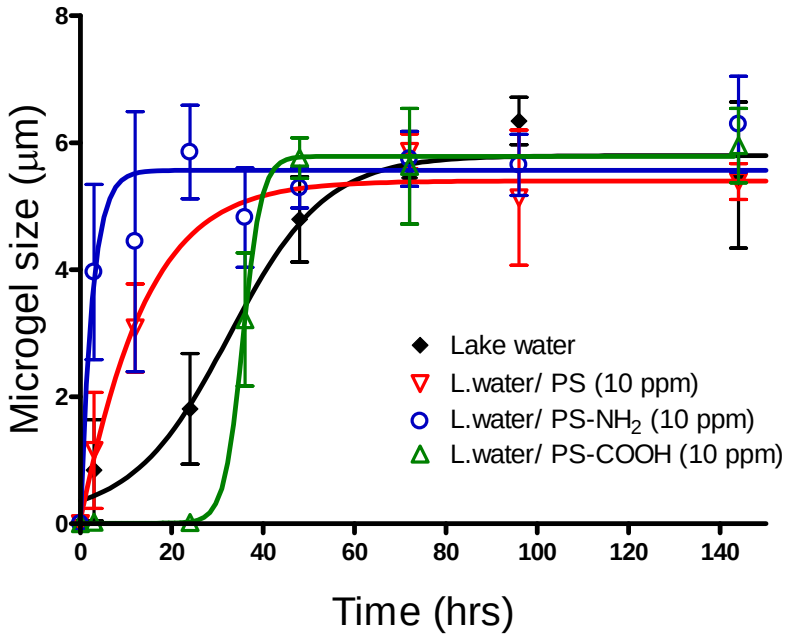

Fig – 3. ENs (25nm, 10 mg L^{-1}) with different surface modifications can significantly alter the assembly kinetics of river DOM (hydrophobic/ red; amine-modification/ blue; carboxyl/green). Both polystyrene and amine-modified surface ENs can accelerate assembly kinetics. Amine-modified surface ENs showed stronger acceleration effects than polystyrene ENs. Carboxyl modified ENs at high concentration (10 mg L^{-1}) can delay assembly kinetics more than 24 hrs. Each data point represents (mean ± SD) of six measurements made in each of six replicate samples.

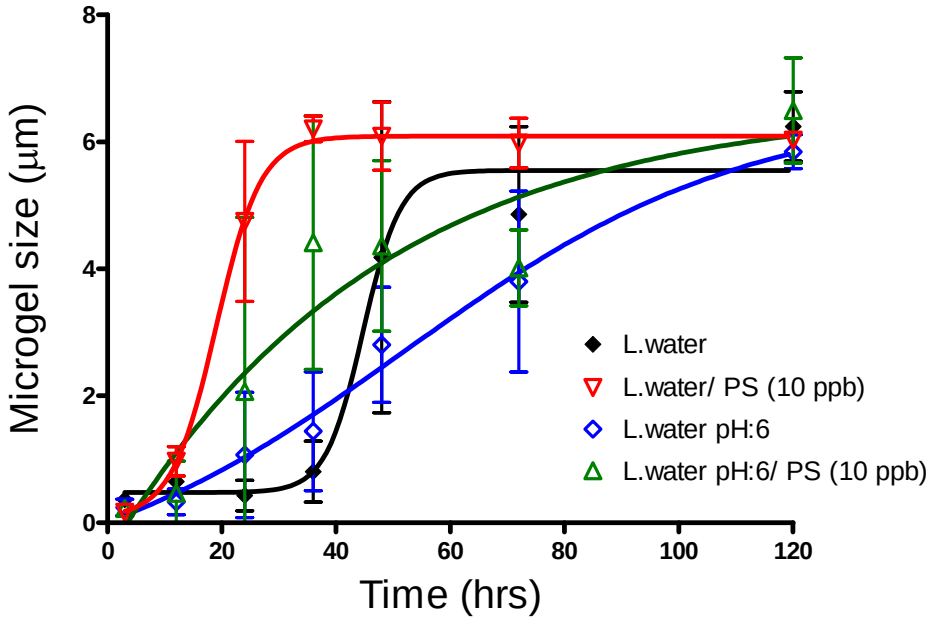

Fig-4. DOM assembly at different pHs. The kinetic of ENs-DOM assembly were studied under natural condition (pH 7.1) and lower pH (pH: 6.0). At low pH, the DOM assembly rate can significantly reduce, and ENs can still accelerate DOM assembly kinetics (DOM at pH 6/ blue; DOM with hydrophobic ENs at pH 6/ green). Each data point represents (mean ± SD) of six measurements made in each of six replicate samples.

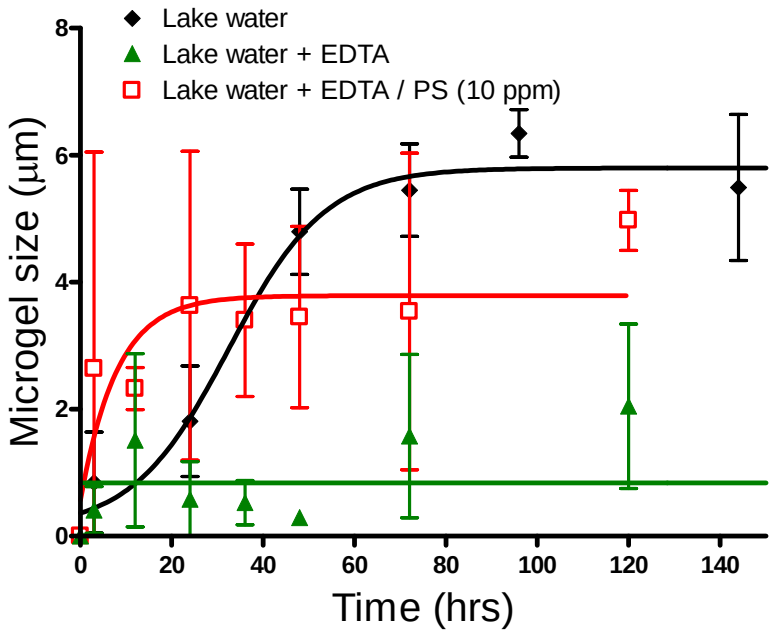

Fig – 5. Assembly kinetics of DOM polymers in absence or presence of 10 mM Ca^{2+} chelator EDTA. In chelating Ca^{2+} in lake water with EDTA, no DOM assembly was observed (lake water + EDTA/ green). Addition of ENs will restore the assemble processes, but the final size of microgels is considerably decreased compared with normal conditions (with Ca^{2+}). (lake water/ black; lake water with EDTA and 10 ppm hydrophobic ENs/ red)

Reference

Amon, R.M.W., Benner, R., 1994. Rapid-Cycling of High-Molecular-Weight Dissolved Organic-Matter in the Ocean. Nature 369, 549-552.
Amon, R.M.W., Benner, R., 1996a. Bacterial utilization of different size classes of dissolved organic matter. Limnol. Oceanogr. 41, 41-51.
Amon, R.M.W., Benner, R., 1996b. Photochemical and microbial consumption of dissolved organic carbon and dissolved oxygen in the Amazon River system. Geochimica Et Cosmochimica Acta 60, 1783-1792.
Benner, R., Pakulski, J.D., McCarthy, M., Hedges, J.I., Hatcher, P.G., 1992. Bulk Chemical Characteristics of Dissolved Organic-Matter in the Ocean. Science 255, 1561-1564.
Bhaskar, P.V., Bhosle, N.B., 2005. Microbial extracellular polymeric substances in marine biogeochemical processes. Current Science 88, 45-53.
Buffle, J., Wilkinson, K.J., Stoll, S., Filella, M., Zhang, J.W., 1998. A generalized description of aquatic colloidal interactions: The three-colloidal component approach. Environmental Science & Technology 32, 2887-2899.
Caruso, F., Caruso, R.A., Mohwald, H., 1998. Nanoengineering of inorganic and hybrid hollow spheres by colloidal templating. Science 282, 1111-1114.
Chin, W.C., Orellana, M.V., Verdugo, P., 1998. Spontaneous assembly of marine dissolved organic matter into polymer gels. Nature 391, 568-572.
Coble, P.G., 1996. Characterization of marine and terrestrial DOM in seawater using excitation emission matrix spectroscopy. Marine Chemistry 51, 325-346.
Ding, Y.-X., Chin, W.-C., Rodriguez, A., Hung, C.-C., Santschi, P.H., Verdugo, P., 2008. Amphiphilic exopolymers from Sagittula stellata induce DOM self-assembly and formation of marine microgels. Marine Chemistry 112, 11-19.
Dunphy Guzman, K.A., Taylor, M.R., Banfield, J.F., 2006. Environmental risks of nanotechnology: National nanotechnology initiative funding, 2000-2004. Environmental Science & Technology 40, 1401-1407.
Elimelech, M., Omelia, C.R., 1990. Effect of Particle-Size on Collision Efficiency in the Deposition of Brownian Particles with Electrostatic Energy Barriers. Langmuir 6, 1153-1163.
Filella, M., Buffle, J., 1993. Factors Controlling the Stability of Submicron Colloids in Natural-Waters. Colloids and Surfaces a-Physicochemical and Engineering Aspects 73, 255-273.
Gennes, P.G.D., 1979. Scaling concepts in polymer physics. Cornell University Press.
Kelly, K.L., Coronado, E., Zhao, L.L., Schatz, G.C., 2003. The optical properties of metal nanoparticles: The influence of size, shape, and dielectric environment. Journal of Physical Chemistry B 107, 668-677.
Kepkay, P.E., 1994. Particle Aggregation and the Biological Reactivity of Colloids. Marine Ecology-Progress Series 109, 293-304.
Kerner, M., Hohenberg, H., Ertl, S., Reckermann, M., Spitzy, A., 2003. Self-organization of dissolved organic matter to micelle-like microparticles in river water. Nature 422, 150-154.
Klaine, S.J., Alvarez, P.J., Batley, G.E., Fernandes, T.F., Handy, R.D., Lyon, D.Y., Mahendra, S., McLaughlin, M.J., Lead, J.R., 2008. Nanomaterials in the environment:

behavior, fate, bioavailability, and effects. Environmental toxicology and chemistry / SETAC 27, 1825-1851.
Kretzschmar, R., Sticher, H., 1997. Transport of humic-coated iron oxide colloids in a sandy soil: Influence of Ca2+ and trace metals. Environmental Science & Technology 31, 3497-3504.
Lecoanet, H.F., Bottero, J.Y., Wiesner, M.R., 2004. Laboratory assessment of the mobility of nanomaterials in porous media. Environmental Science & Technology 38, 5164-5169.
Maynard, A.D., Aitken, R.J., Butz, T., Colvin, V., Donaldson, K., Oberdorster, G., Philbert, M.A., Ryan, J., Seaton, A., Stone, V., Tinkle, S.S., Tran, L., Walker, N.J., Warheit, D.B., 2006. Safe handling of nanotechnology. Nature 444, 267-269.
Mirkin, C.A., Letsinger, R.L., Mucic, R.C., Storhoff, J.J., 1996. A DNA-based method for rationally assembling nanoparticles into macroscopic materials. Nature 382, 607-609.
Murray, C.B., Kagan, C.R., Bawendi, M.G., 2000. Synthesis and characterization of monodisperse nanocrystals and close-packed nanocrystal assemblies. Annual Review of Materials Science 30, 545-610.
Nel, A., Xia, T., Madler, L., Li, N., 2006. Toxic potential of materials at the nanolevel. Science 311, 622-627.
Pellegrino, T., Manna, L., Kudera, S., Liedl, T., Koktysh, D., Rogach, A.L., Keller, S., Radler, J., Natile, G., Parak, W.J., 2004. Hydrophobic nanocrystals coated with an amphiphilic polymer shell: A general route to water soluble nanocrystals. Nano Letters 4, 703-707.
Provencher, S.W., Stepanek, P., 1996. Global analysis of dynamic light scattering autocorrelation functions. Particle & Particle Systems Characterization 13, 291-294.
Santschi, P.H., Balnois, E., Wilkinson, K.J., Zhang, J.W., Buffle, J., Guo, L.D., 1998. Fibrillar polysaccharides in marine macromolecular organic matter as imaged by atomic force microscopy and transmission electron microscopy. Limnol. Oceanogr. 43, 896-908.
Thomas, J.D., 1997. The role of dissolved organic matter, particularly free amino acids and humic substances, in freshwater ecosystems. Freshwater Biology 38, 1-36.
Thurman, E.M., 1985. Organic geochemistry of natural waters. Martinus Nijhoff/ Dr W. Junk publishers.
Verdugo, P., Alldredge, A.L., Azam, F., Kirchman, D.L., Passow, U., Santschi, P.H., 2004a. The oceanic gel phase: a bridge in the DOM-POM continuum. Marine Chemistry 92, 67-85.
Verdugo, P., Alldredge, A.L., Azam, F., Kirchman, D.L., Passow, U., Santschi, P.H., 2004b. The oceanic gel phase: a bridge in the DOMâ€“POM continuum. Marine Chemistry 92, 67-85.
Verdugo, P., Orellana, M.V., Chin, W.C., Petersen, T.W., van den Eng, G., Benner, R., Hedges, J.I., 2008. Marine biopolymer self-assembly: implications for carbon cycling in the ocean. Faraday Discussions 139, 393-398.
Vergugo, P., 2012. Marine microgels. Annual Review of Marine Science 4, 1-25.
Wells, M.L., 1998. Marine colloids - A neglected dimension. Nature 391, 530-531.
Zhang, T.R., Ge, J.P., Hu, Y.P., Yin, Y.D., 2007. A general approach for transferring hydrophobic nanocrystals into water. Nano Letters 7, 3203-3207.

Chapter4 The impact of nanoparticles on the assembly of phytoplankton EPS

Abstract

The unique properties of engineered nanoparticles (ENs) that make their industrial applications so attractive simultaneously raise questions regarding their environmental safety. ENs exhibit behaviors different from bulk materials with identical chemical compositions. Though the nanotoxicity of ENs has been studied intensively, their unintended environmental impacts remain largely unknown. Herein we report experimental results of EN interactions with exopolymeric substances (EPS) from three marine phytoplankton species: *Amphora sp.*, *Ankistrodesmus angustus* and *Phaeodactylum tricornutum*. EPS are polysaccharide-rich anionic colloid polymers released by various microorganisms that can assemble into microgels, possibly by means of hydrophobic and ionic mechanisms. Polystyrene nanoparticles (23 nm) were used in our study as model ENs. The effects of ENs on EPS assembly were monitored with dynamic laser scattering (DLS). We found ENs can induce significant acceleration in *Amphora sp.* EPS assembly; after 72 hours EN-EPS aggregation reached equilibrium, forming microscopic gels of ~4-6 μm in size. In contrast, ENs only cause moderate assembly kinetic acceleration for *A. angustus* and *P. tricornutum* EPS samples. Our results indicate that the effects of ENs on EPS assembly kinetics mainly depend on the hydrophobic interactions of ENs with EPS polymers. The cycling mechanism of EPS is complex. Nonetheless, the change of EPS assembly kinetics induced by ENs can be considered as one potential disturbance to the marine carbon cycle.

4.1 EPS and biofilm formation / nanoparticles

Engineered nanoparticles (ENs) are increasingly being developed to improve and innovate industrial and consumer products; for example, they are used to improve semiconductors, sunscreens and cosmetics and in the medicinal industry for imagery and drug delivery (Nel et al., 2006). As a large fraction of atoms are located at or near their surface, ENs have high electron activities. Cytotoxic interactions between organisms and ENs can occur through various mechanisms such as electro-active groups, heavy-metal effects and reactive oxygen species (ROS) (Nel et al., 2006). Previous studies have demonstrated the ability of algal and protozoan to uptake ENs (WerlinR et al., 2011). The popularity of ENs in the consumer industry raises critical questions regarding their potential impacts on ecological systems (Maynard et al., 2006), especially in the context of oceanic environments. Therefore, any EN-aquatic biota interaction that could alter natural oceanic processes, including the marine carbon cycle or marine food webs, should receive increased attention (Ferry et al., 2009).

In recent years, accumulating plastic debris in the world's oceans has become a major public concern (Artham et al., 2009; Thompson et al., 2004; Zarfl and Matthies). To date, several studies have elucidated the threat by microplastics to marine organisms such as fish, birds, and turtles —mostly through pathways of ingestion (Derraik, 2002; Ward and Shumway, 2004). Few have focused on marine phytoplankton (Bhattacharya et al., 2010) despite the fact that most floating plastic fragments—some with sizes close to 1μm—accumulate at the ocean surface (Zarfl and Matthies); here they can degrade to leave free-floating polymers of appropriate sizes for transportation by ocean currents to neighboring regions (Moret-Ferguson et al., ; Thompson et al., 2004; Watters et al.). These reports suggest that accumulated micropolymers may be interacting with marine phytoplankton. Though it is difficult to quantify the direct ecological influence of nanopolymers on aquatic ecosystems (Werlin et al.), studying the potential threat that nanopolymers released from plastic degradation (Gopferich, 1996) on ecological processes is greatly needed given reported threat by microplastics (Bhattacharya et al., 2010; Ward and Shumway, 2004).

Phytoplankton in the surface ocean account for about half of the global photosynthetic activity (Chisholm, 2000), making them a major driving force to sequester CO_2 from the

atmosphere (Chisholm, 2000; Falkowski et al., 2000). Furthermore, about ~40-60% of the photosynthetic production by phytoplankton is released as EPS into the dissolved organic carbon (DOC) pool, contributing to the primary marine carbon reservoir (Baines and Pace, 1991; Fogg, 1983). The recent discovery that ~ 10% of the DOC pool can assemble to form porous microscopic gels that can be readily colonized and metabolized by marine bacteria opened a novel lens to view DOC and carbon cycling in the oceans (Chin et al., 1998; Ding et al., 2008b; Verdugo et al., 2004; Verdugo et al., 2008; Wells, 1998). Considering that EPS is a major source of both the marine DOC and particulate organic carbon (POC) pools (Baines and Pace, 1991; Fogg, 1983; Hedges, 1992; Wotton and Preston, 2005) understanding EPS assembly in the presence of nanoparticles and their specific mechanisms of microgel formation are critically important.

Recent studies have revealed that EN toxicity can impair phytoplankton function both extra- and intra-cellularly (Navarro et al., 2008). Miao et al. (Miao et al., 2009) found trace metal ions released from the oxidative dissolution of silver ENs in seawater were toxic to the marine diatom *Thalassiosira weissflogii.* These authors also reported that EPS production, particularly in nutrient limited cultures, played an important role in Ag ion detoxification. Zinc oxide ENs have been found to elicit a similar toxicity responses in the marine diatom *Thalassiosira pseudonana* (Miao et al., 2010b); ZnO-EN dissolution rates were accelerated in seawater, whereas ZnO-EN concentration itself only had a very small effect on Zn^{2+} release. Ag-ENs were also found to accumulate inside the freshwater alga *Ochromonas danica* where they exerted their toxic effects (Miao et al., 2010a).

Here we used EPS released by three phytoplankton—*Amphora sp., A. angustus* and *P. tricornutum*—to investigate the effects of ENs on EPS assembly. *Amphora sp.* is a major genus of diatoms that has a world-wide distribution and an ability to grow under a wide range of conditions (Daniel et al., 1980). *Amphora sp.* is also a dominant fouling/biofilm diatom species that produces significant amount of EPS (Daniel et al., 1980) and has been used in many diatom mobility studies (Cooksey and Wigglesworthcooksey, 1995; Wigglesworth-Cooksey and Cooksey, 2005). *Ankistrodesmus* is a major genus of green algae that has been used in many studies (Adrian, 1987; Conner, 1981). *P. tricornutum* is

a model diatom for genomics (De Martino et al., 2007; Scala et al., 2002) and fatty acid metabolism studies (Yongmanitchai and Ward, 1991). To investigate the environmental impacts of nanoplastics released during debris degradation, polystyrene ENs (diameter 23 nm) were used as model ENs. Their high surface ratio and nano-scale particle size provided a suitable model to study the interactions of engineered nanomaterials and natural polymers. In this study, particle sizing by dynamic laser scattering (DLS) was used to monitor the assembly process of EPS and their interactions with ENs. Hydrophobic dye (Nile Red) and protein:carbohydrate ratios were used to quantify the existence of hydrophobic domains on EPS polymers and to investigate the role hydrophobic interactions in EN-induced EPS assembly (Ding et al., 2009).

4.2 Material and methods

Chemicals and solution preparation

HPLC grade reagents and salts including sodium chloride, potassium chloride, calcium chloride, magnesium chloride, magnesium sulfate, sodium bicarbonate, and dimethyl sulfoxide were purchased from Sigma-Aldrich (St. Lious, MO, USA). Polystyrene nanoparticles (Bangs Laboratories, IN, USA) were used in our study as model ENs. The primary size and surface area of these non-fluorescence nanoparticles were 23 nm and 2.48×10^{14} $\mu m^2/g$ (certificate provided by vendor). Fluorescence polystyrene ENs (23 nm, Bangs Laboratories, IN, USA) were used only for fluorescence microscopy. The size of these ENs was independently confirmed by DLS (dynamic laser scattering). Thorough sonication was applied to nanoparticle stock solutions before experiments, as described in our previous study (Chen et al. 1998).

Artificial Seawater (ASW, 423 mM NaCl, 9 mM KCl, 9.27 mM $CaCl_2$, 22.94 mM $MgCl_2$, 25.5 mM $MgSO_4$, 2.14 mM $NaHCO_3$) was prepared using deionized water from a Milli-Q system (Millipore, Billerica, MA, USA) following established protocols from the Marine Biological Laboratory, Woods Hole, MA. The composition of Ca^{2+}- free ASW included: 436.7 mM NaCl, 9 mM KCl, 22.9 mM $MgCl_2$, 25.5 mM $MgSO_4$, 2.1 mM $NaHCO_3$, and 1 mM EGTA. Two different concentrations of ENs were added into the EPS solution (final EN concentration: 10 ppb, 100 ppb). A Nile Red stock solution (1.6 mM) was prepared in DMSO. A Chlortetracycline hydrochloride (CTC) (Sigma-Aldrich, USA) stock solution (10 mM) was prepared in Milli-Q water.

Extraction of exopolymeric substances (EPS) from phytoplankton culture

A. angustus and *P. tricornutum* used for EPS extraction were purchased from the CCMP (The Provasoli-Guillard National Center for Culture of Marine Phytoplankton). Both species were grown under continuous light (35 μmol. photons m^{-2} s^{-1}) at 20ºC. The culture volume was 20 L for each and cultures were aerated. Growth was monitored by measuring the change in optical density at 750 nm with a UV/VIS spectrophotometer. Cultures were harvested during the stationary phase and then EPS was extracted. The phytoplankton culture was centrifuged at 3200 rpm for 30 minutes, after which it was

separated into pellet (cells) and supernatant fractions. The supernatant fraction was used to collect free dissolved EPS according to the previous study (Zhang and Santschi, 2009). In brief, the procedure consisted of a) filtration, b) cross-flow ultrafiltration, c) stirred-cell diafiltration. The pre-filtered supernatant fraction (<0.45 μm) (20 L) was ultrafiltered until 200-300 mL of retentate was left. The cartridge was rinsed with 200 mL of pure water and soaked for 6 hours. After that, the cartridge was rinsed with another 200 mL of water, and this whole process was repeated twice. Subsequently, the retentate solution and four rinse solutions were combined. The resulting 1 L of solution was then further concentrated by stirred-cell diafiltration with a 5 kDa membrane to obtain 50 mL of concentrated EPS solution. EPS of *Amphora sp.* was obtained using the same approach described by Zhang et al. (Zhang et al., 2008).

Compositional characterization of EPS

Carbohydrate concentration was measured using the anthrone method (Zhang and Santschi, 2009), with glucose as a standard. Uronic acids were determined according to Blumenkrantz and Asboe-Hansen with glucuronic acid as a standard (Blumenkr.N and Asboehan.G, 1973). Proteins were measured using a modified Lowry Protein Assay Kit (Pierce, 23240, USA), according to the protocol provided by the manufacture. Additionally, elemental carbon, hydrogen and nitrogen abundance was analyzed by Series II CHNS/O Analyzer 2400 (Perkin Elmer).

Estimation of EPS molecular weight

Size Exclusion Chromatography (SEC) was used to measure the molecular weight of the EPS (Zhang et al., 2008). Briefly, 150 μL of EPS solution was injected into a Tosoh TSK G-4000PW×l (300×7.8 mm) and detected by a Refractive Index detector. The mobile phase was 0.078 M $NaNO_3$ in 10 mM phosphate buffer (pH=6.8) at a flow rate of 0.5 mL/min. Polystyrene standards with a molecular weight of 8 kDa, 35 kDa, 100 kDa, and 780 kDa were used for establishing the calibration curve, whereby the logarithm of molecular weight was plotted vs. corresponding retention time.

Microgel Sizing

EN-induced alterations of EPS assembly were investigated with three different types of EPS (*Amphora sp.*, *A. angustus* and *P. tricornutum*) and at three EN concentrations (0, 10, 100 ppb) in ASW and Ca^{2+}-free ASW. The size of assembled EPS gels (microgels) was monitored by DLS following protocols published previously (Chin et al., 1998). The EPS solution was briefly shaken, and refiltered through a 0.22-μm Millipore membrane (pre-washed with 0.1N HCl) before use. Aliquots were then poured directly into scattering sample vials. Scattering cells were positioned in the goniometer of a Brookhaven laser spectrometer (Brookhaven Instruments, Holtsville, NY, USA). EPS assembly was monitored for two weeks, by analyzing the scattering fluctuations detected at a 45 degree scattering angle. The autocorrelation function of the scattering intensity fluctuations was averaged over a 12-min sampling time, using a Brookhaven BI 9000AT autocorrelator. CONTIN method was adapted to calculate particle size distribution (Chin et al., 1998; Provencher and Stepanek, 1996). Calibration of the DLS method was conducted using standard suspensions of latex microspheres (Polysciences, Warrington, PA, USA). Each measurement was taken in replicate (n=6) at room temperature.

Fluorescence enhancement measurement

Nile Red (Invitrogen, Carlsbad, CA, USA), used as a hydrophobic indicator as in our previous studies (Ding et al., 2009), is a particularly effective solvatochromic dye containing a rigid aromatic group and an exocyclic diethylamine group. The absorbance and fluorescence emission depends on the physical properties of surrounding solvent environment: fluorescence emission is enhanced with hydrophobic environment exposure (Yablon and Schilowitz, 2004). EPS from *Amphora sp.*, *A. angustus* and *P. tricornutum* were mixed with 13 μM Nile Red in triplicate. The fluorescence measurements were obtained with a Shimadzu RF-5000U spectrofluorophotometer ($\lambda_{excitation}$=550 nm; $\lambda_{emission}$= 633 nm). Fluorescence emission of Nile Red showed a very weak signal at 633 nm in the polar ASW with excitation wavelength 550 nm.

CTC was used to reveal bound Ca^{2+} on EPS polymers (Chin et al., 1998; Ding et al., 2007). CTC (100 μM) was added into ASW mixed with each type of EPS. For CTC

fluorescence measurements, the emission was collected at λ= 530 nm (excited at λ= 390 nm) using a Shimadzu RF-5000U spectrofluorophotometer.

Environmental scanning electron microscopy (ESEM)

ESEM was used to investigate EPS polymer networks in their native conformations. This method provides a non-destructive tool to study materials at electron microscopy resolution while still fully hydrated. Samples of EPS were prepared in ASW with/without 23 nm polystyrene nanoparticles, as previously described (Chin et al., 1998; Ding et al., 2008b; Verdugo et al., 2004; Verdugo et al., 2008; Wells, 1998). After being incubated for 10 days in darkness to reach the equilibrium sizes, all EPS aggregations were filtered through a 0.22-μm Millipore Isopore membrane (Fisher Scientific, Pittsburgh, PA, USA). The assembled microgels retained on filters were investigated using FEI Quanta 200 ESEM (North America NanoPort, Portland, OR, USA).

Fluorescence microscopy

The accumulation of ENs within EPS microgels was investigated with Fluorescence Microscopy (Nikon Instruments, Melville, NY, USA). EN-induced EPS microgels were prepared in agreement with our aforementioned protocol with 100 ppb 23 nm fluorescent ENs (Bangs Laboratories, IN, USA) and 13 μM Nile Red. The fluorescent images of microgels retained on Isopore membrane were collected by fluorescence microscopy with at $\lambda_{excitation}$ = 530 nm (Nile red) and at $\lambda_{excitation}$ = 488 nm (fluorescent ENs).

Statistical analysis

Data represent means ± 1 standard deviation (SD). Each experiment was performed in triplicate. A student's t-test analysis was used to determine statistical significance. p values of < 0.05 were used as standard for statistical significance (GraphPad Prism 4.0, GraphPad Software, San Diego, CA).

4.3 Results

Chemical analysis of EPS

EPS from the three phytoplankton species contained varied protein:carbohydrate ratios, which can be taken as an indicator of their relative hydrophobicity. *A. angustus* had a ratio of 0.72, *P. tricornutum* with a ratio of 0.31 while *Amphora sp.* had no detectable level of proteins (Table-1, Zhang et al., 2008). Our chemical analysis indicates that EPS from these three phytoplankton species have similar molecular weight distributions and uronic acid ratios (Table 1). CHN analysis also indicated that *Amphora* EPS has the lowest N content of the three types of EPS (Table-1). Of the different EPS used in this study, EPS from *A. angustus* is the most hydrophobic whilst *Amphora* EPS is the most hydrophilic.

Assembly of EPS from phytoplankton in ASW and Ca^{2+}- free ASW

The spontaneous assembly of 100 μg L^{-1} *Amphora sp.* EPS solutions in ASW containing 9 mM Ca^{2+} (but no ENs) was monitored by DLS for more than 10 days. As shown in Fig. 1a, EPS from *Amphora sp.* cannot assemble to form EPS microgels after 10 days. Similar measurements conducted in 100 μg L^{-1} *Amphora sp.* EPS solutions with ENs (10 or 100 ppb) demonstrated that ENs can facilitate EPS assembly following first-order kinetics, reaching steady-state assembly/dispersion equilibrium in ~60 hrs. The equilibrium size of microgels, ~ 2.5 μm formed with 10 ppb ENs, was significantly smaller than those formed from 100 ppb ENs (4-5 μm) (Fig. 1a).

The same protocol was used to test the spontaneous assembly of EPS from *A. angustus* (Fig. 1b) and *P. tricornutum* (Fig. 1c). Results show that both types of EPS polymers can assemble following almost identical kinetics and reach similar microgel equilibrium sizes (~2 μm) in the absence of ENs. With 10 ppb ENs, for both EPS types, the assembly rate was accelerated and the resulting microgel size was increased to around 4 μm (Fig. 1b, c). With higher concentrations of ENs (100 ppb), the assembly rate was further accelerated; however, the resulting microgel size remained at around 4 μm (Fig. 1b, c). We also

monitored pure ENs in ASW for 10 days with DLS and found no EN self-aggregation (data not shown).

The EN-induced EPS assemblies from those three species were monitored with 100 ppb ENs in Ca^{2+}-free ASW. Without divalent ions (Ca^{2+} or Mg^{2+}), our results show ENs still can promote EPS assembly. EPS from *Amphora sp*, *A. angustus* and *P. tricornutum* assembled into microgels with equilibrium sizes about 4-5 μm within ~120 hrs (Fig. 1a-c).

ESEM images (Fig. 2a-c) showed that ENs (100 ppb) may incorporate into EPS microgel matrices, as granular surface structures were found in these ESEM images (Fig. 2a-c). In addition, ESEM observations confirmed the size measurements with DLS (Fig. 1a-c). The results from fluorescence microscopy supported the hypothesis that ENs may be incorporated into EPS microgels. In our experiments, EPS microgels were stained with Nile Red to determine the gel morphology (Fig-3). Noting EPS assembly in ASW without ENs, green fluorescent ENs were found in EPS matrices of all three species (Fig-3). The data indicate that ENs can accumulate within EPS polymer matrices and may reach a higher concentration than the bulk EN concentration in the water column.

Fluorescence of Nile Red and CTC

We used Nile Red, a widely used hydrophobic fluorescent probe, to detect the presence of hydrophobic regions in EPS from *Amphora sp.*, *A. angustus* and *P. tricornutum* (Fig. 3). The higher Nile Red fluorescence intensity observed in EPS from *A. angustus* and *P. tricornutum* indicated these EPS are much more hydrophobic than EPS from *Amphora sp*. The Nile Red fluorescence results here are consistent with chemical analysis results (Table-1) demonstrating that EPS from *A. angustus* is the most hydrophobic and *Amphora sp.* EPS is the least hydrophobic.

CTC has been used to monitor bound Ca^{2+} in marine microgels (Chin et al., 1998; Ding et al., 2007). CTC fluorescence indicates that all three types of phytoplankton EPS have similar Ca^{2+} binding capacity (Fig. 4).

4.4 Discussion

Both hydrophobic and electrostatic interactions have been demonstrated to play important roles in the assembly of EPS microgels (Ding et al., 2008b; Ding et al., 2009). Our results indicate that only 10 to 100 ppb of released ENs in the aquatic environment can cause significant EPS-assembly changes (Fig. 1a-c). The results from *A. angustus* and *P. tricornutum* show that ENs can accelerate the assembly kinetics and increase the equilibrium microgel sizes of EPS. For EPS from *Amphora*, ENs can effectively induce their assembly, resulting in microgels with an equilibrium size of 4-6 μm, similar to *A. angustus* and *P. tricornutum* EPS.

EPS polymers from marine organisms are polysaccharide-rich, containing uronic acids and various proteins. Slight changes in their compositions would therefore affect their physic-chemical, e.g., biosurfactant and emulsifying, properties. Their role and fate in biogeochemical cycles is largely unexplored (Bhaskar and Bhosle, 2005; Wotton, 2004). Generally, the acidic groups in EPS are carboxylate, sulphate, and phosphate. Protein constituents have been proposed to be the major contributor for the hydrophobic domains of EPS (Ding et al., 2009; Quiroz et al., 2006).

Different protein:carbohydrate ratios were found in our chemical analysis of EPS (Table-1). Nile Red and CTC were used to detect the presence of hydrophobic domains and Ca^{2+} binding on different EPS polymers (Chin et al., 1998; Ding et al., 2008b; Ding et al., 2007; Ding et al., 2009). Our Nile Red fluorescence results indicate greater hydrophobic domains on EPS polymers with higher protein:carbohydrate ratios, which are in agreement with previous reports showing protein content contributes to amphiphilic and emulsifying properties of hydrocolloids such as EPS (Dickinson, 2003; Stenstrom, 1989). Spontaneous assembly was only observed with EPS from *A. angustus* and *P. tricornutum*, which have higher protein:carbohydrate ratios, and not from *Amphora sp.* EPS (Fig. 1a-c), which has a low protein:carbohydrate ratio (i.e., no detectable protein, lack of sufficient hydrophobic domains, Table 1). Our data indicate that the hydrophobic domains on EPS polymers potentially serve as the essential aggregation sites for EPS assembly (Fig. 1a-c) (Ding et al., 2008a). For EPS with a relatively low protein (hydrophobic) fraction, such

as *Amphora sp.*, 100 ppb ENs is required to trigger significant EPS assembly. However, for both partially hydrophobic EPS from *A. angustus* and *P. tricornutum,* 10 ppb ENs are sufficient to significantly change assembly kinetics, resulting in larger microgels (4-5 μm) (Fig. 1b-c). Our data thus confirm the importance of hydrophobic interactions and the total amount of EPS, as well as indicate the threshold of released nanowaste that can disturb the EPS assembly, which may be related to the specific protein:carbohydrate ratio of EPS.

The Ca^{2+} -free ASW data further confirmed that hydrophobic interactions play a critical role in phytoplankton ENs-induced EPS assembly (Fig. 1). With a lack of divalent ions serving as cross-linkers, similar EN-induced EPS assembly was observed in 100 ppb EN concentrations. Our results provide evidence that hydrophobic interactions play critical roles in the assembly of these marine EPS, consistent with the previous findings (Ding et al., 2008b).

The chemical analysis in our study indicates that EPS from these three phytoplankton species have similar molecular weight distributions (*Amphora*: 1000 kD; *A. angustus*: 1028 kD; *P. tricornutum*: 1006 kD) (Table-1). These observations are consistent with the predictions from a previous polymer model that states the equilibrium size of entangled polymer matrices depends on the polymer length (Degennes, 1979; Degennes and Leger, 1982). Due to the heterogeneous chemical compositions, the mechanism of EPS assembly remains elusive. In order to quantify the accelerations effects of ENs, the assembly kinetics was fitted with a sigmoidal curve and $T_{1/2}$ was used to represent the time needed for the microgel to reach half of the equilibrium size. *A. angustus* showed a dramatically decreased $T_{1/2}$: from ~178 hrs (control, without ENs) to ~16 hrs with 100 ppb ENs. Similar positive correlations between $T_{1/2}$ decrease and ENs dosages were found in *P. tricornutum* and *Amphora sp.* EPS (Table-2). The acceleration of assembly kinetics shown here demonstrated that ENs are able to promote EPS assembly. In addition, we used Hill coefficients to investigate the cooperative interactions between ENs and EPS polymers (Ding et al., 2008a) . For *Amphora* EPS, the Hill coefficient was ~2.28 for 100 ppb ENs concentration. Positive EN-EPS cooperative effects were also

observed in EPS assembly of *A. angustus* and *P. tricornutum* (Table-2). Similar positive cooperation was also found to correlate with hydrophobic interactions between ENs and EPS.

EPS play critical roles in aquatic ecosystems and have been shown to be key sources for marine DOC and POC. If the EN-induced changes of EPS assembly highlighted in this study are applicable to the natural environment, ENs can lead to deleterious environmental impacts. With varying assembly characteristics, EPS released from diverse phytoplankton contribute to different organic carbon pools in the ocean. Our data reported here indicate that 10 ppb ENs can unexpectedly induce assembly of EPS of *Amphora sp.,* indicating the re-direction of the organic carbon flux from the DOC to POC pool. The alterations of EPS assembly kinetics from *A. angustus* and *P. tricornutum* also indicate the change of the time scale for carbon flow between DOC and POC.

EPS assembly changes can also affect the microbial ecosystem and marine trophic cycle. Described as the dark matter of biofilms and transparent exopolymeric particles (TEP), EPS play crucial roles in the formation and maintenance of structured multicelluar microbial communities (Azam, 1998; Azam and Long, 2001; Azam and Malfatti, 2007; Flemming et al., 2007; Flemming and Wingender, ; Passow, 2002; Passow and Alldredge, 1994; Verdugo et al., 2004). The concentration, cohesion, charge, sorption capacity, specificity and nature of the individual components of EPS, as well as the three-dimensional architecture of the matrix (the dense areas, pores and channels), determine the mode of community life. In this study, our data showed that ENs can drastically change the assembly behavior of EPS. The change of sedimentation velocity, caused by assembly size changes, can reshape the plume leaking from microgel and influence the nutrient utilization of free-living microbes in the water column (Azam and Long, 2001; Kiorboe and Jackson, 2001). Moreover, higher concentrations of ENs accumulated within EPS microgel matrices were shown with ESEM and fluorescence microscopy (Fig 2a-c). Because microgels also serve as important nutrition source for the marine food web in the deep ocean, the possibility of ENs impacting direct up-take by higher-level organisms, such as protozoa and metazoan, needs to also be considered (Kerner et al., 2003).

Our data thus show the EPS gel matrices serve as a concentrating sponge (Fig-3). This new pathway of nanowaste accumulation facilitated by EPS suggests an urgent need to consider lower concentration limits for nanowaste in marine environments (Leppard, 2008; Maynard et al., 2006). In summary, our results clearly demonstrate how nanowaste (e.g. nanoparticles) can potentially disturb the marine carbon cycle and ecosystem (Azam and Malfatti, 2007). Whereas most environmental impact studies of nanomaterials have focused on "nanotoxicity"—investigating the direct harmful effects on phytoplankton cells or various organisms—our study indicates that indirect influences from ENs can potentially pose greater environmental threats than those of direct toxicity.

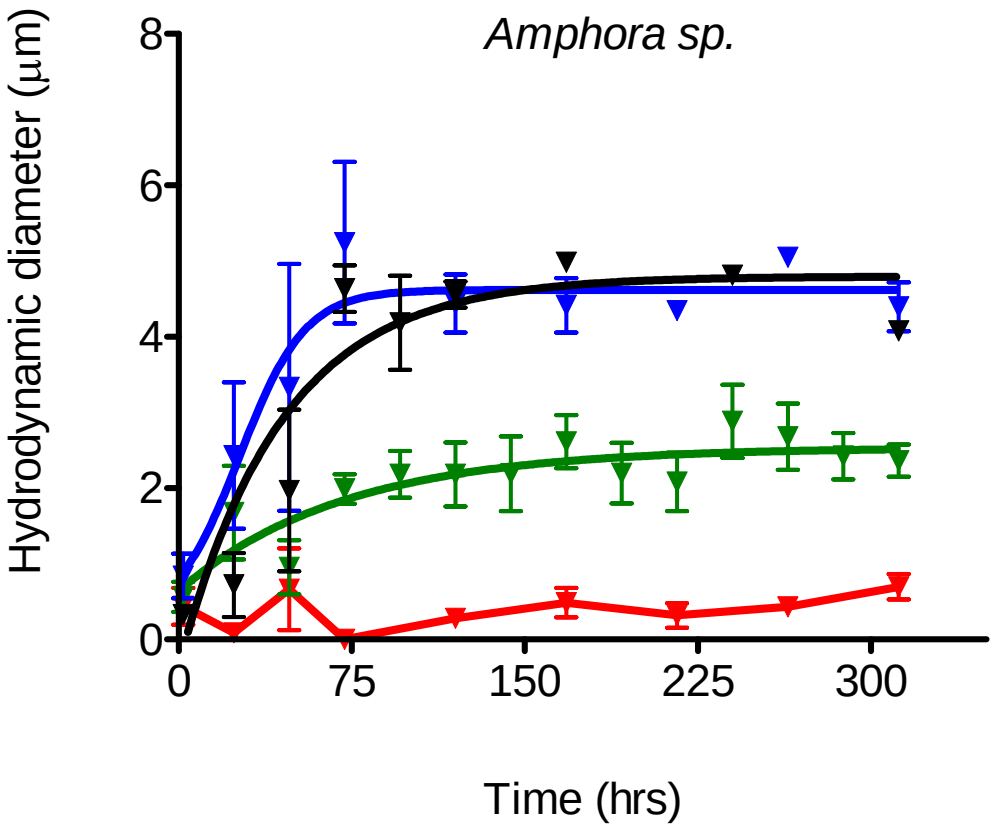

Fig. 1a Assembly kinetics of EPS of *Amphora sp.* monitored with DLS. EPS assembly in Ca^{2+}-free ASW (black) was monitored to investigate assembly kinetics with decreased divalent ion availability. Different concentrations of ENs (polystyrene nanoparticles): 0 (red), 10 (green) and 100 ppb (blue), were added to investigate the effect of ENs on EPS microgel formation.

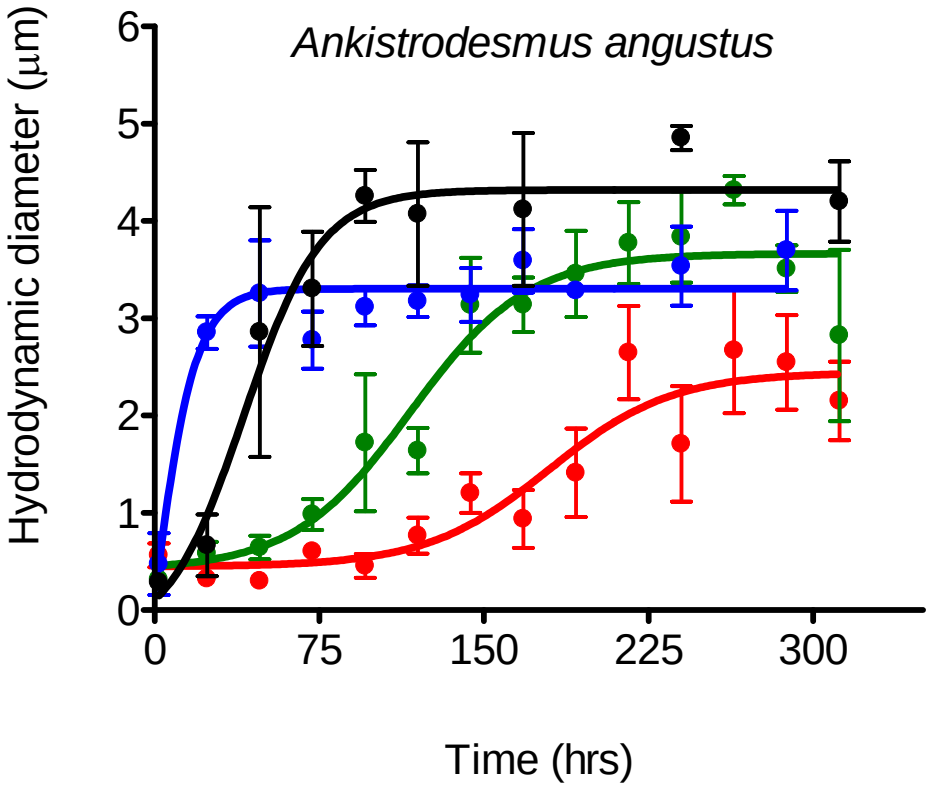

Fig. 1b Assembly kinetics of EPS of *Ankistrodesmus angustus* monitored with DLS. EPS assembly in Ca^{2+}-free ASW (black) was monitored to investigate assembly kinetics with decreased divalent ion availability. Different concentrations of ENs (polystyrene nanoparticles): 0 (red), 10 (green) and 100 ppb (blue), were added to investigate the effect of ENs on EPS microgel formation.

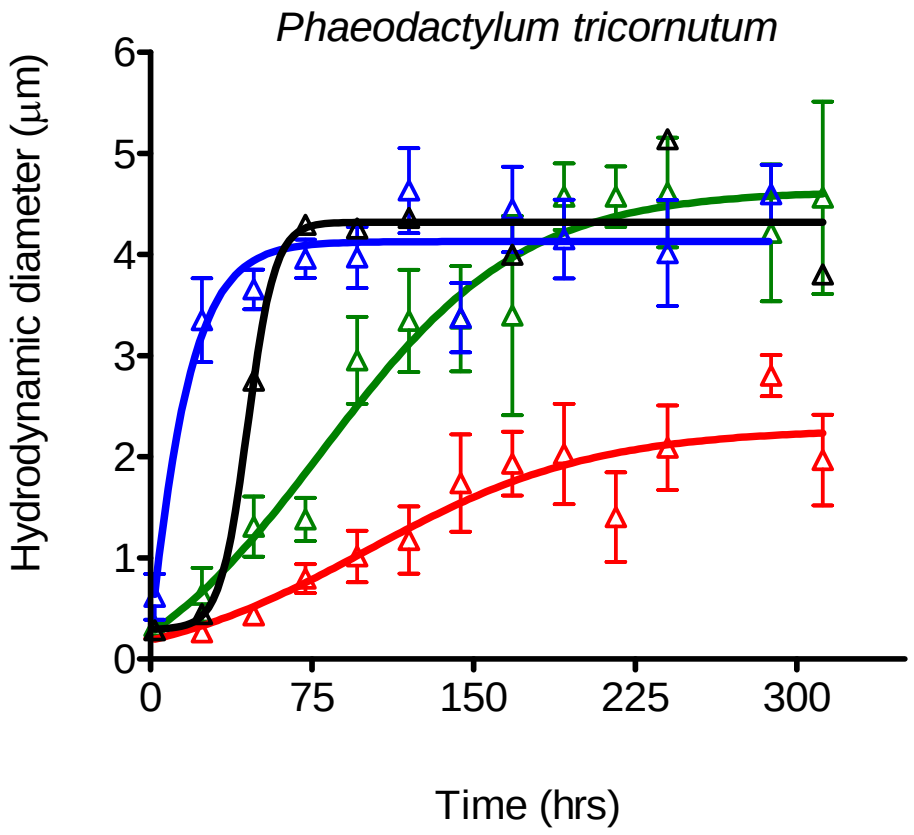

Fig.1c Assembly kinetics of EPS of *Phaeodactylum tricornutum* monitored with DLS. EPS assembly in Ca^{2+}-free ASW (black) was monitored to investigate assembly kinetics with decreased divalent ion availability. Different concentrations of ENs (polystyrene nanoparticles): 0 (red), 10 (green) and 100 ppb (blue), were added to investigate the effect of ENs on EPS microgel formation.

a

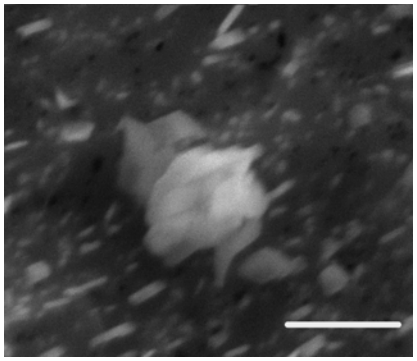

b

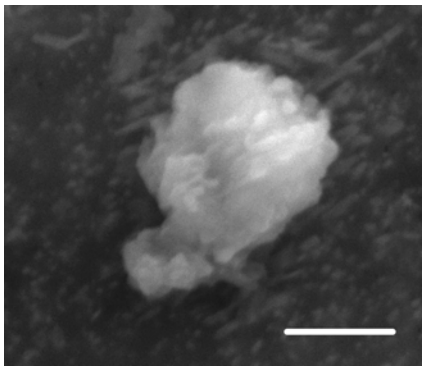

c

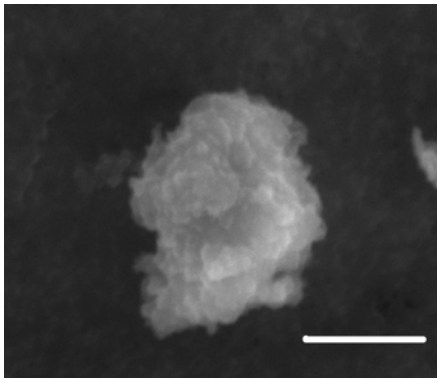

Fig. 2 ESEM images. (a) *Amphora sp.* (Scale Bar = 4 μm) (b) *Ankistrodesmus angustus* (Scale Bar = 5 μm) (c) *Phaeodactylum tricornutum* (Scale Bar = 5 μm)

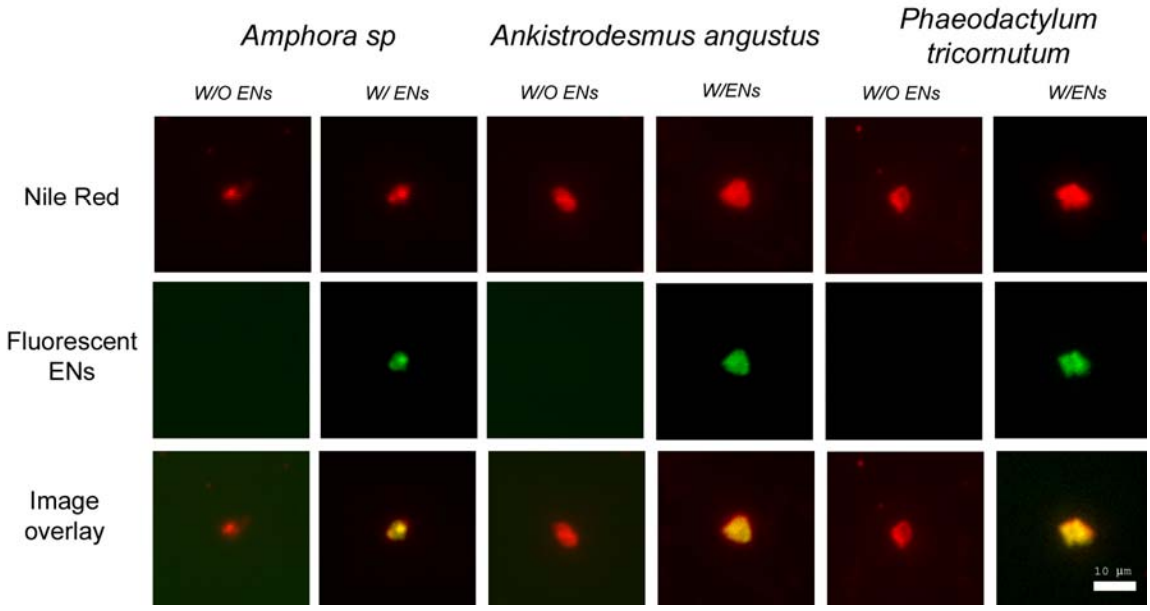

Fig. 3 Fluorescence images of EPS and ENs-induced EPS microgels. Nile Red was used to determine the microgel morphology. Green fluorescent signals indicated the fluorescent ENs. From the overlay images, results showed that the ENs incorporated within EPS matrixes. Scale bar is 10 µm.

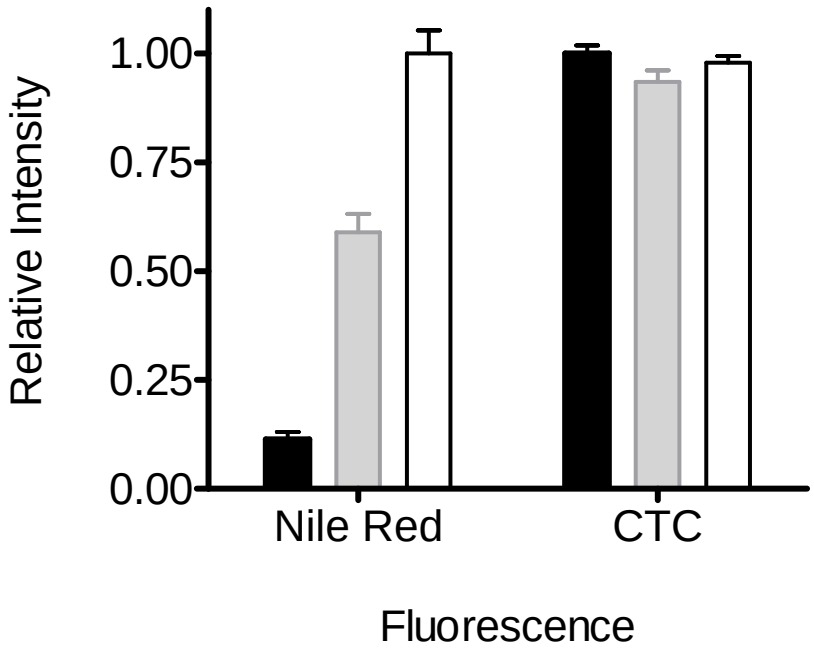

Fig. 4 Fluorescence measurements of Nile red and CTC for EPS of *Amphora sp.* (black), *Phaeodactylum tricornutum* (grey) , and *Ankistrodesmus angustus* (white).

Table-1 Chemical analysis of EPS

Marine Phytoplankton	Molecular weight distribution (kDa)	Protein/carbohydrate Ratio	Uronic acid/carbohydrate Ratio	C %	H %	N %
*Amphora sp.**	1000.0	~0	0.5	37.7	6.27	1.37
Ankistrodesmus angustus	1026.7, 123, 13.2, 2.6	0.72	0.48	41.8	7.34	5.83
Phaeodactylum tricornutum	1005.9, 126.4, 36.1, 22.7, 12.8	0.31	0.5	37.6	5.71	4.5

* Zhange et al., (2008) [40]

Table-2 EPS Assembly analysis

Phytoplankton	*Amphora sp.**			*Ankistrodesmus angustus*			*Phaeodactylum tricornutum*		
ENs concentration (ppb)	*N.A*	10	100	*N.A*	10	100	*N.A*	10	100
$T_{1/2}$ (hrs)	--	46	28	*178*	116	16	119	96	16
Hill coefficient	--	0.84	2.28	--	1.97	1.33	--	2.38	1.46

Adrian, R., 1987. Viability of Phytoplankton in Fecal Pellets of 2 Cyclopoid Copepods. Archiv Fur Hydrobiologie 110, 321-330.
Artham, T., Sudhakar, M., Venkatesan, R., Nair, C.M., Murty, K., Doble, M., 2009. Biofouling and stability of synthetic polymers in sea water. International Biodeterioration & Biodegradation 63, 884-890.
Azam, F., 1998. Microbial control of oceanic carbon flux: The plot thickens. Science 280, 694-696.
Azam, F., Long, R.A., 2001. Oceanography - Sea snow microcosms. Nature 414, 495-+.
Azam, F., Malfatti, F., 2007. Microbial structuring of marine ecosystems. Nature Reviews Microbiology 5, 782-791.
Baines, S.B., Pace, M.L., 1991. The Production of Dissolved Organic-Matter by Phytoplankton and Its Importance to Bacteria - Patterns across Marine and Fresh-Water Systems. Limnology and Oceanography 36, 1078-1090.
Bhaskar, P.V., Bhosle, N.B., 2005. Microbial extracellular polymeric substances in marine biogeochemical processes. Current Science 88, 45-53.
Bhattacharya, P., Lin, S.J., Turner, J.P., Ke, P.C., 2010. Physical Adsorption of Charged Plastic Nanoparticles Affects Algal Photosynthesis. Journal of Physical Chemistry C 114, 16556-16561.
Blumenkr.N, Asboehan.G, 1973. New Method for Quantitative-Determination of Uronic Acids. Analytical Biochemistry 54, 484-489.
Chen, E.Y.T., Wang, Y.C., Chen, C.S., Chin, W.C., Functionalized Positive Nanoparticles Reduce Mucin Swelling and Dispersion. Plos One 5.
Chin, W.C., Orellana, M.V., Verdugo, P., 1998. Spontaneous assembly of marine dissolved organic matter into polymer gels. Nature 391, 568-572.
Chisholm, S.W., 2000. Oceanography - Stirring times in the Southern Ocean. Nature 407, 685-687.
Conner, A.J., 1981. The Differential Sensitivity of Phytoplankton to Polychlorinated-Biphenyls When Cultured Heterotrophically and Photoautotrophically. Environmental and Experimental Botany 21, 241-247.
Cooksey, K.E., Wigglesworthcooksey, B., 1995. Adhesion of Bacteria and Diatoms to Surfaces in the Sea - a Review. Aquatic Microbial Ecology 9, 87-96.
Daniel, G.F., Chamberlain, A.H.L., Jones, E.B.G., 1980. Ultrastructural Observations on the Marine Fouling Diatom Amphora. Helgolander Meeresuntersuchungen 34, 123-149.
De Martino, A., Meichenin, A., Shi, J., Pan, K.H., Bowler, C., 2007. Genetic and phenotypic characterization of Phaeodactylum tricornutum (Bacillariophyceae) accessions. Journal of Phycology 43, 992-1009.
Degennes, P.G., 1979. Scaling concepts in polymer physics. Cornell University Press.
Degennes, P.G., Leger, L., 1982. Dynamics of Entangled Polymer-Chains. Annual Review of Physical Chemistry 33, 49-61.
Derraik, J.G.B., 2002. The pollution of the marine environment by plastic debris: a review. Marine Pollution Bulletin 44, 842-852.
Dickinson, E., 2003. Hydrocolloids at interfaces and the influence on the properties of dispersed systems. Food Hydrocolloids 17, 25-39.

Ding, Y.-X., Chin, W.-C., Rodriguez, A., Hung, C.-C., Santschi, P.H., Verdugo, P., 2008a. Amphiphilic exopolymers from Sagittula stellata induce DOM self-assembly and formation of marine microgels. Marine Chemistry 112, 11-19.
Ding, Y.X., Chin, W.C., Rodriguez, A., Hung, C.C., Santschi, P.H., Verdugo, P., 2008b. Amphiphilic exopolymers from Sagittula stellata induce DOM self-assembly and formation of marine microgels. Marine Chemistry 112, 11-19.
Ding, Y.X., Chin, W.C., Verdugo, P., 2007. Development of a fluorescence quenching assay to measure the fraction of organic carbon present in self-assembled gels in seawater. Marine Chemistry 106, 456-462.
Ding, Y.X., Hung, C.C., Santschi, P.H., Verdugo, P., Chin, W.C., 2009. Spontaneous Assembly of Exopolymers from Phytoplankton. Terrestrial Atmospheric and Oceanic Sciences 20, 741-747.
Falkowski, P., Scholes, R.J., Boyle, E., Canadell, J., Canfield, D., Elser, J., Gruber, N., Hibbard, K., Hogberg, P., Linder, S., Mackenzie, F.T., Moore, B., Pedersen, T., Rosenthal, Y., Seitzinger, S., Smetacek, V., Steffen, W., 2000. The global carbon cycle: A test of our knowledge of earth as a system. Science 290, 291-296.
Ferry, J.L., Craig, P., Hexel, C., Sisco, P., Frey, R., Pennington, P.L., Fulton, M.H., Scott, I.G., Decho, A.W., Kashiwada, S., Murphy, C.J., Shaw, T.J., 2009. Transfer of gold nanoparticles from the water column to the estuarine food web. Nature nanotechnology 4, 441-444.
Flemming, H.C., Neu, T.R., Wozniak, D.J., 2007. The EPS matrix: The "House of Biofilm cells". Journal of Bacteriology 189, 7945-7947.
Flemming, H.C., Wingender, J., The biofilm matrix. Nature Reviews Microbiology 8, 623-633.
Fogg, G.E., 1983. The Ecological Significance of Extracellular Products of Phytoplankton Photosynthesis. Botanica Marina 26, 3-14.
Gopferich, A., 1996. Mechanisms of polymer degradation and erosion. Biomaterials 17, 103-114.
Hedges, J.I., 1992. Global Biogeochemical Cycles - Progress and Problems. Marine Chemistry 39, 67-93.
Kerner, M., Hohenberg, H., Ertl, S., Reckermann, M., Spitzy, A., 2003. Self-organization of dissolved organic matter to micelle-like microparticles in river water. Nature 422, 150-154.
Kiorboe, T., Jackson, G.A., 2001. Marine snow, organic solute plumes, and optimal chemosensory behavior of bacteria. Limnology and Oceanography 46, 1309-1318.
Leppard, G.G., 2008. Nanoparticles in the environment as revealed by transmission electron microscopy: Detection, characterisation and activities. Current Nanoscience 4, 278-301.
Maynard, A.D., Aitken, R.J., Butz, T., Colvin, V., Donaldson, K., Oberdorster, G., Philbert, M.A., Ryan, J., Seaton, A., Stone, V., Tinkle, S.S., Tran, L., Walker, N.J., Warheit, D.B., 2006. Safe handling of nanotechnology. Nature 444, 267-269.
Miao, A.J., Luo, Z., Chen, C.S., Chin, W.C., Santschi, P.H., Quigg, A., 2010a. Intracellular uptake: a possible mechanism for silver engineered nanoparticle toxicity to a freshwater alga Ochromonas danica. PLoS One 5, e15196.

Miao, A.J., Schwehr, K.A., Xu, C., Zhang, S.J., Luo, Z., Quigg, A., Santschi, P.H., 2009. The algal toxicity of silver engineered nanoparticles and detoxification by exopolymeric substances. Environ Pollut 157, 3034-3041.
Miao, A.J., Zhang, X.Y., Luo, Z.P., Chen, C.S., Chin, W.C., Santschi, P.H., Quigg, A., 2010b. Zinc Oxide Engineered Nanoparticles Dissolution and Toxicity to Marine Phytoplankton. Environmental Toxicology and Chemistry 29, 2814-2822.
Moret-Ferguson, S., Law, K.L., Proskurowski, G., Murphy, E.K., Peacock, E.E., Reddy, C.M., The size, mass, and composition of plastic debris in the western North Atlantic Ocean. Marine Pollution Bulletin 60, 1873-1878.
Navarro, E., Baun, A., Behra, R., Hartmann, N.I.B., Filser, J., Miao, A.-J., Quigg, A., Santschi, P.H., Sigg, L., 2008. Ecotoxicity of nanoparticles on algae, plants and fungi: state of the art and future needs. Special issue on Ecotoxicology: Chemistry and Risk Assessment of Nanoparticles 17, 372-386.
Nel, A., Xia, T., Madler, L., Li, N., 2006. Toxic potential of materials at the nanolevel. Science 311, 622-627.
Passow, U., 2002. Transparent exopolymer particles (TEP) in aquatic environments. Progress in Oceanography 55, 287-333.
Passow, U., Alldredge, A.L., 1994. Distribution, Size and Bacterial-Colonization of Transparent Exopolymer Particles (Tep) in the Ocean. Marine Ecology-Progress Series 113, 185-198.
Provencher, S.W., Stepanek, P., 1996. Global analysis of dynamic light scattering autocorrelation functions. Particle & Particle Systems Characterization 13, 291-294.
Quiroz, N.G.A., Hung, C.C., Santschi, P.H., 2006. Binding of thorium(IV) to carboxylate, phosphate and sulfate functional groups from marine exopolymeric substances (EPS). Marine Chemistry 100, 337-353.
Scala, S., Carels, N., Falciatore, A., Chiusano, M.L., Bowler, C., 2002. Genome properties of the diatom Phaeodactylum tricornutum. Plant Physiology 129, 993-1002.
Stenstrom, T.A., 1989. Bacterial Hydrophobicity, an Overall Parameter for the Measurement of Adhesion Potential to Soil Particles. Applied and Environmental Microbiology 55, 142-147.
Thompson, R.C., Olsen, Y., Mitchell, R.P., Davis, A., Rowland, S.J., John, A.W.G., McGonigle, D., Russell, A.E., 2004. Lost at sea: Where is all the plastic? Science 304, 838-838.
Verdugo, P., Alldredge, A.L., Azam, F., Kirchman, D.L., Passow, U., Santschi, P.H., 2004. The oceanic gel phase: a bridge in the DOM-POM continuum. Marine Chemistry 92, 67-85.
Verdugo, P., Orellana, M.V., Chin, W.C., Petersen, T.W., van den Eng, G., Benner, R., Hedges, J.I., 2008. Marine biopolymer self-assembly: implications for carbon cycling in the ocean. Faraday Discuss. 139, 393-398.
Ward, J.E., Shumway, S.E., 2004. Separating the grain from the chaff: particle selection in suspension- and deposit-feeding bivalves. Journal of Experimental Marine Biology and Ecology 300, 83-130.
Watters, D.L., Yoklavich, M.M., Love, M.S., Schroeder, D.M., Assessing marine debris in deep seafloor habitats off California. Marine Pollution Bulletin 60, 131-138.
Wells, M.L., 1998. Marine colloids - A neglected dimension. Nature 391, 530-531.

Werlin, R., Priester, J.H., Mielke, R.E., Kramer, S., Jackson, S., Stoimenov, P.K., Stucky, G.D., Cherr, G.N., Orias, E., Holden, P.A., Biomagnification of cadmium selenide quantum dots in a simple experimental microbial food chain. Nature nanotechnology 6, 65-71.
WerlinR, Priester, J.H., Mielke, R.E., KramerS, JacksonS, Stoimenov, P.K., Stucky, G.D., Cherr, G.N., OriasE, Holden, P.A., 2011. Biomagnification of cadmium selenide quantum dots in a simple experimental microbial food chain. Nat Nano 6, 65-71.
Wigglesworth-Cooksey, B., Cooksey, K.E., 2005. Use of fluorophore-conjugated lectins to study cell-cell interactions in model marine biofilms. Applied and Environmental Microbiology 71, 428-435.
Wotton, R.S., 2004. The ubiquity and many roles of exopolymers (EPS) in aquatic systems. Scientia Marina 68, 13-21.
Wotton, R.S., Preston, T.M., 2005. Surface films: Areas of water bodies that are often overlooked. Bioscience 55, 137-145.
Yablon, D.G., Schilowitz, A.M., 2004. Solvatochromism of Nile Red in nonpolar solvents. Applied Spectroscopy 58, 843-847.
Yongmanitchai, W., Ward, O.P., 1991. Growth of and Omega-3-Fatty-Acid Production by Phaeodactylum-Tricornutum under Different Culture Conditions. Applied and Environmental Microbiology 57, 419-425.
Zarfl, C., Matthies, M., Are marine plastic particles transport vectors for organic pollutants to the Arctic? Marine Pollution Bulletin 60, 1810-1814.
Zhang, S.J., Santschi, P.H., 2009. Application of cross-flow ultrafiltration for isolating exopolymeric substances from a marine diatom (Amphora sp.). Limnology and Oceanography-Methods 7, 419-429.
Zhang, S.J., Xu, C., Santschi, P.H., 2008. Chemical composition and Th-234 (IV) binding of extracellular polymeric substances (EPS) produced by the marine diatom Amphora sp. Marine Chemistry 112, 81-92.

Chapter5 The synergistic effect of ocean acidification and global warming on marine dissolved matter assembly

Abstract

The oceans have historically been effective in buffering atmospheric carbon dioxide (CO_2) fluctuations (Caldeira and Wickett, 2003; Solomon and (eds.), 2007). However, recent increasing CO_2 levels exacerbated by fossil fuel consumption have resulted in measurable changes in seawater temperature and pH (Solomon and (eds.), 2007), with little known effects on the global carbon cycle—of which the ocean plays a critical role. Indeed, understanding the direct influence of climate changes, such as sea surface warming and acidification, on carbon cycles remains a great challenge (Caldeira and Wickett, 2003). Marine dissolved organic matter (DOM) is one of the largest carbon pools on Earth (Benner et al., 1992), yet DOM research has been mainly focused on its complex chemical composition, neglecting macromolecular polymeric characteristics. Here we report that a moderate temperature increase (from 30°C to 32°C) can change the ratio of surface hydrophobic/hydrophilic domains on DOM polymers to decelerate—and even block—DOM assembly into microgels (particulate organic matter, POM). Furthermore, such temperature increases can disperse microgels, which carry significant implications for the marine carbon cycle. We found that the critical dispersion temperature decreases concurrently with pH: from 32^{o}C at pH 8.2, to 28˚C at pH 7.5. Left alone, this synergetic effect to reduce microgel assembly can decrease downward carbon and nutrient flux to the deep ocean, disturbing marine trophic and trace element cycles. This finding—the first to link direct environmental changes to a resulting aberrant DOM behavior—highlights the need to consider aspects of climate changes as parts of an integrated system and serves to inform the broader framework of carbon emission discussion.

5.1 Ocean acidification and global warming on the ocean carbon cycle

Rising atmospheric CO_2 has prompted both public concern and scientific debates regarding climate changes and global carbon cycle (Caldeira and Wickett, 2003; Fung et al., 2005). Since pre-industrial times the ocean has served as an effective carbon sink, buffering almost as much carbon as the atmosphere itself (Solomon and (eds.), 2007) (Jiao et al., 2010). As a major oceanic active carbon pool, DOM has been shown to play essential roles in the global carbon cycle (Chin et al., 1998; del Giorgio and Duarte, 2002). Existing as part of an organic matter continuum, the ability of DOM polymers to spontaneously assemble between less bioactive DOM and more bioactive POM influences the biogeochemical cycle, sedimentation processes and microbial communities in the ocean (Azam and Long, 2001; Chin et al., 1998; Suess, 1980) and represents a critical link in the trophic cycle (Azam and Long, 2001; Azam and Malfatti, 2007; Kiorboe, 2001; Kiorboe and Jackson, 2001). DOM has been shown to be refractory with complex chemical composition and macromolecular structures (Benner et al., 1992; Verdugo et al., 2004). Considering structural (conformational) changes play a determining role in the function and behavior of many macromolecules and polymers, investigating potential environmentally-induced DOM conformational changes is critical, though yet to be considered. Moderate environmental variations insufficient to induce a chemical reaction may nonetheless alter polymer behaviors owing to a conformational changes (Ćosović and Kozarac, 1993; Vergugo, 2012). Minute perturbations in the DOM pool—integrated over the entire ocean—would have a significant effect on the ocean carbon flux and marine ecosystem (David M, 2002).

5.2 Material and methods

Water sampling and filtration

Seawater samples collected at Puget Sound (WA, USA) near Friday Harbor Marine Laboratories in August 2009 were filtered through a GF/F fiberglass membrane and a 0.22-µm membrane (prewashed with 0.1 N HCl), treated with 0.02% sodium azide—a microbial biocide—and stored in clean, sealed bottles in dark at 4°C until further processing.

Particle Sizing

Microgel assembly was monitored with dynamic laser scattering (DLS) as described previously (Chin et al., 1998). Seawater aliquots (10 ml) were syringe filtered through a 0.22-µm membrane (low-protein binding Durapore®, Millipore) directly into scattering vials. Scattering cells were placed in the goniometer of a Brookhaven laser spectrometer (Brookhaven Instruments, NY) and the scattering fluctuation signals were detected at 45° scattering angle. The autocorrelation function of scattering intensity fluctuations was averaged over a 12-minute sampling time. Hydrodynamic diameters of polymer gels were analyzed by the CONTIN method (Chin et al., 1998). In temperature-dependent experiments (Fig-1), samples in sealed scattering vials were incubated at 22˚C, 32˚C and 35˚C for 24 hrs and stored/monitored for 15 d at 22˚C. For microgel dispersion-temperature experiments (Fig-3), 10 ml of seawater was syringe filtered into vials and incubated in dark for 10 d at 22˚C. After confirming microgel equilibrium sizes by DLS, seawater sample pHs were adjusted with 0.1N HCL and incubated at desired experimental temperatures for 24 hrs. Microgel sizes were measured with DLS immediately after pH/temperatures adjustments. For the pH/temperature impact on microgels experiment, DOM assembly was monitored under pHs ranging from 7.3 to 8.0 and temperatures ranging from 22˚C to 32˚C (Fig-4). 0.1N HCl was used to acidify sea water samples to desired pH, and scattering vials were incubated/measured at each experimental temperature over 15 d.

Nile red and CTC fluorescence

For DOM polymer property assays, seawater samples were sealed in vials and incubated at experimental temperatures for 24 hrs. Nile red (13 μm, Sigma-Aldrich, USA) served as a hydrophobic indicator and fluorescence measurements were performed with a Shimadzu RF-5000U spectrofluorophotometer ($\lambda_{excitation}$ = 550 nm; $\lambda_{emission}$=633 nm). Chlortetracycline (100 μM, Sigma-Aldrich, USA) was used to reveal bound Ca^{2+} on DOM polymers(Chin et al., 1998), also performed with a Shimadzu RF-5000U (λ = 390 nm excitation; λ = 530 nm emission). Nile red and CTC serve as complementary indicators of cross-linking: whereas Nile red quantifies hydrophobicity changes, CTC provides a reliable quantification of bound Ca^{2+}.

5.3 Results and Discussion

Sea surface temperature is projected to increase 3 ˚C, relative to the 1961-1990 mean (Johnson and Xie), in some ocean regions by 2100. To investigate temperature effects on DOM assembly we monitored microgel size as a function of time using dynamic laser scattering spectroscopy (DLS) as described previously (Chin et al., 1998). DOM polymers in 0.22 μm-filtered seawater were incubated (at 22, 30, 32 and 35 ˚C) for 24 hrs; assembly was monitored at 22˚C. Our control group (22˚C) results showed DOM polymers spontaneously assembled into microgels with sizes ranging from 200 nm to 1 μm within 30 minutes. Microgels continued to grow following a characteristic sigmoid time course of second order kinetics to reach equilibrium sizes (about 5 μm) within 100 hrs, which is consistent with our previous finding (Chin et al., 1998). Our results show that DOM assembly was completely blocked above 32 ˚C (Fig-1). This critical (non-linear) temperature dependency supports the polymer characters of microgel kinetics (Chin et al., 1998). The temperature-dependent assembly also implies that the danger of sea surface warming carries the capacity to decrease downward carbon flux by altering DOM assembly.

In addition to rising seawater temperatures, numerous studies point to acidification as a major outcome of excessive carbon emissions, projecting in some regions 7.5 pH units by 2300 (Caldeira and Wickett, 2003; Sunda, 2010). To address a potential compounding effect of temperature and pH yet to be considered on DOM assembly, we monitored assembly kinetics and the equilibrium size of microgels at 3 different pH units coupled with 3 different temperatures. Equilibrium microgel size decreased with increased temperature, although microgel diameter at pH 8.0 remained ~4 μm, even at 32˚C (Fig. 4). Lowering pH from 8.0 to 7.5 at 22˚C, DOM assembly rates decreased (from 120 hrs to 200 hrs) as well as equilibrium sizes (from ~6 μm to ~4 μm). When temperature increased to above 30˚C, microgel sizes further decreased (to < 2 μm). Moreover, the disruption of DOM assembly induced by increased temperature was amplified with a concurrent pH decrease: at pH 7.5, the microgel size could grow no greater than ~0.5 μm at 32˚C. Such an unexpected synergistic relationship highlights the potential far-reaching ecological influence of increasing temperature and acidification at the surface ocean (Smith et al., 2009).

A polymer gel model successfully adapted in our previous microgel study (Chin et al., 1998) on DOM assembly dynamics may help explain this synergetic relationship. An increase of polymer reptation concomitants a decrease of entangle frictions. Due to an abundance of anionic charges and functional groups on DOM polymers, as H^+ concentration increases owing to a pH decrease, H^+ ions can pronate some acidic functional groups on DOM polymers, causing fewer available binding sites on DOM for divalent Ca^{+2} cross-linking (Chin et al., 1998; Verdugo et al., 2004). Decreased binding sites on the polymer chains can result in longer correlation lengths and decreased entangle friction (De Gennes, 1979) with fewer Ca^{2+} crosslinking. This situation would lead to smaller equilibrium microgel sizes as shown our results (Fig-3). The critical dispersion temperature, consistent with our model prediction, decreased to 30˚C at pH 7.7 and again to 28˚C at pH 7.5 (fig. 3).

Our results reveal an aberrant "denatured" characteristic of DOM. Similar to most macromolecules, e.g., proteins, the denatured state generally corresponds to a macromolecular behavior change. In this study DOM polymers lost or diminished their ability to spontaneously assemble into microgels owing to warming and acidification, a feature consistent with denaturation. Our results raise the possibility that the history of DOM plays a determining role in their fate. If applicable to the natural environment, current DOM behaviors and functions may potentially be considered an integration of past oceanic environmental changes, e.g., of higher temperature or ocean chemistry fluctuations. Environmental influences—temperature, pH or pressure—that DOM experience through ocean currents and mixing during their course, might also determine DOM polymer behavior (Ćosović and Kozarac, 1993).

Based on this polymer model, microgel assembly is related to Ca^{2+} cross-linking within a DOM-POM polymer matrix. It has been shown that bicarbonate in microenvironment can decrease the viscosity of polymer matrices by reducing Ca^{2+} cross-linking. As a result, the change of marine carbonic acid under different pH and temperature conditions warrants this consideration . The balance of carbonate ions and bicarbonate ions can be described with following equations:.

$$CO_2\ (g) = CO_2\ (aq) \qquad (1)$$

$$CO_2\ (aq) = H^+ + HCO_3^- \qquad (2)$$

$$K_1 = [H^+]\ [HCO_3^-]\ /[\ CO_2] \qquad (3)$$

$$HCO_3^- = H^+ + CO_3^{2-} \qquad (4)$$

$$K_2 = [H^+][\ CO_3^{2-}]/[\ HCO_3^-] \qquad (5)$$

Considering the influence of salinity and temperature, the equilibrium constant for the reactions can be expressed as (Lueker et al., 2000):

1. $\mathrm{Log}_{10}\ (K_1\ /k) = -3633.86/\ (T/K) + 61.2172 - 9.67770\ \ln\ (T/K) + 0.011555S - 0.0001152S^2$

2. $\text{Log}_{10}(K_2/k) = -471.78/(T/K) - 25.9290 + 3.16967 \ln(T/K) + 0.0178\,S - 0.0001122\,S^2$

, where k = 1 mole / kg-sol, *S* is salinity, and t is temperature (K).

From field study data, seawater salinity varies from 10 to ~37.5, depending on location. In our model, we used a conservative salinity value of 30, and estimated change of the carbonic acids at various temperatures and pH conditions. At 22 ˚C, the $\text{Log}_{10}(K_1/k)$ and $\text{Log}_{10}(K_2/k)$ are -5.89484 and -9.0691, respectively. Once the temperature is raised to 27 ˚C, the $\text{Log}_{10}(K_1/k)$ and $\text{Log}_{10}(K_2/k)$ are -5.85219 and -8.98917 respectively. The $\text{Log}_{10}(K_1/k)$ and $\text{Log}_{10}(K_2/k)$ are -5.81359 and -8.911, respectively, at 32 ˚C. For temperatures between 22˚C to 32˚C under constant pH value, the concentration of HCO_3^- led by the equilibrium constant change raises ~ 20%, and the CO_3^{2-} increases 74%. However, if we consider the pCO2 increase and the pH drop from 8.1 to 7.5, the HCO_3^- will decrease ~14% and CO_3^{2-} will decrease ~74%. Because only 3-10% of HCO_3^- dissociate into CO_3^{2-} within pH and temperature ranges studied, the influence of CO_3^{2-} can be neglected in our model. Considering the variation of DLS measurements, the moderate HCO_3^- changes may not have shown an obvious influence on the DLS results.

These results that demonstrate DOM susceptibility to moderate environmental changes provide alternative realizations to recalcitrant DOM (RDOM) formation. Current biogeochemistry models propose RDOM can be produced from several sources, such as ectoenzyme conversion and exudation during bacterial production (Jiao et al., 2010). Hydrophobicity and micelle-like macromolecular structures have been proposed to contribute to degradation resistance of DOM (Dittmar and Kattner, 2003). The hydrophobicity increase induced by environmental changes observed here permits an understanding of an abiotic mechanism for RDOM formation in terms of past events: the turbulent fluctuations of ocean acidification and temperature may to help explain the surprising abundance of DOM resistant to microbial decomposition (Jiao et al., 2010) .

The sensitivity of microgels to temperature and pH may lead to a reduced downward organic carbon flux. The decreased burial of organic carbon on the seafloor could

ultimately diminish the capacity of the oceanic carbon sink. Ocean stratification caused by increased temperature reduces the downward water current, resulting in further dampened downward carbon flux (Fung et al., 2005). Taken together, increased surface ocean temperature can significantly reduce the carbon sequestering capacity of the ocean, forming a positive feedback loop to aggravate global warming. Furthermore, a decrease in POM (microgels) downward flux will reduce nutrition transport from the ocean surface to the deep-sea community (Azam, 1998; Azam and Malfatti, 2007; Suess, 1980). This lack of organic carbon supply to the deep sea microbial communities may cause undesired environmental selection pressures (Smith et al., 2009)(ref). In the upper ocean, smaller microgels can limit the nutrition availability of colonized bacterial communities (Kiorboe et al., 2002). The altered plume profile of these reduced-size microgels has potential to restructure the biodiversity of free-living bacteria in the water column (Kiorboe et al., 2002; (Kiorboe and Jackson, 2001; Stocker et al., 2008) . These situations that impact the microbial loop are worrisome given the sensitivity of atmospheric CO_2 concentrations to ocean remineralization processes driven primarily by surface microbial communities (Cermeno et al., 2008).

Low dissolved iron concentration has been found to limit phytoplankton growth and thereby carbon fixation that primarily drives the CO_2 sequestration capacity of the surface ocean (Sunda, 2010). The labile metal fraction is a function of metal/organic ligand concentrations and binding-constants between metal ions and DOM (David M, 2002). Once pH and temperature block DOM assembly and disperse microgels, accumulating DOM—now functioning as metal chelators—in the upper ocean may effectively compete with phytoplankton communities for dissolved iron or other limiting nutrients to reduce the carbon sequestration capacity of the surface ocean.

Whether the ocean is as a carbon sink or potential source has yet to be determined (Caldeira and Wickett, 2003); its fate rests on the relative contributions of organic matter production to biological respiration(Azam and Long, 2001; Caldeira and Wickett, 2003; del Giorgio and Duarte, 2002). Predicting how climate changes will affect these processes is one of Earth sciences' great challenges. Our results demonstrate that pH and

temperature work synergetically—inclusive of the "dark side" of the marine carbon cycle—to disperse microgels and reduce DOM assembly. This relationship highlights uncertainties on the marine carbon cycle: additional DOM chelation may reduce primary production, but marine gel dispersion may decrease biological respiration. Compounding climate changes on the marine carbon cycle may not only limit the ocean's carbon sequestration capacity, but carry the potential risk of reversion from presumed carbon sink[1] to impending source (Caldeira and Wickett, 2003). Yet undiscovered potential synergisms from presumably independent factors may too hold significant influence on carbon cycle dynamics and stress the urgency to study marine processes as parts of integrated systems.

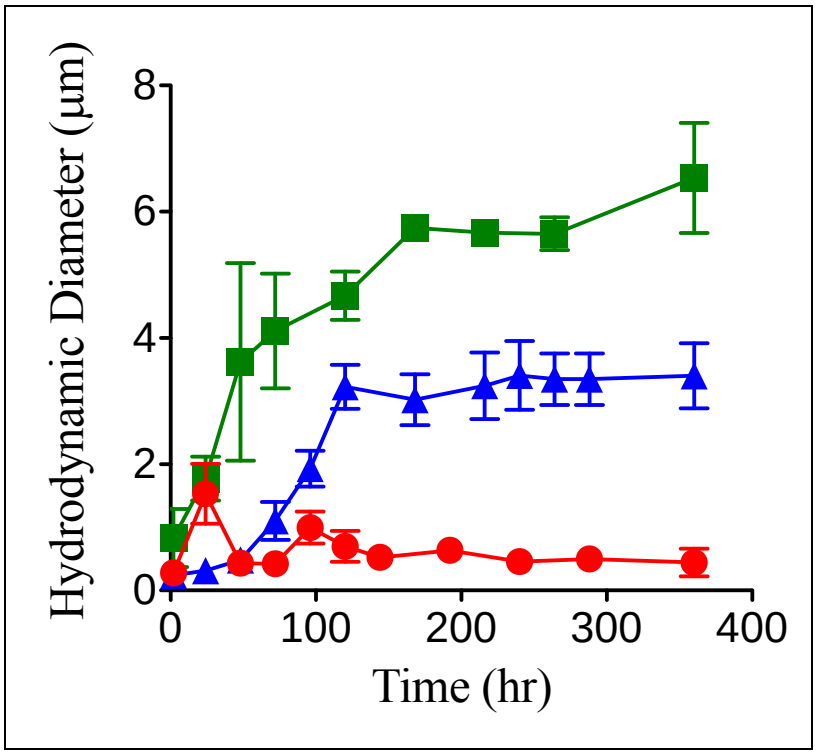

Fig-1

Microgel assembly rate and equilibrium size decreased with increased temperature. Samples were heat-treated at 22^{oC} (green), 32^{oC} (blue) and 35^{oC} (red) for 24 hour, and then stored in dark at 22^{oC}. Assembly was measured using dynamic laser scattering at 22^{oC}. Each data point represents (mean ± SD) in six replicate. Data highlights that short-term temperature exposure above 35^{oC} confers significant DOM assembly loss with no obvious recovery.

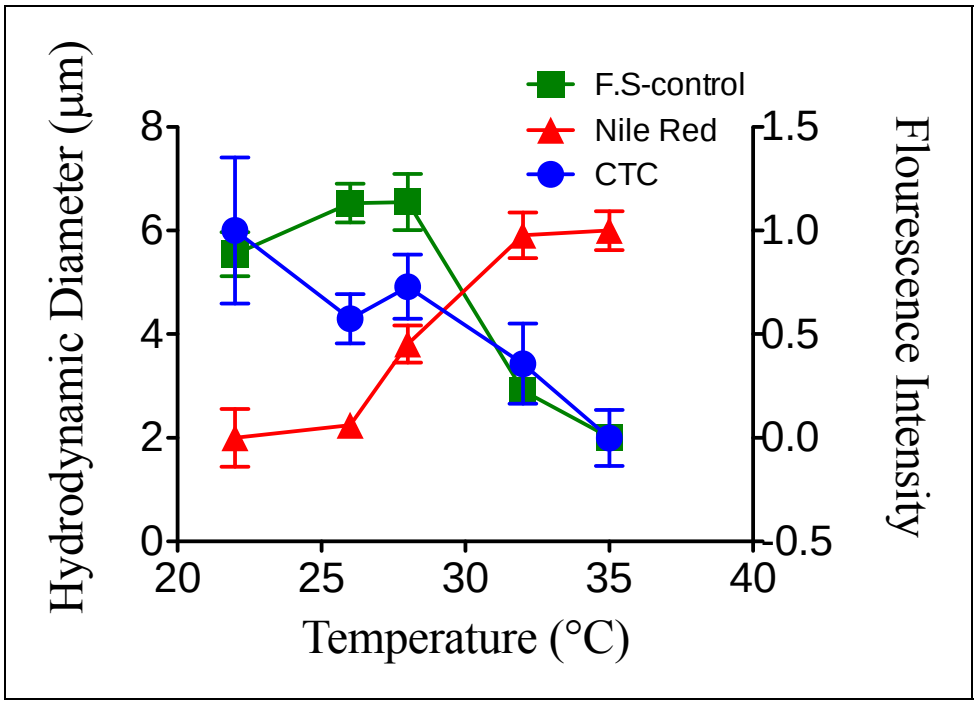

Fig-2

Decreased microgel equilibrium size (green) and bound Ca^{2+} (blue) with concomitant increase in hydrophobicity (red). The non-linear rate of declining microgel size with increased temperature indicates potential cooperativity; 32^{oC} reveal all three parameters experienced the most pronounced associative effect— major drop in microgel size and bound Ca^{2+}, and rise in hydrophobicity.

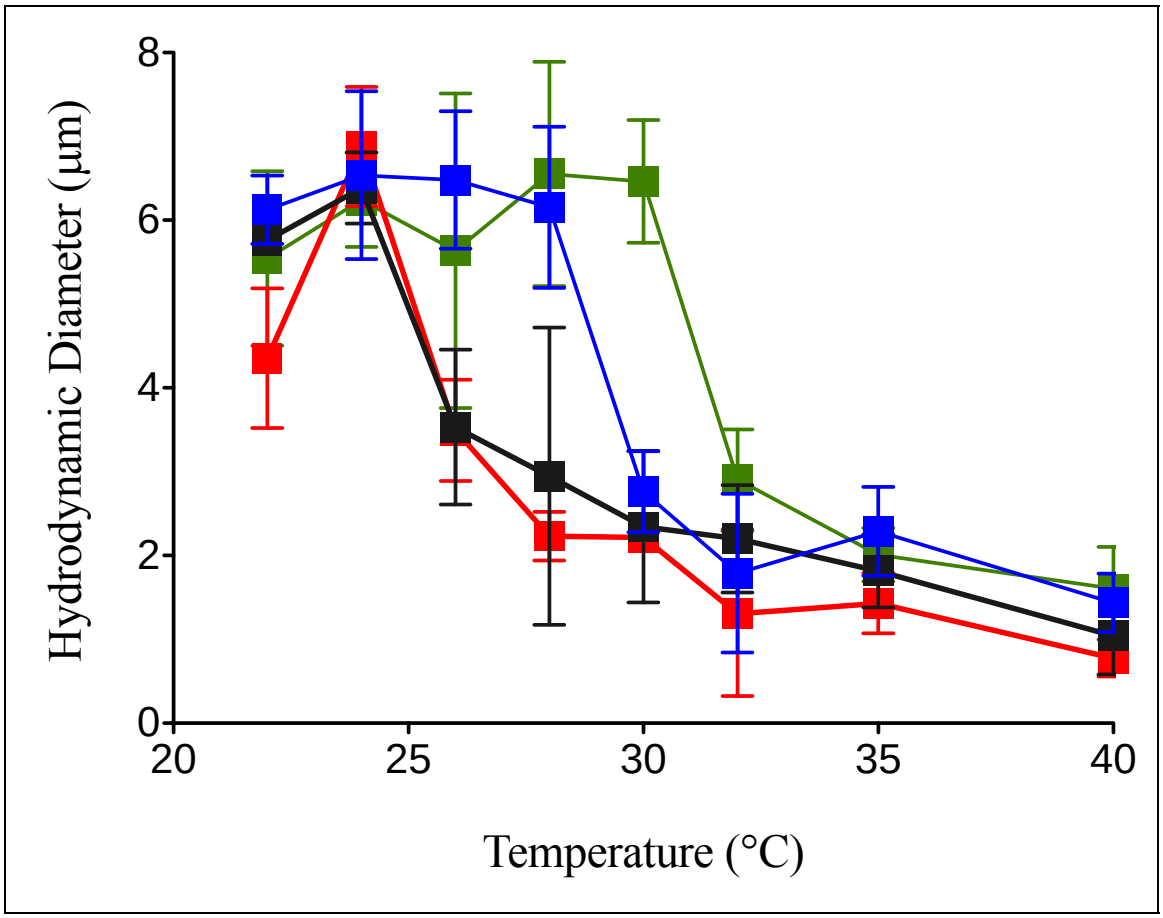

Fig-3

Microgel dispersion-temperature decreases with pH decrease. As pH is reduced from 8.0 (green) to 7.7 (blue) to 7.5 (black) to 7.3 (red), non-linear microgel dispersion-temperature shift were observed while pH decreases. Dispersion temperature dropped ~2^{oC} with pH decrease 0.2 occurred between pH 8.0 to pH 7.5. Each data point (mean ± SD) was performed in six replicate.

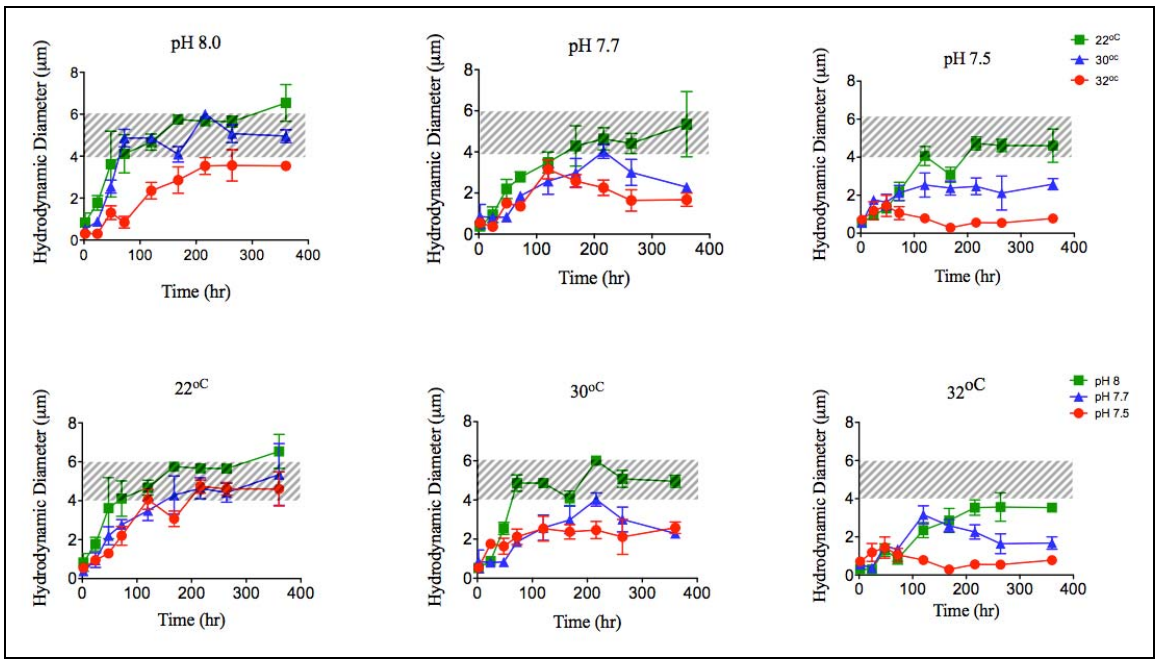

Fig-4

DOM assembly monitored with temperature and pH reveals as either pH decreases or temperature increases, microgel equilibrium size and assembly rates decrease at a non-linear rate. a. DOM assembly at three temperatures—22^{oC} (green), 30^{oC} (blue), 32^{oC} (red)—over time at three pH units. Each data point (mean ± SD) was performed in six replicate. b. DOM assembly at three pHs—8.0 (green), 7.7 (blue), 7.5 (red)—over time at three constant temperature incubations. Microgels assembled in identical pH conditions showed equilibrium size reduction and decelerate non-linear assembly rates when exposed to increased temperature. Each data point (mean ± SD) was performed in six replicate. Shaded window represents microgel equilibrium size range (ref).

Azam, F., 1998. Microbial control of oceanic carbon flux: The plot thickens. Science 280, 694-696.
Azam, F., Long, R.A., 2001. Sea snow microcosms. Nature 414, 495, 497-498.
Azam, F., Malfatti, F., 2007. Microbial structuring of marine ecosystems. Nat. Rev. Microbiol. 5, 782-791.
Benner, R., Pakulski, J.D., McCarthy, M., Hedges, J.I., Hatcher, P.G., 1992. Bulk Chemical Characteristics of Dissolved Organic-Matter in the Ocean. Science (New York, N.Y 255, 1561-1564.
Caldeira, K., Wickett, M.E., 2003. Oceanography: anthropogenic carbon and ocean pH. Nature 425, 365.
Cermeno, P., Dutkiewicz, S., Harris, R.P., Follows, M., Schofield, O., Falkowski, P.G., 2008. The role of nutricline depth in regulating the ocean carbon cycle. Proceedings of the National Academy of Sciences of the United States of America 105, 20344-20349.
Chin, W.C., Orellana, M.V., Verdugo, P., 1998. Spontaneous assembly of marine dissolved organic matter into polymer gels. Nature 391, 568-572.
Ćosović, B., Kozarac, Z., 1993. Temperature and pressure effects upon hydrophobic interactions in natural waters. Marine Chemistry 42, 1-10.
David M, K., 2002. Nutrient dynamics in the deep blue sea. Trends in Microbiology 10, 410-418.
De Gennes, P.G., 1979. Scaling concepts in polymer physics. Cornell University Press.
del Giorgio, P.A., Duarte, C.M., 2002. Respiration in the open ocean. Nature 420, 379-384.
Dittmar, T., Kattner, G., 2003. Recalcitrant dissolved organic matter in the ocean: major contribution of small amphiphilics. Marine Chemistry 82, 115-123.
Fung, I.Y., Doney, S.C., Lindsay, K., John, J., 2005. Evolution of carbon sinks in a changing climate. Proc Natl Acad Sci U S A 102, 11201-11206.
Jiao, N., Herndl, G.J., Hansell, D.A., Benner, R., Kattner, G., Wilhelm, S.W., Kirchman, D.L., Weinbauer, M.G., Luo, T., Chen, F., Azam, F., 2010. Microbial production of recalcitrant dissolved organic matter: long-term carbon storage in the global ocean. Nat Rev Micro 8, 593-599.
Johnson, N.C., Xie, S.P., Changes in the sea surface temperature threshold for tropical convection. Nature Geoscience 3, 842-845.
Kiorboe, T., 2001. Formation and fate of marine snow: small-scale processes with large-scale implications. Scientia Marina 65, 57-71.
Kiorboe, T., Grossart, H.P., Ploug, H., Tang, K., 2002. Mechanisms and rates of bacterial colonization of sinking aggregates. Applied and Environmental Microbiology 68, 3996-4006.
Kiorboe, T., Jackson, G.A., 2001. Marine snow, organic solute plumes, and optimal chemosensory behavior of bacteria. Limnology and Oceanography 46, 1309-1318.
Lueker, T.J., Dickson, A.G., Keeling, C.D., 2000. Ocean pCO2 calculated from dissolved inorganic carbon, alkalinity, and equations for K1 and K2: validation based on laboratory measurements of CO2 in gas and seawater at equilibrium. Marine Chemistry 70, 105-119.
Smith, K.L., Ruhl, H.A., Bett, B.J., Billett, D.S.M., Lampitt, R.S., Kaufmann, R.S., 2009. Climate, carbon cycling, and deep-ocean ecosystems. Proceedings of the National Academy of Sciences of the United States of America 106, 19211-19218.

Solomon, S., D. Qin, M. Manning, Z. Chen, M. Marquis, K.B. Averyt, M. Tignor and, (eds.), H.L.M., 2007. Climate Change 2007: The Physical Science Basis. Contribution of Working Group I to the Fourth Assessment Report of the Intergovernmental Panel on Climate Change. Cambridge Univ Press, Cambridge, UK.
Stocker, R., Seymour, J.R., Samadani, A., Hunt, D.E., Polz, M.F., 2008. Rapid chemotactic response enables marine bacteria to exploit ephemeral microscale nutrient patches. Proceedings of the National Academy of Sciences of the United States of America 105, 4209-4214.
Suess, E., 1980. Particulate Organic-Carbon Flux in the Oceans - Surface Productivity and Oxygen Utilization. Nature 288, 260-263.
Sunda, W.G., 2010. Oceans. Iron and the carbon pump. Science 327, 654-655.
Verdugo, P., Alldredge, A.L., Azam, F., Kirchman, D.L., Passow, U., Santschi, P.H., 2004. The oceanic gel phase: a bridge in the DOMâ€“POM continuum. Marine Chemistry 92, 67-85.
Vergugo, P., 2012. Marine microgels. Annual Review of Marine Science 4, 1-25.

Chapter 6 Conclusion and Future Direction

The goal of this study is to apply the principle of polymer physic to examine anthropogenic influence on marine DOM-POM transitions. We found that low concentrations of ENs (parts per billion) in the ocean can significantly accelerate DOM assembly—by as much as by 200%. Moreover, these kinetic accelerations are not dominated by the modified-charge on ENs. We further investigated the hydrophobic interactions in EN-DOM matrices at temperatures above 22^{o}C. Our results indicated hydrophobic interactions play important roles in marine EN-DOM assembly and stabilize microgels incubated at temperatures up to 40˚C. Considering the ocean is the largest carbon sink, it is possible that the EN-induced POM formation may enhance its carbon sequester efficiency. The impact of nutrition and trace metal distribution caused by the ENs-induced POM formation needs thorough investigation. In addition, the fate of EN-induced POM impact on the marine microbial loop warrants further exploration.

In contrast to the critical role of hydrophobic interactions in marine EN-DOM assembly, we found that electrostatic forces can influence DOM-POM transition in a freshwater system. Non-charged and positive-charged ENs accelerated the kinetics of DOM assembly, but the negative-charged ENs can delay the process more than 24 hrs. In addition, we noticed a size-dependent effect; smaller (diameter 25 nm) ENs showed greater acceleration effects on DOM-POM kinetic than the larger ones (diameter 100 nm). The different outcomes observed in our study highlight the diversity of DOM chemical compositions in natural environments. Moreover, the aquatic environments, such as salinity and pH, can also influence the ENs-DOM interaction. In order to fully understand the fates of ENs in aquatic systems, the interactions between various types of ENs and natural DOM polymers should be systematically studied.

In the surface ocean, ~40-60% of photosynthetic production is released as exopolymeric substances (EPS). In this study, we analyzed the chemical composition and surface properties of EPS from three phytoplankton . Our study indicates EPS polymers with a high fraction of relative hydrophobic domain are more sensitive to environmental ENs.

Moreover, the high concentration of ENs (100ppb) accumulated within EPS gel matrices was observed. Our findings not only demonstrate the peculiar selection pressure on marine microbial community caused by nanopollutants, but also imply a new concentrating pathway of nanowaste accumulation in ecosystems.

We investigated the influences of ocean acidification and surface warming on marine DOM assembly. We found the DOM-POM transition keeps relatively stable under only single environmental changes, either pH or temperature. However, the unexpected synergetic, compounding effect of slight pH drop and moderate temperature increase can dramatically block the DOM assembly process. These environmental changes can also disperse microgels in the ocean. The critical dispersion temperature decreases concurrently with pH: from 32^{o}C at pH 8.2, to 28˚C at pH 7.5. Because the DOM-POM transition serve critical linkages of marine carbon/nutrition cycles in ocean, the unanticipated change on DOM-POM transition may impact the marine ecosystem in various respects. The potential DOM conformation changes found in this study raise important questions: How do DOM conformation changes influence the binding affinity of organic ligand/metal ions? Can this abiotic pathway contribute to the refractory DOM formation by means of temperature/pH-induced denaturation? The remineralization of changed DOM into the microbial loop needs to be addressed as well.

Under the anthropogenic stresses imposed on the ocean by means of increased atmospheric carbon, the feasibility of the DOM pool serving as carbon sink is called into question. We studied DOM-POM transitions with polymer physics model(s) and investigated the changes caused by anthropogenic activity. The complex EN-DOM interactions and the synergetic effects of temperature and pH on DOM both indicate the intricate and unpredicted nature of the DOM-POM shunt. In order to establish sensible regulations for nanotechnology and carbon emission strategies, more studies are needed to further understand the DOM-POM link, a neglected, but not missing relationship.

Appendix

Selected Publications

1. C.-S Chen, J Anaya, S Zhang, J Spurgin, C.-Y Chuang, C Xu, A-J Miao, E Chen, K Shwehr, Y Jiang, A Quigg, PH Santschi“Effects of engineered nanoparticles on the assembly of exopolymeric substances from phytoplankton” PLoS ONE 2011

2. C.-S Chen, W.Ju Chung, Ian C. Hsu, C.-M Wu , W.-C Chin “ Force field measurements within exclusion zone of water” Journal of Biological Physics 2011

3. C.-S Chen, S Soni, C Le, M Biasca, E Farr, Y-T. E Chen, W.-C Chin “ Huamn Stem Cell Neuronal Differentiation on Silk-Conbon Nanotube Composite” Nanoscale Reserch letter (in press)

Patents

1. “Processes for Rapid Microfabrication Using Thermoplastics and Devices Thereof ” US/World patent WO/2009/064816 **;** US2008/083283

2. “Apparatus and Method for Culturing Stem Cells”, 1/26/2009, US provisional patent 61/147,424.

3. “Cell Culture Media to Differentiate Embryonic Stem Cells into Neuronal Lineages”, 8/26/2010, US patent application 12/869,599.

4. “Cell culture device to differentiate stem cells in a specific orientation”, 8/26/2010, US patent application 12/869,616.

5. “Energy-free Concentrator and Energy-free Pump for micro-meter scale system” US provision patent 61/429,392

OPEN ACCESS Freely available online

PLoS one

Effects of Engineered Nanoparticles on the Assembly of Exopolymeric Substances from Phytoplankton

Chi-Shuo Chen[1☯], Jesse M. Anaya[1☯], Saijin Zhang[2,4], Jessica Spurgin[2,4], Chia-Ying Chuang[2,4], Chen Xu[2,4], Ai-Jun Miao[5], Eric Y-T Chen[1], Kathleen A. Schwehr[2,4], Yuelu Jiang[2,4], Antonietta Quigg[2,3,4], Peter H. Santschi[2,4], Wei-Chun Chin[1]*

1 Bioengineering, University of California, Merced, Merced, California, United States of America, **2** Department of Marine Science, Texas A & M University at Galveston, Galveston, Texas, United States of America, **3** Department of Marine Biology, Texas A & M University at Galveston, Galveston, Texas, United States of America, **4** Department of Oceanography, Texas A & M University, College Station, Texas, United States of America, **5** State Key Laboratory of Pollution Control and Resource Reuse, School of Environment, Nanjing University, Nanjing, Jiangsu Province, People's Republic of China

Abstract

The unique properties of engineered nanoparticles (ENs) that make their industrial applications so attractive simultaneously raise questions regarding their environmental safety. ENs exhibit behaviors different from bulk materials with identical chemical compositions. Though the nanotoxicity of ENs has been studied intensively, their unintended environmental impacts remain largely unknown. Herein we report experimental results of EN interactions with exopolymeric substances (EPS) from three marine phytoplankton species: *Amphora sp.*, *Ankistrodesmus angustus* and *Phaeodactylum tricornutum*. EPS are polysaccharide-rich anionic colloid polymers released by various microorganisms that can assemble into microgels, possibly by means of hydrophobic and ionic mechanisms. Polystyrene nanoparticles (23 nm) were used in our study as model ENs. The effects of ENs on EPS assembly were monitored with dynamic laser scattering (DLS). We found that ENs can induce significant acceleration in *Amphora sp.* EPS assembly; after 72 hours EN-EPS aggregation reached equilibrium, forming microscopic gels of ~4–6 μm in size. In contrast, ENs only cause moderate assembly kinetic acceleration for *A. angustus* and *P. tricornutum* EPS samples. Our results indicate that the effects of ENs on EPS assembly kinetics mainly depend on the hydrophobic interactions of ENs with EPS polymers. The cycling mechanism of EPS is complex. Nonetheless, the change of EPS assembly kinetics induced by ENs can be considered as one potential disturbance to the marine carbon cycle.

Citation: Chen C-S, Anaya JM, Zhang S, Spurgin J, Chuang C-Y, et al. (2011) Effects of Engineered Nanoparticles on the Assembly of Exopolymeric Substances from Phytoplankton. PLoS ONE 6(7): e21865. doi:10.1371/journal.pone.0021865

Editor: Stephen J. Johnson, University of Kansas, United States of America

Received February 8, 2011; **Accepted** June 10, 2011; **Published** July 21, 2011

Funding: This work was supported, in part, by the National Science Foundation to Peter H. Santschi and Antonietta Quigg (CBET-0933137), and to Wei-Chun Chin (CBET-0932404) and California Sea Grant (NA10OAR4170060) to Wei-Chun Chin. CSC, JMA and EYTC were supported by UC Merced Center of Excellence on Health Disparities (1P20MD005049-01 from the National Center on Minority Health and Health Disparities), UC LEADS program, California Sea Grant trainee program and GRC summer fellowship from UC Merced. The funders had no role in study design, data collection and analysis, decision to publish, or preparation of the manuscript.

Competing Interests: Dr. Chin is a member of the editorial board of PLoS ONE. This does not alter the authors' adherence to all the PLoS ONE policies on sharing data and materials.

* E-mail: wchin2@ucmerced.edu

☯ These authors contributed equally to this work.

Introduction

Engineered nanoparticles (ENs) are increasingly being developed to improve and innovate industrial and consumer products; for example, they are used to improve semiconductors, sunscreens and cosmetics and in the medicinal industry for imagery and drug delivery [1]. As a large fraction of atoms are located at or near their surface, ENs have high electron activities. Cytotoxic interactions between organisms and ENs can occur through various mechanisms such as electro-active groups, heavy-metal effects and reactive oxygen species (ROS) [1]. Previous studies have demonstrated the ability of algal and protozoan to uptake ENs [2]. The popularity of ENs in the consumer industry raises critical questions regarding their potential impacts on ecological systems [3], especially in the context of oceanic environments. Therefore, any EN-aquatic biota interaction that could alter natural oceanic processes, including the marine carbon cycle or marine food webs, should receive increased attention [4].

In recent years, accumulating plastic debris in the world's oceans has become a major public concern [5,6,7]. To date, several studies have elucidated the threat by microplastics to marine organisms such as fish, birds, and turtles —mostly through pathways of ingestion [8,9]. Few have focused on marine phytoplankton [10] despite that fact that most floating plastic fragments—some with sizes close to 1 μm— accumulate at the ocean surface [7]; here they can degrade to leave free-floating polymers of appropriate sizes for transportation by ocean currents to neighboring regions [6,11,12]. These reports suggest that accumulated micropolymers may be interacting with marine phytoplankton. Though it is difficult to quantify the direct ecological influence of nanopolymers on aquatic ecosystems [13], studying the potential threat that nanopolymers released from plastic degradation [14] on ecological processes is greatly needed given reported threat by microplastics [8,10].

Phytoplankton in the surface ocean account for about half of the global photosynthetic activity [15], making them a major driving force to sequester CO_2 from the atmosphere [15,16]. Furthermore, about ~40–60% of the photosynthetic production by phytoplankton is released as EPS into the dissolved organic carbon (DOC) pool, contributing to the primary marine carbon reservoir [17,18]. The recent discovery that ~10% of the DOC pool can assemble to form porous microscopic gels that can be readily colonized and metabolized by marine bacteria opened a novel lens to view DOC and carbon cycling in the oceans [19,20,21,22,23]. Considering that EPS is a major source of both the marine DOC and particulate organic carbon (POC) pools [17,18,24,25] understanding EPS assembly in the presence of nanoparticles and their specific mechanisms of microgel formation are critically important.

Recent studies have revealed that EN toxicity can impair phytoplankton function both extra- and intra-cellularly [26]. Miao et al. [27] found trace metal ions released from the oxidative dissolution of silver ENs in seawater were toxic to the marine diatom *Thalassiosira weissflogii*. These authors also reported that EPS production, particularly in nutrient limited cultures, played an important role in Ag ion detoxification. Zinc oxide ENs have been found to elicit a similar toxicity responses in the marine diatom *Thalassiosira pseudonana* [28]; ZnO-EN dissolution rates were accelerated in seawater, whereas ZnO-EN concentration itself only had a very small effect on Zn^{2+} release. Ag-ENs were also found to accumulate inside the freshwater alga *Ochromonas danica* where they exerted their toxic effects [29].

Here we used EPS released by three phytoplankton—*Amphora sp.*, *A. angustus* and . *tricornutum*—to investigate the effects of ENs on EPS assembly. *Amphora sp.* is a major genus of diatoms that has a world-wide distribution and an ability to grow under a wide range of conditions [30]. *Amphora sp.* is also a dominant fouling/biofilm diatom species that produces significant amount of EPS [30] and has been used in many diatom mobility studies [31,32]. *Ankistrodesmus* is a major genus of green algae that has been used in many studies [33,34]. *P. tricornutum* is a model diatom for genomics [35,36] and fatty acid metabolism studies [37]. To investigate the environmental impacts of nanoplastics released during debris degradation, polystyrene ENs (diameter 23 nm) were used as model ENs. Their high surface ratio and nano-scale particle size provided a suitable model to study the interactions of engineered nanomaterials and natural polymers. In this study, particle sizing by dynamic laser scattering (DLS) was used to monitor the assembly process of EPS and their interactions with ENs. Hydrophobic dye (Nile Red) and protein:carbohydrate ratios were applied to quantify the existence of hydrophobic domains on EPS polymers and to investigate the role hydrophobic interactions in EN-induced EPS assembly [38].

Materials and Methods

Chemicals and solution preparation

HPLC grade reagents and salts including sodium chloride, potassium chloride, calcium chloride, magnesium chloride, magnesium sulfate, sodium bicarbonate, and dimethyl sulfoxide were purchased from Sigma-Aldrich (St. Lious, MO, USA). Polystyrene nanoparticles (Bangs Laboratories, IN, USA) were used in our study as model ENs. The primary size and surface area of these non-fluorescence nanoparticles were 23 nm and 2.48×10^{14} $\mu m^2/g$ (certificate provided by vendor). Fluorescence polystyrene ENs (23 nm, Bangs Laboratories, IN, USA) were used only for fluorescence microscopy. The size of these ENs was independently confirmed by DLS (dynamic laser scattering) in lab. Thorough sonication was applied to nanoparticle stock solutions before experiments, as described in our previous study [39].

Artificial Seawater (ASW, 423 mM NaCl, 9 mM KCl, 9.27 mM $CaCl_2$, 22.94 mM $MgCl_2$, 25.5 mM $MgSO_4$, 2.14 mM $NaHCO_3$) was prepared using deionized water from a Milli-Q system (Millipore, Billerica, MA, USA) following established protocols from the Marine Biological Laboratory, Woods Hole, MA. The composition of Ca^{2+}- free ASW included: 436.7 mM NaCl, 9 mM KCl, 22.9 mM $MgCl_2$, 25.5 mM $MgSO_4$, 2.1 mM $NaHCO_3$, and 1 mM EGTA. Two different concentrations of ENs were added into the EPS solution (final EN concentration: 10 ppb, 100 ppb). A Nile Red stock solution (1.6 mM) was prepared in DMSO. A Chlortetracycline hydrochloride (CTC) (Sigma-Aldrich, USA) stock solution (10 mM) was prepared in Milli-Q water.

Extraction of exopolymeric substances (EPS) from phytoplankton culture

A. angustus and *P. tricornutum* used for EPS extraction were purchased from the CCMP (The Provasoli-Guillard National Center for Culture of Marine Phytoplankton). Both species were grown under continuous light (35 μmol. photons m^{-2} s^{-1}) at 20°C. The culture volume was 20 L for each and cultures were aerated. Growth was monitored by measuring the change in optical density at 750 nm with a UV/VIS spectrophotometer. Cultures were harvested during the stationary phase and then EPS was extracted. The phytoplankton culture was centrifuged at 3200 rpm for 30 minutes, after which it was separated into pellet (cells) and supernatant fractions. The supernatant fraction was used to collect free dissolved EPS according to the previous study [40]. In brief, the procedure consisted of a) filtration, b) cross-flow ultrafiltration, c) stirred-cell diafiltration. 20 L of the pre-filtered supernatant fraction (<0.45 μm) was ultrafiltered until 200–300 mL of retentate was left. The cartridge was rinsed with 200 mL of pure water and soaked for 6 hours. After that, the cartridge was rinsed with another 200 mL of water, and this whole process was repeated twice. Subsequently, the retentate solution and four rinse solutions were combined. The resulting 1 L of solution was then further concentrated by stirred-cell diafiltration with a 5 kDa membrane to obtain 50 mL of concentrated EPS solution. EPS of *Amphora sp.* was obtained using the same approach described by Zhang et al. [41].

Compositional characterization of EPS

Carbohydrate concentration was measured using the anthrone method [40], with glucose as a standard. Uronic acids were determined according to Blumenkrantz and Asboe-Hansen with glucuronic acid as a standard [42]. Proteins were measured using a modified Lowry Protein Assay Kit (Pierce, 23240, USA), according to the protocol provided by the manufacture. Additionally, elemental carbon, hydrogen and nitrogen abundance was analyzed by Series II CHNS/O Analyzer 2400 (Perkin Elmer).

Estimation of EPS molecular weight

Size Exclusion Chromatography (SEC) was used to measure the molecular weight of the EPS [41]. Briefly, 150 μL of EPS solution was injected into a Tosoh TSK G-4000PW×l (300×7.8 mm) and detected by a Refractive Index detector. The mobile phase was 0.078 M $NaNO_3$ in 10 mM phosphate buffer (pH = 6.8) at a flow rate of 0.5 mL/min. Polystyrene standards with a molecular weight of 8 kDa, 35 kDa, 100 kDa, and 780 kDa were used for establishing the calibration curve, whereby the logarithm of molecular weight was plotted vs. corresponding retention time.

Microgel Sizing

EN-induced alterations of EPS assembly were investigated with three different types of EPS (*Amphora sp.*, *A. angustus* and *P. tricornutum*) and at three EN concentrations (0, 10, 100 ppb) in ASW and Ca^{2+}-free ASW. The size of assembled EPS gels (microgels) was monitored by DLS following protocols published previously [19]. The EPS solution was briefly shaken, and refiltered through a 0.22-μm Millipore membrane (pre-washed with 0.1N HCl) before use. Aliquots were then poured directly into scattering sample vials. Scattering cells were positioned in the goniometer of a Brookhaven laser spectrometer (Brookhaven Instruments, Holtsville, NY, USA). EPS assembly was monitored for two weeks, by analyzing the scattering fluctuations detected at a 45 degree scattering angle. The autocorrelation function of the scattering intensity fluctuations was averaged over a 12-min sampling time, using a Brookhaven BI 9000AT autocorrelator. CONTIN method was adapted to calculate particle size distribution [19,43]. Calibration of the DLS method was conducted using standard suspensions of latex microspheres (Polysciences, Warrington, PA, USA). Each measurement was taken in replicate (n = 6) at room temperature.

Fluorescence enhancement measurement

Nile Red (Invitrogen, Carlsbad, CA, USA), used as a hydrophobic indicator as in our previous studies [38], is a particularly effective solvatochromic dye containing a rigid aromatic group and an exocyclic diethylamine group. The absorbance and fluorescence emission depends on the physical properties of surrounding solvent environment: fluorescence emission is enhanced with hydrophobic environment exposure [44]. EPS from *Amphora sp.*, *A. angustus* and *P. tricornutum* were mixed with 13 μM Nile Red in triplicate. The fluorescence measurements were obtained with a Shimadzu RF-5000U spectrofluorophotometer ($\lambda_{excitation} = 550$ nm; $\lambda_{emission} = 633$ nm). Fluorescence emission of Nile Red showed a very weak signal at 633 nm in the polar ASW with excitation wavelength 550 nm.

CTC was used to reveal bound Ca^{2+} on EPS polymers [19,45]. CTC (100 μM) was added into ASW mixed with each type of EPS. For CTC fluorescence measurements, the emission was collected at $\lambda = 530$ nm (excited at $\lambda = 390$ nm) using a Shimadzu RF-5000U spectrofluorophotometer.

Environmental scanning electron microscopy (ESEM)

ESEM was used to investigate EPS polymer networks in their native conformations. This method provides a non-destructive tool to study materials at electron microscopy resolution while still fully hydrated. Samples of EPS were prepared in ASW with/without 23 nm polystyrene nanoparticles, as previously described [19,20,21,22,23]. After being incubated for 10 days in darkness to reach the equilibrium sizes, all EPS aggregations were filtered through a 0.22-μm Millipore Isopore membrane (Fisher Scientific, Pittsburgh, PA, USA). The assembled microgels retained on filters were investigated using FEI Quanta 200 ESEM (North America NanoPort, Portland, OR, USA).

Fluorescence microscopy

The accumulation of ENs within EPS microgels was investigated with Fluorescence Microscopy (Nikon Instruments, Melville, NY, USA). EN-induced EPS microgels was prepared in agreement with our aforementioned protocol with 100 ppb 23 nm fluorescent ENs (Bangs Laboratories, IN, USA) and 13 μM Nile Red. The fluorescent images of microgels retained on Isopore membrane were collected by fluorescence microscopy with at $\lambda_{excitation} = 530$ nm (Nile red) and at $\lambda_{excitation} = 488$ nm (fluorescent ENs).

Statistical analysis

Data represent means ±1 standard deviation (SD). Each experiment was performed in triplicate. A student's t-test analysis was used to determine statistical significance. p values of <0.05 were used as standard for statistical significance (GraphPad Prism 4.0, GraphPad Software, San Diego, CA).

Results

Chemical analysis of EPS

EPS from the three phytoplankton species contained varied protein:carbohydrate ratios, which can be taken as an indicator of their relative hydrophobicity. *A. angustus* had a ratio of 0.72, *P. tricornutum* with a ratio of 0.31 while *Amphora sp.* had no detectable level of proteins (Table 1, Zhang et al 2008). Our chemical analysis indicates that EPS from these three phytoplankton species have similar molecular weight distributions and uronic acid ratios (Table 1). CHN analysis also indicated that *Amphora* EPS has the lowest N content of the three types of EPS (Table 1). Of the different EPS used in this study, EPS from *A. angustus* is the most hydrophobic whilst *Amphora* EPS is the most hydrophilic.

Assembly of EPS from phytoplankton in ASW and Ca^{2+}- free ASW

The spontaneous assembly of 100 μg L^{-1} *Amphora sp.* EPS solutions in ASW containing 9 mM Ca^{2+} (but no ENs) was monitored by DLS for more than 10 days. As shown in Fig. 1a, EPS from *Amphora sp.* cannot assemble to form EPS microgels after 10 days. Similar measurements conducted in 100 μg L^{-1} *Amphora sp.* EPS solutions with ENs (10 or 100 ppb) demonstrated that ENs can facilitate EPS assembly following first-order kinetics, reaching steady-state assembly/dispersion equilibrium in ~60 hrs. The equilibrium size of microgels, ~2.5 μm formed with 10 ppb ENs, was significantly smaller than those formed from100 ppb ENs (4–5 μm) (Fig. 1a).

The same protocol was used to test the spontaneous assembly of EPS from *A. angustus* (Fig. 1b) and *P. tricornutum* (Fig. 1c). Results show that both types of EPS polymers can assemble following almost

Table 1. Chemical analysis of EPS.

Marine Phytoplankton	Molecular weight distribution (kDa)	Protein/carbohydrate Ratio	Uronic acid/carbohydrate Ratio	C %	H %	N %
*Amphora sp.**	1000.0	~0	0.5	37.7	6.27	1.37
Ankistrodesmus angustus	1026.7, 123, 13.2, 2.6	0.72	0.48	41.8	7.34	5.83
Phaeodactylum tricornutum	1005.9, 126.4, 36.1, 22.7, 12.8	0.31	0.5	37.6	5.71	4.5

*Zhange et al., (2008) [40].

doi:10.1371/journal.pone.0021865.t001

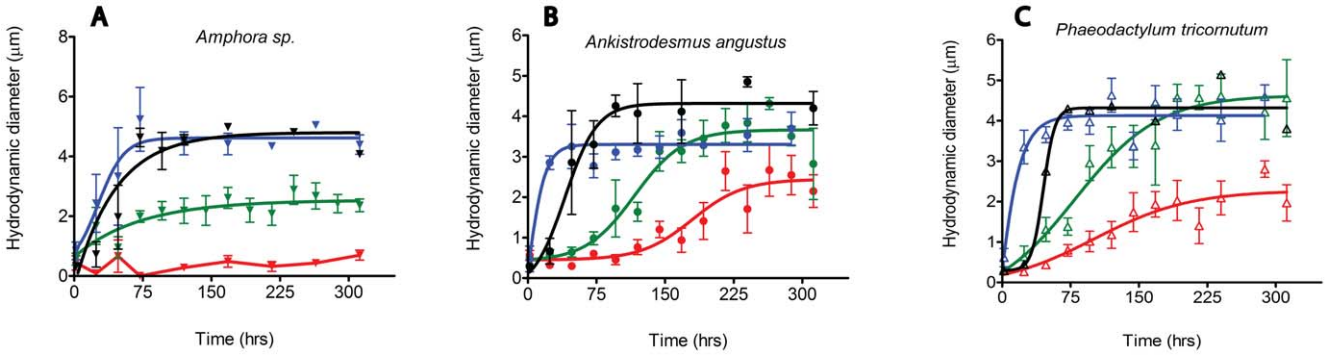

Figure 1. Assembly kinetics of EPS monitored with DLS. (A) Assembly kinetics of EPS of *Amphora sp.* (B) Assembly kinetics of EPS of *Ankistrodesmus angustus* (C) Assembly kinetics of EPS of *Phaeodactylum tricornutum* EPS assembly in Ca^{2+}-free ASW (black) was monitored to investigate assembly kinetics with decreased divalent ion availability. Different concentrations of ENs (polystyrene nanoparticles): 0 (red), 10 (green) and 100 ppb (blue), were added to investigate the effect of ENs on EPS microgel formation.
doi:10.1371/journal.pone.0021865.g001

identical kinetics and reach similar microgel equilibrium sizes (~2 μm) in the absence of ENs. With 10 ppb ENs, for both EPS types, the assembly rate was accelerated and the resulting microgel size was increased to around 4 μm (Fig. 1b, c). With higher concentrations of ENs (100 ppb), the assembly rate was further accelerated; however, the resulting microgel size remained at around 4 μm (Fig. 1b, c). We also monitored pure ENs in ASW for 10 days with DLS and found no EN self-aggregation (data not shown).

The EN-induced EPS assemblies from those three species were monitored with 100 ppb ENs in Ca^{2+}-free ASW. Without divalent ions (Ca^{2+} or Mg^{2+}), our results show ENs still can promote EPS assembly. EPS from *Amphora sp*, *A. angustus* and *P. tricornutum* assembled into microgels with equilibrium sizes about 4–5 μm within ~120 hrs (Fig. 1a–c).

ESEM images (Fig. 2a–c) showed that ENs (100 ppb) may incorporate into EPS microgel matrices, as granular surface structures were found in these ESEM images (Fig. 2a–c). In addition, ESEM observations confirmed the size measurements with DLS (Fig. 1a–c). The results from fluorescence microscopy supported the hypothesis that ENs may be incorporated into EPS microgels. In our experiments, EPS microgels were stained with Nile Red to determine the gel morphology (Fig. 3). Noting EPS assembly in ASW without ENs, green fluorescent ENs were found in EPS matrices of all three species (Fig. 3). The data indicate that ENs can accumulate within EPS polymer matrices and may reach a higher concentration than the bulk EN concentration in the water column.

Fluorescence of Nile Red and CTC

We used Nile Red, a widely used hydrophobic fluorescent probe, to detect the presence of hydrophobic regions in EPS from *Amphora sp.*, *A. angustus* and *P. tricornutum* (Fig. 3). The higher Nile Red fluorescence intensity observed in EPS from *A. angustus* and *P. tricornutum* indicated these EPS are much more hydrophobic than EPS from *Amphora sp*. The Nile Red fluorescence results here are consistent with chemical analysis results (Table 1) demonstrating that EPS from *A. angustus* is the most hydrophobic and *Amphora sp.* EPS is the least hydrophobic.

CTC has been used to monitor bound Ca^{2+} in marine microgels [19,45]. CTC fluorescence indicates that all three types of phytoplankton EPS have similar Ca^{2+} binding capacity (Fig. 4).

Discussion

Both hydrophobic and electrostatic interactions have been demonstrated to play important roles in the assembly of EPS microgels [23,38]. Our results indicate that only 10 to 100 ppb of ENs released to the aquatic environment can cause significant EPS-assembly changes (Fig. 1a–c). The results from *A. angustus* and *P. tricornutum* show that ENs can accelerate the assembly kinetics and increase the equilibrium microgel sizes of EPS. For EPS from *Amphora*, ENs can effectively induce their assembly, resulting in microgels with an equilibrium size of 4–6 μm, similar to *A. angustus* and *P. tricornutum* EPS.

EPS polymers from marine organisms are polysaccharide-rich, containing uronic acids and various proteins. Slight changes in their compositions would therefore affect their physic-chemical, e.g., biosurfactant and emulsifying, properties. Their role and fate in biogeochemical cycles is largely unexplored [46,47]. Generally, the acidic groups in EPS are carboxylate, sulphate, and phosphate. Protein constituents have been proposed to be the major contributor for the hydrophobic domains of EPS [38,48].

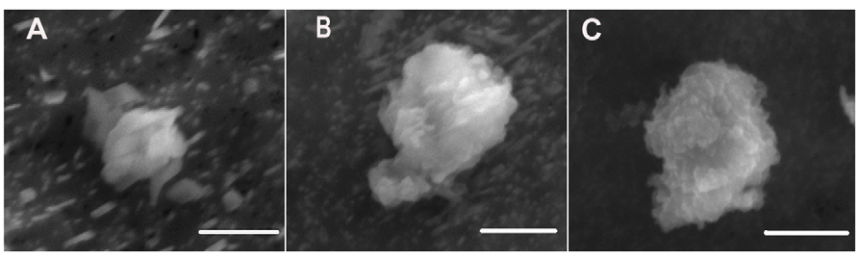

Figure 2. ESEM images of EPS microgel. (A) *Amphora sp.* (Scale Bar = 4 μm) (B) *Ankistrodesmus angustus* (Scale Bar = 5 μm) (C) *Phaeodactylum tricornutum* (Scale Bar = 5 μm).
doi:10.1371/journal.pone.0021865.g002

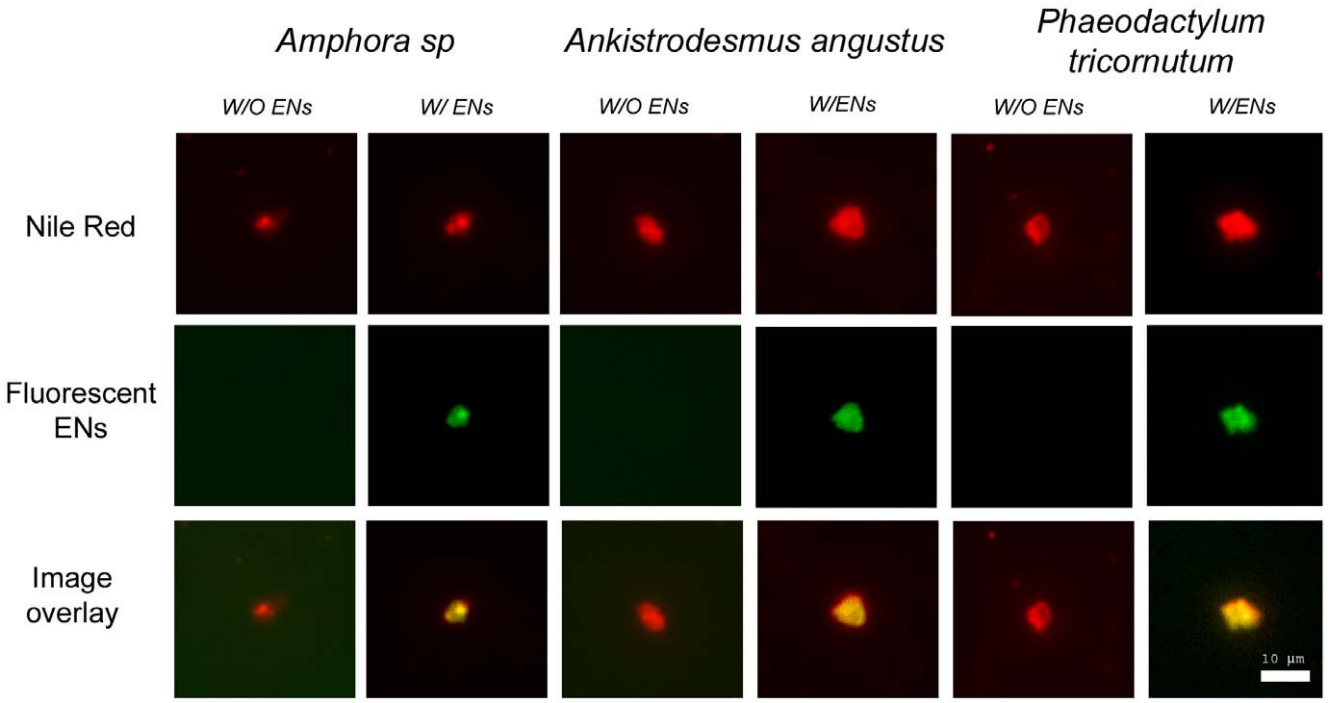

Figure 3. Fluorescence images of EPS and ENs-induced EPS microgels. Nile Red was used to determine the microgel morphology. Green fluorescent signals indicated the fluorescent ENs. From the overlay images, results showed that the ENs incorporated within EPS matrixes. Scale bar is 10 μm.
doi:10.1371/journal.pone.0021865.g003

Different protein:carbohydrate ratios were found in our chemical analysis of EPS (Table 1). Nile Red and CTC were used to detect the presence of hydrophobic domains and Ca^{2+} binding on different EPS polymers [19,23,38,45]. Our Nile Red fluorescence results indicate greater hydrophobic domains on EPS polymers with higher protein:carbohydrate ratios, which are in agreement with previous reports showing protein content contributes to amphiphilic and emulsifying properties of hydrocolloids such as EPS [49,50]. Spontaneous assembly was only observed with EPS from *A. angustus* and *P. tricornutum*, which have higher protein:carbohydrate ratios, and not from *Amphora sp*. EPS (Fig. 1a–c), which has a low protein:carbohydrate ratio (i.e., no detectable protein, lack of sufficient hydrophobic domains, Table 1). Our data indicate that the hydrophobic domains on EPS polymers potentially serve as the essential aggregation sites for EPS assembly (Fig. 1a–c) [51]. For EPS with a relatively low protein (hydrophobic) fraction, such as *Amphora sp*., 100 ppb ENs is required to trigger significant EPS assembly. However, for both partially hydrophobic EPS from *A. angustus* and *P. tricornutum*, 10 ppb ENs are sufficient to significantly change assembly kinetics, resulting in larger microgels (4–5 μm) (Fig. 1b–c). Our data thus confirm the importance of hydrophobic interactions and the total amount of EPS, as well as indicate the threshold of released nanowaste that can disturb the EPS assembly, which may be related to the specific protein:carbohydrate ratio of EPS.

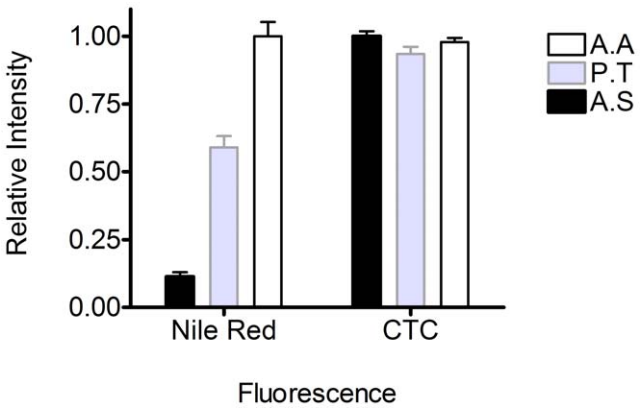

Figure 4. Fluorescence measurements of Nile red and CTC for EPS. EPS extracted from various phytoplankton, *Amphora sp.* (black), *Phaeodactylum tricornutum* (grey) , and *Ankistrodesmus angustus* (white).
doi:10.1371/journal.pone.0021865.g004

The Ca^{2+} -free ASW data further confirmed that hydrophobic interactions play a critical role in phytoplankton ENs-induced EPS assembly (Fig. 1). With a lack of divalent ions serving as cross-linkers, similar EN-induced EPS assembly was observed in 100 ppb EN concentrations. Our results provide evidence that hydrophobic interactions play critical roles in the assembly of these marine EPS, consistent with the previous findings [23].

The chemical analysis in our study indicates that EPS from these three phytoplankton species have similar molecular weight distributions (*Amphora*: 1000 kD; *A. angustus*: 1028 kD; *P. tricornutum*: 1006 kD) (Table 1). These observations are consistent with the predictions from a previous polymer model that states the equilibrium size of entangled polymer matrices depends on the polymer length [52,53]. Due to the heterogeneous chemical compositions, the mechanism of EPS assembly remains elusive. In order to quantify the accelerations effects of ENs, the assembly kinetics was fitted with a sigmoidal curve and $T_{1/2}$ was used to represent the time needed for the microgel to reach half of the equilibrium size. *A. angustus* showed a dramatically decreased $T_{1/2}$: from ~178 hrs (control, without ENs) to ~16 hrs with 100 ppb

Table 2. EPS Assembly analysis.

Phytoplankton	*Amphora sp.**			*Ankistrodesmus angustus*			*Phaeodactylum tricornutum*		
ENs concentration (ppb)	*N.A*	10	100	*N.A*	10	100	*N.A*	10	100
$T_{1/2}$ (hrs)	–	46	28	*178*	116	16	119	96	16
Hill coefficient	–	0.84	2.28	–	1.97	1.33	–	2.38	1.46

doi:10.1371/journal.pone.0021865.t002

ENs. Similar positive correlations between $T_{1/2}$ decrease and ENs dosages were found in *P. tricornutum* and *Amphora sp*. EPS (Table 2). The acceleration of assembly kinetics shown here demonstrated that ENs are able to promote EPS assembly. In addition, we used Hill coefficients to investigate the cooperative interactions between ENs and EPS polymers [51] . For *Amphora* EPS, the Hill coefficient was ~2.28 for 100 ppb ENs concentration. Positive EN-EPS cooperative effects were also observed in EPS assembly of *A. angustus* and *P. tricornutum* (Table 2). Similar positive cooperation was also found to correlate with hydrophobic interactions between ENs and EPS.

EPS play critical roles in aquatic ecosystems and have been shown to be key sources for marine DOC and POC. If the EN-induced changes of EPS assembly highlighted in this study are applicable to the natural environment, ENs can lead to deleterious environmental impacts. With varying assembly characteristics, EPS released from diverse phytoplankton contribute to different organic carbon pools in the ocean. Our data reported here indicate that 10 ppb ENs can unexpectedly induce assembly of EPS of *Amphora sp*., indicating the re-direction of the organic carbon flux from the DOC to POC pool. The alterations of EPS assembly kinetics from *A. angustus* and *P. tricornutum* also indicate the change of the time scale for carbon flow between DOC and POC.

EPS assembly changes can also affect the microbial ecosystem and marine trophic cycle. Described as the dark matter of biofilms and transparent exopolymeric particles (TEP), EPS play crucial roles in the formation and maintenance of structured multicelluar microbial communities [21,54,55,56,57,58,59,60]. The concentration, cohesion, charge, sorption capacity, specificity and nature of the individual components of EPS, as well as the three-dimensional architecture of the matrix (the dense areas, pores and channels), determine the mode of community life. In this study, our data showed that ENs can drastically change the assembly behavior of EPS. The change of sedimentation velocity, caused by assembly size changes, can reshape the plume leaking from microgel and influence the nutrient utilization of free-living microbes in the water column [54,61]. Moreover, higher concentrations of ENs accumulated within EPS microgel matrices were shown with ESEM and fluorescence microscopy (Fig. 2a–c). Because microgels also serve as important nutrition source for the marine food web in the deep ocean, the possibility of ENs impacting direct up-take by higher-level organisms, such as protozoa and metazoan, needs to also be considered [62].

Our data thus show the EPS gel matrices serve as a concentrating sponge (Fig. 3). This new pathway of nanowaste accumulation facilitated by EPS suggests an urgent need to consider lower concentration limits for nanowaste in marine environments [3,63]. In summary, our results clearly demonstrate how nanowaste (e.g. nanoparticles) can potentially disturb the marine carbon cycle and ecosystem [58]. Whereas most environmental impact studies of nanomaterials have focused on "nanotoxicity"—investigating the direct harmful effects on phytoplankton cells or various organisms—our study indicates that indirect influences from ENs can potentially pose greater environmental threats than those of direct toxicity.

Acknowledgments

We thank Mike Dunlap for his assistance with ESEM, and the anonymous reviewers for constructive suggestions for improving the manuscript.

Author Contributions

Conceived and designed the experiments: CSC SZ WCC. Performed the experiments: CSC JMA SZ JS. Analyzed the data: CSC JMA SZ. Contributed reagents/materials/analysis tools: SZ CYC CX AJM EYTC KAS YJ. Wrote the manuscript: CSC JMA SZ AQ PHS WCC.

References

1. Nel A, Xia T, Madler L, Li N (2006) Toxic potential of materials at the nanolevel. Science 311: 622–627.
2. Werlin R, Priester JH, Mielke RE, Kramer S, Jackson S, et al. (2011) Biomagnification of cadmium selenide quantum dots in a simple experimental microbial food chain. Nat Nano 6: 65–71.
3. Maynard AD, Aitken RJ, Butz T, Colvin V, Donaldson K, et al. (2006) Safe handling of nanotechnology. Nature 444: 267–269.
4. Ferry JL, Craig P, Hexel C, Sisco P, Frey R, et al. (2009) Transfer of gold nanoparticles from the water column to the estuarine food web. Nature Nanotechnology 4: 441–444.
5. Artham T, Sudhakar M, Venkatesan R, Nair CM, Murty K, et al. (2009) Biofouling and stability of synthetic polymers in sea water. International Biodeterioration & Biodegradation 63: 884–890.
6. Thompson RC, Olsen Y, Mitchell RP, Davis A, Rowland SJ, et al. (2004) Lost at sea: Where is all the plastic? Science 304: 838–838.
7. Zarfl C, Matthies M. Are marine plastic particles transport vectors for organic pollutants to the Arctic? Marine Pollution Bulletin 60: 1810–1814.
8. Ward JE, Shumway SE (2004) Separating the grain from the chaff: particle selection in suspension- and deposit-feeding bivalves. Journal of Experimental Marine Biology and Ecology 300: 83–130.
9. Derraik JGB (2002) The pollution of the marine environment by plastic debris: a review. Marine Pollution Bulletin 44: 842–852.
10. Bhattacharya P, Lin SJ, Turner JP, Ke PC (2010) Physical Adsorption of Charged Plastic Nanoparticles Affects Algal Photosynthesis. Journal of Physical Chemistry C 114: 16556–16561.
11. Moret-Ferguson S, Law KL, Proskurowski G, Murphy EK, Peacock EE, et al. The size, mass, and composition of plastic debris in the western North Atlantic Ocean. Marine Pollution Bulletin 60: 1873–1878.
12. Watters DL, Yoklavich MM, Love MS, Schroeder DM. Assessing marine debris in deep seafloor habitats off California. Marine Pollution Bulletin 60: 131–138.
13. Werlin R, Priester JH, Mielke RE, Kramer S, Jackson S, et al. Biomagnification of cadmium selenide quantum dots in a simple experimental microbial food chain. Nat Nanotechnol 6: 65–71.
14. Gopferich A (1996) Mechanisms of polymer degradation and erosion. Biomaterials 17: 103–114.
15. Chisholm SW (2000) Oceanography - Stirring times in the Southern Ocean. Nature 407: 685–687.
16. Falkowski P, Scholes RJ, Boyle E, Canadell J, Canfield D, et al. (2000) The global carbon cycle: A test of our knowledge of earth as a system. Science 290: 291–296.
17. Fogg GE (1983) The Ecological Significance of Extracellular Products of Phytoplankton Photosynthesis. Botanica Marina 26: 3–14.
18. Baines SB, Pace ML (1991) The Production of Dissolved Organic-Matter by Phytoplankton and Its Importance to Bacteria - Patterns across Marine and Fresh-Water Systems. Limnology and Oceanography 36: 1078–1090.

19. Chin WC, Orellana MV, Verdugo P (1998) Spontaneous assembly of marine dissolved organic matter into polymer gels. Nature 391: 568–572.
20. Wells ML (1998) Marine colloids - A neglected dimension. Nature 391: 530–531.
21. Verdugo P, Alldredge AL, Azam F, Kirchman DL, Passow U, et al. (2004) The oceanic gel phase: a bridge in the DOM-POM continuum. Marine Chemistry 92: 67–85.
22. Verdugo P, Orellana MV, Chin WC, Petersen TW, van den Eng G, et al. (2008) Marine biopolymer self-assembly: implications for carbon cycling in the ocean. Faraday Discussions 139: 393–398.
23. Ding YX, Chin WC, Rodriguez A, Hung CC, Santschi PH, et al. (2008) Amphiphilic exopolymers from Sagittula stellata induce DOM self-assembly and formation of marine microgels. Marine Chemistry 112: 11–19.
24. Wotton RS, Preston TM (2005) Surface films: Areas of water bodies that are often overlooked. Bioscience 55: 137–145.
25. Hedges JI (1992) Global Biogeochemical Cycles - Progress and Problems. Marine Chemistry 39: 67–93.
26. Navarro E, Baun A, Behra R, Hartmann NIB, Filser J, et al. (2008) Ecotoxicity of nanoparticles on algae, plants and fungi: state of the art and future needs. Special issue on Ecotoxicology: Chemistry and Risk Assessment of Nanoparticles 17: 372–386.
27. Miao AJ, Schwehr KA, Xu C, Zhang SJ, Luo Z, et al. (2009) The algal toxicity of silver engineered nanoparticles and detoxification by exopolymeric substances. Environ Pollut 157: 3034–3041.
28. Miao AJ, Zhang XY, Luo ZP, Chen CS, Chin WC, et al. (2010) Zinc Oxide Engineered Nanoparticles Dissolution and Toxicity to Marine Phytoplankton. Environmental Toxicology and Chemistry 29: 2814–2822.
29. Miao AJ, Luo Z, Chen CS, Chin WC, Santschi PH, et al. (2010) Intracellular uptake: a possible mechanism for silver engineered nanoparticle toxicity to a freshwater alga Ochromonas danica. PLoS One 5: e15196.
30. Daniel GF, Chamberlain AHL, Jones EBG (1980) Ultrastructural Observations on the Marine Fouling Diatom Amphora. Helgolander Meeresuntersuchungen 34: 123–149.
31. Cooksey KE, Wigglesworthcooksey B (1995) Adhesion of Bacteria and Diatoms to Surfaces in the Sea - a Review. Aquatic Microbial Ecology 9: 87–96.
32. Wigglesworth-Cooksey B, Cooksey KE (2005) Use of fluorophore-conjugated lectins to study cell-cell interactions in model marine biofilms. Applied and Environmental Microbiology 71: 428–435.
33. Adrian R (1987) Viability of Phytoplankton in Fecal Pellets of 2 Cyclopoid Copepods. Archiv Fur Hydrobiologie 110: 321–330.
34. Conner AJ (1981) The Differential Sensitivity of Phytoplankton to Polychlorinated-Biphenyls When Cultured Heterotrophically and Photoautotrophically. Environmental and Experimental Botany 21: 241–247.
35. Scala S, Carels N, Falciatore A, Chiusano ML, Bowler C (2002) Genome properties of the diatom Phaeodactylum tricornutum. Plant Physiology 129: 993–1002.
36. De Martino A, Meichenin A, Shi J, Pan KH, Bowler C (2007) Genetic and phenotypic characterization of Phaeodactylum tricornutum (Bacillariophyceae) accessions. Journal of Phycology 43: 992–1009.
37. Yongmanitchai W, Ward OP (1991) Growth of and Omega-3-Fatty-Acid Production by Phaeodactylum-Tricornutum under Different Culture Conditions. Applied and Environmental Microbiology 57: 419–425.
38. Ding YX, Hung CC, Santschi PH, Verdugo P, Chin WC (2009) Spontaneous Assembly of Exopolymers from Phytoplankton. Terrestrial Atmospheric and Oceanic Sciences 20: 741–747.
39. Chen EYT, Wang YC, Chen CS, Chin WC. Functionalized Positive Nanoparticles Reduce Mucin Swelling and Dispersion. Plos One 5.
40. Zhang SJ, Santschi PH (2009) Application of cross-flow ultrafiltration for isolating exopolymeric substances from a marine diatom (Amphora sp.). Limnology and Oceanography-Methods 7: 419–429.
41. Zhang SJ, Xu C, Santschi PH (2008) Chemical composition and Th-234 (IV) binding of extracellular polymeric substances (EPS) produced by the marine diatom Amphora sp. Marine Chemistry 112: 81–92.
42. Blumenkr N, Asboehan G (1973) New Method for Quantitative-Determination of Uronic Acids. Analytical Biochemistry 54: 484–489.
43. Provencher SW, Stepanek P (1996) Global analysis of dynamic light scattering autocorrelation functions. Particle & Particle Systems Characterization 13: 291–294.
44. Yablon DG, Schilowitz AM (2004) Solvatochromism of Nile Red in nonpolar solvents. Applied Spectroscopy 58: 843–847.
45. Ding YX, Chin WC, Verdugo P (2007) Development of a fluorescence quenching assay to measure the fraction of organic carbon present in self-assembled gels in seawater. Marine Chemistry 106: 456–462.
46. Wotton RS (2004) The ubiquity and many roles of exopolymers (EPS) in aquatic systems. Scientia Marina 68: 13–21.
47. Bhaskar PV, Bhosle NB (2005) Microbial extracellular polymeric substances in marine biogeochemical processes. Current Science 88: 45–53.
48. Quiroz NGA, Hung CC, Santschi PH (2006) Binding of thorium(IV) to carboxylate, phosphate and sulfate functional groups from marine exopolymeric substances (EPS). Marine Chemistry 100: 337–353.
49. Dickinson E (2003) Hydrocolloids at interfaces and the influence on the properties of dispersed systems. Food Hydrocolloids 17: 25–39.
50. Stenstrom TA (1989) Bacterial Hydrophobicity, an Overall Parameter for the Measurement of Adhesion Potential to Soil Particles. Applied and Environmental Microbiology 55: 142–147.
51. Ding Y-X, Chin W-C, Rodriguez A, Hung C-C, Santschi PH, et al. (2008) Amphiphilic exopolymers from Sagittula stellata induce DOM self-assembly and formation of marine microgels. Marine Chemistry 112: 11–19.
52. Degennes PG, Leger L (1982) Dynamics of Entangled Polymer-Chains. Annual Review of Physical Chemistry 33: 49–61.
53. Degennes PG (1979) Scaling concepts in polymer physics: Cornell University Press.
54. Azam F, Long RA (2001) Oceanography - Sea snow microcosms. Nature 414: 495–+.
55. Passow U (2002) Transparent exopolymer particles (TEP) in aquatic environments. Progress in Oceanography 55: 287–333.
56. Passow U, Alldredge AL (1994) Distribution, Size and Bacterial-Colonization of Transparent Exopolymer Particles (Tep) in the Ocean. Marine Ecology-Progress Series 113: 185–198.
57. Azam F (1998) Microbial control of oceanic carbon flux: The plot thickens. Science 280: 694–696.
58. Azam F, Malfatti F (2007) Microbial structuring of marine ecosystems. Nature Reviews Microbiology 5: 782–791.
59. Flemming HC, Wingender J. The biofilm matrix. Nature Reviews Microbiology 8: 623–633.
60. Flemming HC, Neu TR, Wozniak DJ (2007) The EPS matrix: The "House of Biofilm cells". Journal of Bacteriology 189: 7945–7947.
61. Kiorboe T, Jackson GA (2001) Marine snow, organic solute plumes, and optimal chemosensory behavior of bacteria. Limnology and Oceanography 46: 1309–1318.
62. Kerner M, Hohenberg H, Ertl S, Reckermann M, Spitzy A (2003) Self-organization of dissolved organic matter to micelle-like microparticles in river water. Nature 422: 150–154.
63. Leppard GG (2008) Nanoparticles in the environment as revealed by transmission electron microscopy: Detection, characterisation and activities. Current Nanoscience 4: 278–301.

J Biol Phys
DOI 10.1007/s10867-011-9237-5

ORIGINAL PAPER

Force field measurements within the exclusion zone of water

Chi-Shuo Chen · Wei-Ju Chung · Ian C. Hsu · Chien-Ming Wu · Wei-Chun Chin

Received: 27 March 2011 / Accepted: 16 August 2011

Abstract Water molecules play critical roles in many biological functions, such as protein dynamics, enzymatic activities, and cellular responses. Previous nuclear magnetic resonance and neutron scattering studies have shown that water molecules bind to specific sites on surfaces and form localized clusters. However, most current experimental techniques cannot measure dynamic behaviors of ordered water molecules on cell-size (10 μm) scale. Recently, the long-distance effect of structured water has been demonstrated by Pollack and his colleagues. Namely, there is a structured water layer near the hydrophilic surface that can exclude solutes (Zheng et al, Adv Colloid Interface Sci 127:19–27, 2006; Pollack 2006, Adv Colloid Interface Sci 103:173–196, 2003). The repelling forces of water clusters inside this exclusion region are investigated in this study. With a laser tweezers system, we found the existence of an unexpected force fields inside the solute-free exclusion zone near a Nafion surface. Our results suggest that the water clusters could transduce mechanical signals on the micrometer range within the exclusion zone. This unexpected inhomogeneous force field near the hydrophilic surface would provide a new insight into cellular activities, leading to a potential new physical chemistry mechanism for cell biology.

Keywords Water · Exclusion zone · Nafion · Laser tweezers

1 Introduction

Water molecules play critical roles in many aspects of life, such as protein dynamics and cellular activities [4]. Nuclear magnetic resonance and neutron scattering measurements

C.-S. Chen · W.-C. Chin (✉)
Bioengineering, University of California, Merced, CA, USA
e-mail: wchin2@ucmerced.edu

W.-J. Chung · I. C. Hsu · C.-M. Wu
Department of Biomedical Engineering and Environmental Sciences,
National Tsing-Hua University, Hsinchu, Taiwan

Published online: 09 September 2011

have shown that water molecules can form localized molecular clusters on protein surfaces [5]. Recent studies also showed that solutes are excluded from the structured water layers immediately adjacent to various gel and biological surfaces. The solute-exclusion (EZ) zone is considerably larger than anticipated by conventional theories: nominally on the order of 100 μm or more [1]. The identification of the EZ zone provides unique opportunities to understand the basic mechanism of biomolecular interactions within water structures and to explore the importance of water organization in life [6].

The concept of layered or "structured" water has a long history, which began with a hypothesis put forth a century ago by Fischer and Moore [7]. The idea was strongly advocated by the Hungarian biophysics school [8]. Gilbert Ling suggested that structuring originated at charged protein surfaces, to which water molecules would associate because of their polar nature [9]. Once a single layer adhered, additional layers would adhere one upon another to form a layered network [10, 11]. Structured water was also the centerpiece of Albert Szent-Gyorgyi's classic book (1972), in which interactions between macromolecules and surrounding water were argued to be the living state's dominant feature [12].

Modern biophysical approaches have begun addressing water layers in a more quantitative way, particularly using the surface-force apparatus and atomic force microscopy [13]. Classical (such as DLVO) theory predicts that as surface-to-surface separation diminishes, the force will increase monotonically (ultimately diminishing sharply as the surfaces get extremely close together). But experimental results indicate that the force is oscillatory. Different solvents have been used and in each instance the spatial period of the oscillation was equal to the diameter of the sandwiched (solvent) molecules [13, 14]. These experiments confirm that layering of solvent molecules between closely juxtaposed, charged surfaces is possible, although the exact mechanism of layering is still unsettled and may not involve dipolar structuring [15].

Since Ashkin established the laser-based optical trapping in early 1970s, the applications of laser tweezers have been demonstrated in many biophysical studies [16–23]. In the single beam laser tweezers systems, most platforms are based on modified microscopes. Briefly, with different optical designs and settings [20–23], the parallel laser beam passed through a high numerical aperture microscopy objective is highly focused on the sample plane. The targeted samples are trapped within the high gradient energy field generated by the focused laser beam. Two different theoretical models (Mie scattering and Rayleigh scattering) have been developed to interpret the trapping mechanism, and mainly depends on the diameters of trapped samples [21, 22]. Near the central equilibrium region of the laser beam, the force applied on the trapped sample is a function of the displacement of the sample from the gradient centers, refractive index of the sample and surrounding solution, laser power, and the gradient of the focused laser beam [18, 21]. By measuring the sample displacement, the displacement can be converted into the force applied on the targeted samples. Because of the high spatial resolution (∼nm) and precise force measurement (pN), this non-destructive tool has been intensively applied in various biophysical studies, such as kinesin stepping, DNA structure, enzyme affinity, etc [19, 21, 23–25].

Although the EZ zone has been demonstrated as a general phenomenon in the vicinity of various hydrophilic surfaces [1, 26], the properties of force-caused exclusion is not yet understood. Moreover, the establishment of a feasible platform to explore the molecular interactions in structured water networks (EZ zone) is critical and necessary. Hence, we investigate the potential of an optical tweezers system to measure the force field in the vicinity of hydrophilic surfaces. The force vectors within the EZ zone were analyzed with

different surface-modified probes. Due to the importance of force translation in cell biology, these measurements within EZ zone provide a new insight for the role of water dynamics in cellular functions.

2 Materials and methods

2.1 Laser tweezers system

To measure structured water's mechanical properties with minimum disturbance, we used a dielectric microsphere (2 μm diameter) as the force probe. The infrared laser tweezers system can be operated as a two-dimensional force measuring apparatus, applying a specific magnitude of force load to a trapped microsphere moving in designed directions [20, 27]. The applied force on the microsphere can be calculated by the microsphere's relative movement and the laser power. An inverted microscope (TE-2000E, Nikon) was modified to integrate with other optical components (Fig. 1). To achieve more precise spatial movement measurements two different lasers were set separately for trapping (1,064 nm, Nd:YVO4, BL-106C, Spectra-Physics, Newport, Irvine, CA, USA) and position detection (828 nm, LDS-series, Point Source, Optodyne, Compton, CA). The quadrant photodiode (QPD, SPOT9-DM1, UDT, San Diego, CA) was adapted to collect the movement of the probe with 20 k bandwidth. Data analysis and force calibration were performed using custom software developed using LabVIEW® (National Instruments, Austin, TX, USA) and MATLAB® (MathWorks, Natick, MA, USA) [27].

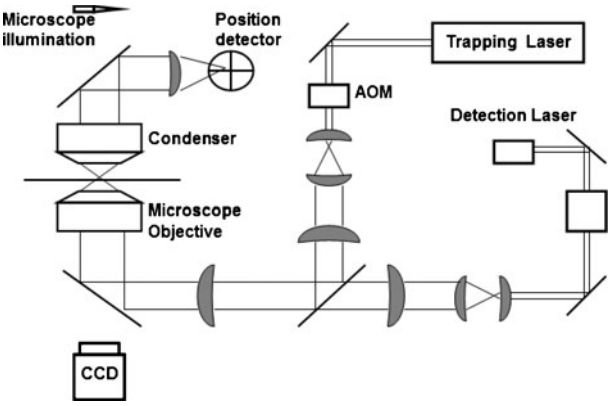

Fig. 1 Layout of IR laser tweezers system. A trap laser (1,064 nm) and a separate detection laser (828 nm) were used in our system. An acousto-optical modulator was used to steer the trap laser beam. Laser output beams were expended to overfill the back aperture of the objective. A telescopic lens was used for manually steering the position of the optical trap in the specimen plane. The laser beam was highly focused by an oil immersion objective lens (100×/N.A 1.40) to form the optical trap in the specimen plane. A computer controlled three-axis piezo stage was incorporated to provide precise specimen positioning. Trapped samples were imaged with a camera, and the forward scattered light signals were coupled onto the position detector on the back focal plane of the condenser. Scattering signals were translated into sample displacements and converted into force units with post signal processing

2.2 Exclusion zone

In previous studies, the long-impact exclusion zone was observed on the Nafion surface in aquatic environment. The width of this solute-free zone is usually several hundred micrometers from the various hydrophilic surfaces [1]. Various ions, such as imidazole or TES (2-[[1,3-dihydroxy-2-(hydroxymethyl)propan-2-yl]amino]ethanesulfonic acid), and different ion concentrations are applied to influence the formation of the EZ zone [28]. Similar EZ zones have been reported in polar solvents as well [26]. Here, we placed a Nafion film into the glass slide chamber with 10 mM imidazole solution as described previously [1, 26].

2.3 Experimental methods

To measure the force field within the exclusion zone, we trapped single microsphere in the laser beam center and dragged the microsphere toward the hydrophilic surface. Force calibration can be achieved with determined stiffness of the optical trap and measured displacement from the equilibrium trap position [21]; through Hooke's law $F = -\alpha\chi$, where F is the applied force, α is the stiffness, and χ is the displacement. The stiffness of the optical trap mainly depends on the laser power, light wavelength, and trapped bead diameters. In each set of experiments, laser power and other parameters were kept constant, and 2 μm polystyrene microspheres with differ surface modifications were used as our scanning probes [21]. Once microspheres of known radius are trapped, the physics of Brownian motion in a harmonic potential can be used to obtain the stiffness. The thermal fluctuations of the trapped bead can be described as a Lorentzian spectrum [21]. The power spectrum can be fit with a rolloff frequency, from which the stiffness can be calculated [21]. The applied force can be determined by measured displacements from the equilibrium trap position multiplied by the known stiffness.

3 Results

A distinct EZ zone formed next to the surface 5 minutes after Nafion surface was placed in 10 mM imidazole solution (Fig. 2). To measure the mechanical force in the EZ zone, 2 μm non-functionalized polystyrene microspheres were used as the force sensing probe. To calibrate the force probe, we set a lower optical trap stiffness ($\sim 8.2 \times 10^{-6}$ N/m), which is more sensitive to the force changes induced by the environment. Then, the laser beam was moved 1 mm away from the Nafion surface, and the microsphere was trapped at the equilibrium position within the laser beam. The piezo stage was adapted to preciously control the distance between the force probe and the Nafion surface. Under different distance settings, the displacements of the microsphere from the equilibrium center were recorded and converted into the force applied by the EZ zone. The results showed that the repelling force decreases from 3 to 0 pN as the distance increases from the surface to 60 μm. The exclusion range was consistent with previous studies [1, 26]. However, the data demonstrated the force field is not homogeneous throughout the exclusion zone, but is a rather a gradient field across the region (Fig. 3). Once the microsphere was dragged closer to the surface (~10 μm), the force applied by the optical trap was not sufficient to overcome the repelling force from the EZ zone. The trapped microsphere was pushed out from the equilibrium position and escaped from the laser beam. An impenetrable barrier exists close to the hydrophilic surface (~10 μm).

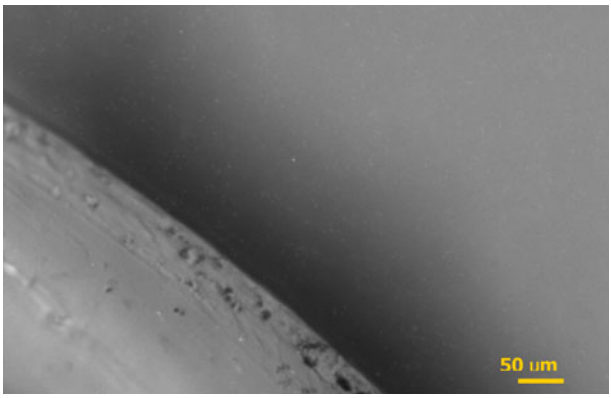

Fig. 2 The exclusion zone under fluorescence microscopy. Nafion film is placed in the glass slide chamber with 10 mM imidazole solution: the microsphere (2 μm) exclusion formed in the vicinity of the Nafion surface and lasted for more than 1 h. Force field measurements were performed under the same condition

To further study the impenetrable barrier, under the same experimental settings, we increased the stiffness of the optical trap (1.78×10^{-5} N/m) with a higher laser intensity (100 mW). The results showed the repelling force increases from 0 to 0.5 pN at 60 μm away from the surface. The observed EZ expansion phenomenon here was consistent with a previous observation [29]. With stronger applied force (∼3.5 pN), the trapped microsphere can be pushed much closer to the surface (∼5 μm).

In our study, various microspheres, 2 μm polystyrene microspheres with non-functionalized, amine-functionalized and carboxyl-functionalized surfaces, were used as force probes. We measured the magnitude of the repelling (+)/attracting (−) force applied on the trapped microsphere within the exclusion zone with micrometer spatial resolution. The results showed the different force response with three different surface modifications of the microspheres (Fig. 4). The repelling force, ranging from 1 to 5 pN, applied on non-functionalized/carboxyl-functionalized microspheres. In contrast, there was an attracting force (approximately −1 to −3 pN) pulling positive-charged microspheres toward the surface. Though the force response curves are variable, similar impermeable barriers (∼10 μm from the surface) were observed under all experimental conditions with the same probe stiffness.

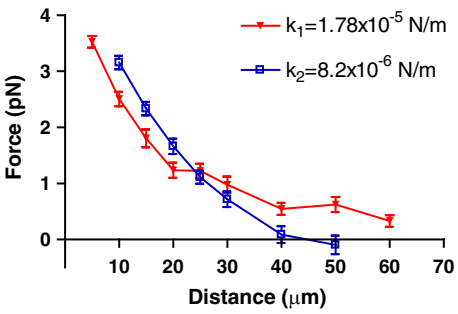

Fig. 3 The force response curves of hydrophobic microspheres as a function of the distance from the Nafion surface. The distance shown on the x-axis indicates the microsphere's relative position to the film surface, and the exclusion force extended to tens of micrometers under both laser tweezers stiffness settings

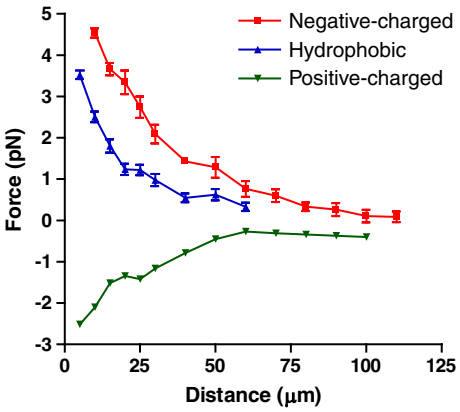

Fig. 4 The different force response curves of microspheres with three different surface modifications. On the y-axis, we defined the force direction as positive while a microsphere experienced the repelling force opposite to the Nafion surface

4 Discussion

The EZ zone has been identified near many types of surfaces, including various biological or synthetic gel surfaces [1]. Our results clearly demonstrate the existence of forces as a function of distance from the surface within the EZ zone. We also confirmed that the range of this force extends more than 50 μm from the surface (Fig. 3), and that the gradient profiles are relatively consistent with the stable charge potential profile demonstrated in a previous study [1]. The negative potential gradients sustained within the EZ zone were proposed to result from the formation of organized water networks and induced dipoles on water molecules (Figs. 4 and 5).

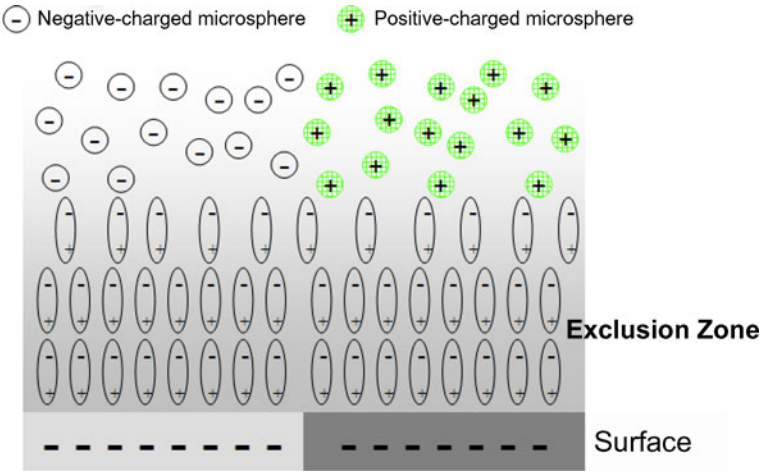

Fig. 5 Water molecules in the exclusion zone "imprint" the charge distribution by dipole arrangement. Charged microspheres are excluded to show the charge-distribution information preserved in the exclusion zone by water molecules

Through the interaction of dipole–dipole interactions, surface charges and hydrogen bonds, various simulation models have been developed to investigate the orientation and dynamics of water networks in the vicinity of various surfaces [30–33]. Though the mechanism of the long-distance force gradient is elusive, we hypothesize that the force transformation within the EZ zone is relative to the water structure and induced dipoles (Fig. 5). Our results show that different charged microspheres experienced different force fields near a Nafion surface (negative surface). For neutral and negative microspheres, the gradient repulsive force field was recorded up to 50 μm away from the Nafion surface. The repelling force may from the exclusive effect for water network formation. The larger force field applied on the carboxyl-functionalized microsphere may come from a synergistic effect of the negative induced dipoles and water structure. In the region far from the surface, the negative charge gradient may potentially dominate the attractive forces found for positive microspheres within the EZ zone; however, due to the compact formation of structured water networks, positive microspheres are excluded from this region closer to the Nafion surface (∼10 μm) (Fig. 5).

Water structures play critical roles on different biological scales. On a biomolecular level, water molecules attached to specific sites of biomolecules and influence their activities [34, 35]; the water molecules form specific organization that are proposed to influence the cytoskeletons [15, 34]; a long distance of repulsion was also observed in the vicinity of rabbit psoas muscle samples. However, the lack of adequate tools limits the investigation of biomolecular interactions in water structures (networks). In our study, we demonstrated the specific directional pico-Newton scale force field recorded by laser tweezers systems that also have been successfully applied to various biomolecular studies, such as enzyme kinetics and DNA structure folding [23, 24]. In addition to the demonstration of the feasibility of optical tweezers systems in structured water studies, our results also provide much-needed experimental evidence for the exclusive forces within the EZ zone.

Acknowledgements This work was in part supported by the National Science Foundation (CBET-0932404). Chi-Shuo Chen was supported by UC Merced Center of Excellence on Health Disparities (1P20MD005049-01 from the National Center on Minority Health and Health Disparities) and Jane Vilas Fellowship.

References

1. Zheng, J.-M., Chin, W.-C., Khijniak, E., Khijniak, J.E., Pollack, G.H.: Surfaces and interfacial water: evidence that hydrophilic surfaces have long-range impact. Adv. Colloid Interface Sci. **127**, 19–27 (2006)
2. Pollack, G.H.: Water and the Cell. Springer, New York (2006)
3. Pollack, G.H.: The role of aqueous interfaces in the cell. Adv. Colloid Interface Sci. **103**, 173–196 (2003)
4. Wiggins, P.M.: Role of water in some biological processes. Microbiol. Rev. **54**, 432–449 (1990)
5. Chaplin, M.F.: The memory of water: an overview. Homeopathy **96**, 143–150 (2007)
6. Wilson, E.K.: Watering down science? Chem. Eng. News **87**, 32–33 (2009)
7. Fischer, M.H., Moore, G.: On the swelling of fibrin. Am. J. Physiol. **20**, 330–342 (1907)
8. Ernst, E.: Bound water in physics and biology. Acta Biochim. Biophys. Acad. Sci. Hung. **5**, 57–69 (1970)
9. Ling, G.N.: Physical state of water in living cell and model systems. Ann. N.Y. Acad. Sci. **125**, 401–417 (1965)
10. Ling, G.N.: Life at the Cell and Below Cell Level. Pacific, New York (2001)
11. Ling, G.N.: In Search of the Physical Basis of Life. Plenum, New York (1984)
12. Szent-Gyorgyi, A.: The Living State: with Remarks on Cancer. Academic Press, New York (1972)
13. Israelachvili, J.N., McGuiggan, P.M.: Forces between surfaces in liquids. Science **241**, 795–800 (1988)
14. Israelachvili, J., Wennerstrom, H.: Role of hydration and water structure in biological and colloidal interactions. Nature **379**, 219–225 (1996)

15. Rand, R.P., Parsegian, V.A., Rau, D.C.: Intracellular osmotic action. Cell. Mol. Life Sci. **57**, 1018–1032 (2000)
16. Ashkin, A., Dziedzic, J.M.: Optical trapping and manipulation of viruses and bacteria. Science **235**, 1517–1520 (1987)
17. Ashkin, A., Dziedzic, J.M., Bjorkholm, J.E., Chu, S.: Observation of a single-beam gradient force optical trap for dielectric particles. Opt. Lett. **11**, 288 (1986)
18. Ashkin, A., Dziedzic, J.M., Yamane, T.: Optical trapping and manipulation of single cells using infrared laser beams. Nature **330**, 769–771 (1987)
19. Ashkin, A., Schutze, K., Dziedzic, J.M., Euteneuer, U., Schliwa, M.: Force generation of organelle transport measured in vivo by an infrared laser trap. Nature **348**, 346–348 (1990)
20. Lang, M.J., Asbury, C.L., Shaevitz, J.W., Block, S.M.: An automated two-dimensional optical force clamp for single molecule studies. Biophys. J. **83**, 491–501 (2002)
21. Neuman, K.C., Block, S.M.: Optical trapping. Rev. Sci. Instrum. **75**, 2787–2809 (2004)
22. Svoboda, K., Block, S.M.: Optical trapping of metallic Rayleigh particles. Opt. Lett. **19**, 930–932 (1994)
23. Wang, M.D., Yin, H., Landick, R., Gelles, J., Block, S.M.: Stretching DNA with optical tweezers. Biophys. J. **72**, 1335–1346 (1997)
24. Bustamante, C., Smith, S.B., Liphardt, J., Smith, D.: Single-molecule studies of DNA mechanics. Curr. Opin. Struct. Biol. **10**, 279–285 (2000)
25. Svoboda, K., Block, S.M.: Force and velocity measured for single kinesin molecules. Cell **77**, 773–784 (1994)
26. Chai, B., Pollack, G.H.: Solute-free interfacial zones in polar liquids. J. Phys. Chem. B **114**, 5371–5375 (2010)
27. Yang, T.S., Cui, Y., Wu, C.M., Lo, J.M., Chiang, C.S., Shu, W.Y., Chung, W.J., Yu, C.S., Chiang, K.N., Hsu, I.C.: Determining the zero-force binding energetics of an intercalated DNA complex by a single-molecule approach. Chemphyschem **10**, 2791–2794 (2009)
28. Zheng, J.-M., Wexler, A., Pollack, G.H.: Effect of buffers on aqueous solute-exclusion zones around ion-exchange resins. J. Colloid Interface Sci. **332**, 511–514 (2009)
29. Chai, B., Yoo, H., Pollack, G.H.: Effect of radiant energy on near-surface water. J. Phys. Chem. B **113**, 13953–13958 (2009)
30. Marry, V., Rotenberg, B., Turq, P.: Structure and dynamics of water at a clay surface from molecular dynamics simulation. Phys. Chem. Chem. Phys. **10**, 4802–4813 (2008)
31. Mittal, J., Hummer, G.: Static and dynamic correlations in water at hydrophobic interfaces. Proc. Natl. Acad. Sci. U. S. A. **105**, 20130–20135 (2008)
32. Lambeth, B.P., Junghans, C., Kremer, K., Clementi, C., Delle Site, L.: Communication: On the locality of hydrogen bond networks at hydrophobic interfaces. J. Chem. Phys. **133**, 221101 (2010)
33. Koefinger, J., Hummer, G., Dellago, C.: Macroscopically ordered water in nanopores. Proc. Natl. Acad. Sci. U. S. A. **105**, 13218–13222 (2008)
34. Chaplin, M.: Do we underestimate the importance of water in cell biology? Nat. Rev. Mol. Cell Biol. **7**, 861–866 (2006)
35. Chaplin, M.F.: Water: its importance to life. Biochem. Mol. Biol. Educ. **29**, 54–59 (2001)

Human stem cell neuronal differentiation on silk-carbon nanotube composite

Chi-Shuo Chen[1], Sushant Soni[1], Catherine Le[2], Matthew Biasca[2], Erik Farr[2], Eric Y-T Chen[1], and Wei-Chun Chin*[1]

[1]Bioengineering Program, School of Engineering, University of California, Merced, CA, USA
[2]School of Nature Sciences, University of California, Merced, CA, USA

*Corresponding author: wchin2@ucmerced.edu

Email addresses:
CSC: cchen32@ucmerced.edu
SS: ssoni@ucmerced.edu
CL: cle24@ucmerced.edu
MB: mbiasca@ucmerced.edu
EF: efarr@ucmerced.edu
EYTC: echen6@ucmerced.edu
WCC: wchin2@ucmerced.edu

Abstract
Human embryonic stem cells [hESCs] are able to differentiate into specific lineages corresponding to regulated spatial and temporal signals. This unique attribute holds great promise for regenerative medicine and cell-based therapy for many human diseases such as spinal cord injury [SCI] and multiple sclerosis [MS]. Carbon nanotubes [CNTs] have been successfully used to promote neuronal differentiation, and silk has been widely applied in tissue engineering. This study aims to build silk-CNT composite scaffolds for improved neuron differentiation efficiency from hESCs.

Two neuronal markers (β-III tubulin and nestin) were utilized to determine the hESC neuronal lineage differentiation. In addition, axonal lengths were measured to evaluate the progress of neuronal development. The results demonstrated that cells on silk-CNT scaffolds have a higher β-III tubulin and nestin expression, suggesting augmented neuronal differentiation. In addition, longer axons with higher density were found to associate with silk-CNT scaffolds.

Our silk-CNT-based composite scaffolds can promote neuronal differentiation of hESCs. The silk-CNT composite scaffolds developed here can serve as efficient supporting matrices for stem cell-derived neuronal transplants, offering a promising opportunity for nerve repair treatments for SCI and MS patients.

Keywords: CNT; silk; fibroin; human stem cell; neuron differentiation; scaffold.

Background
There are about 250,000 to 400,000 patients in the US suffering from spinal cord injury [SCI] [1], usually due to trauma or traffic accidents, which could lead to death or life-long paralysis. According to the National Multiple Sclerosis Society, there are about 400,000 multiple sclerosis [MS] patients in the US, and this number is steadily growing: about 200 people are diagnosed each week. Currently, there is no effective cure for SCI or MS since adult humans do not fully regenerate their damaged neurons and axons. The inability for the body to regenerate and re-innervate target neuronal axons greatly limits therapy feasibility [1, 2]. The unique abilities of human embryonic stem cells [hESCs] - namely, their self-renewal and potency - hold great promise for regenerative medicine. For SCI and MS patients, the capacity of hESCs to differentiate into specific neuronal lineages through effective induction is highly encouraging. The unique appeal of hESC-based transplantation for SCI and MS is the possibility of those transplanted cells to repair damaged neuronal tissues. However, the harsh microenvironment and the lack of supportive substrates during transplantation result in a low survival rate of transplanted cells and diminish the feasibility of stem cell-related cell therapy [3]. In regenerative medicine and tissue engineering, both naturally derived and synthetic materials have been extensively explored and provided their respective advantages [4]. For instance, nanofibers incorporated with the pentapeptide epitope, isolucine-lysin-valine-alanine-valine, were constructed to induce rapid differentiation of cells into neurons. Biomaterials synthesized with synthetic or natural polymers were fabricated to facilitate the complex tissue formations [4-9]. Generally, due to their inherent properties of biological recognition, extracted natural proteins present better cell-triggered proteolysis degradation and biocompatibility; synthetic materials provide more flexible material properties with specific designs. In this study, we aimed to integrate

natural silk fibroin protein with synthetic carbon nanotubes [CNTs] to construct scaffolds for neuronal developments.

CNTs are a conductive biomaterial with sizes comparable to extracellular matrix molecules such as collagens and laminins, which have been reported to favor neuronal growth [10, 11]. In addition, due to their excellent mechanical strength and flexibility, CNTs can contribute to the structural integrity of scaffolds. Substrates prepared with CNTs have been demonstrated to be biocompatible and can support neuronal growth and differentiation [10]. It has also been proposed that neurons grown on a CNT meshwork displayed better signal transmission, possibly due to tight contacts between the CNTs and neural membranes, favoring electrical shortcuts [12]. All of the above characteristics make CNTs a promising biomaterial to repair damaged neuronal tissues.

Silks are natural polymers (protein) that have been widely used as biomaterials for many years. Fibroin protein is extracted from silk (*Bombyx mori*), consisting of 90% of amino acids such as glycine, alanine, and serine. Various ratios of amino acids are distributed on the supramolecular structure of fibroin, consisting of a hydrophobic heavy chain (350 kD to 370 kD) and hydrophilic light chain (25 kD) [13, 14]. Due to its mechanically robust and flexible nature in thin film form, biocompatibility, and *in vivo* reabsorbing and water-dissolvable properties, fibroin protein has been used as a building material for scaffolds for various tissue engineering applications and stem cell researches [8, 15-18]. For instance, fibroin scaffolds have been successfully applied to human mesenchymal stem cell differentiation, especially for ligament, bone, or cartilage tissue engineering [17, 19]. In addition, successful bio-integrated electronics has been developed based on dissolvable silk fibroin films [20].

Unmodified CNTs tend to aggregate rather than disperse in aqueous solutions due to their hydrophobic nature. These heterogeneous aggregations of CNTs not only bring about difficulties in scaffold preparation, but also limit their applications. In an effort to resolve this problem, various surfactants were adapted to disaggregate and uniformly disperse CNTs in different solvents. However, the bio-toxicity of residuals still remains as one of the major concerns for cell scaffolding fabrication [21-23]. Since fibroin consists of 75% of nonpolar hydrophobic amino acids [14], it has been shown that the amphiphilic fibroin protein can effectively serve as a dispersant for CNTs [24]. Here, we used fibroin extraction to disperse CNTs homogeneously to build silk-CNT composite scaffolds. This study aims to combine the unique advantages of these two biocompatible materials to build silk-CNT scaffolds in order to acquire sufficient neuronal differentiation efficiency from hESCs for effective neuronal cell transplantation.

Methods

Silk fibroin preparation

Based on the protocol published by Kaplan et al. [7, 8], *B. mori* silk was in boiling 0.02 M Na_2CO_3 (Sigma-Aldrich, St. Louis, MO, USA) for 1 h and rinsed thoroughly with deionized [DI] water to remove sericin protein associated with fibroin. The washed silk was then dissolved in 9.3 M LiBr (Fisher Scientific, Pittsburgh, PA, USA) for 3 h at 60°C. The fibroin solution was then dialyzed (MWCO 1,000, Spectrum Laboratories, Inc., Rancho Dominguez, CA, USA) in DI water for 48 h.

Following which, the silk solution was centrifuged at 800×*g*, and the supernatant was collected [25].

Silk-CNT scaffolds and poly-L-ornithine coating

Multi-wall CNTs [MWCNTs] (Nano-Lab, Waltham, MA, USA) were dispersed in DI water and sonicated for 2 h to help disperse the MWCNT. Glass micro-coverslips were boiled in a mild surfactant for 30 min and rinsed with DI water. The coverslips were then washed with 2 N HCl overnight and cleaned with DI water. The concentration of the MWCNT/silk mixture was 1 mg/ml MWCNT in 2 wt.% silk fibroin solution. For the preparation of silk scaffolding, 600 µl of 2 wt.% silk fibroin solution was deposited on the coverslip surface at 60°C. Silk-CNT scaffolds were prepared with the silk-CNT mixed solution following a similar protocol. In order to increase cell attachment on silk fibroin [26], laminin (20 µg/ml, Sigma-Aldrich, St. Louis, MO, USA) was used to coat the scaffold surfaces [27]. Poly-L-ornithine [PLO] (Sigma-Aldrich, St Louis, MO, USA), a common substrate for neuronal differentiation, was used as the control substrate coating. PLO solution (0.1 mg/ml) was applied to the coverslip surface and incubated at 37°C overnight. Excess PLO solution was aspirated; then, the surface was rinsed with DPBS before use [27]. Silk-CNT substrates were exposed to UV for 1 h for sterilization purposes.

Maintenance and differentiation of human embryonic stem cells

H9 hESC lines from Wicell (Madison, WI, USA; passage 32 to 55) were cultured on feeder layers of mitomycin C-treated mouse embryonic fibroblasts [MEFs] as described in our previous study [13]. The medium was changed daily, and differentiated cells were moved manually after 7 days.

The hESC cell colonies were detached from the MEF feeder layer with dispase (1 U/ml) and transferred to ultra-low contact wells. The suspended hESCs aggregated as an embryoid body [EB] and was allowed to grow for 4 to 6 days before plating on substrates. With respect to the influence of cell density on differentiations, seven to ten EB cell aggregations were seeded onto each PLO, silk, and silk/CNT substrates, with a neuron induction medium consisting of F12/DMEM, N2 supplement, and FGF2 (20 ng/ml). The medium was changed once daily for the first 2 days and then once every other day.

Immunocytochemistry and fluorescence measurements

We stained cells using β-III tubulin (Millipore Co., Billerica, MA, USA) as a marker for neuronal differentiation with a ratio of 1:500, nestin (Millipore Co., Billerica, MA, USA) as markers for motor neuron progenitor [10], and DAPI (Invitrogen, Carlsbad, CA, USA) as nuclei markers. Cells were fixed with 4% paraformaldehyde on the seventh day for immunostaining.

Images were taken with a Nikon Eclipse TE2000-U fluorescent microscope (Nikon, Tokyo, Japan). Fluorescence intensities and axon lengths were quantified using an image analysis software (SimplePCI, Compix Inc., Sewickley, PA, USA). Statistical analysis was performed using the paired Student's *t* test.

Scanning electron microscopy

Scanning electron microscopy [SEM] was used to investigate the substrate degradation and morphology of cells grown on the different substrates. The cells were

fixed with 4% paraformaldehyde in PBS at 4°C for 20 min, followed by a series of ethanol dehydration. Carbon dioxide critical point drying was preformed to avoid specimen distortion during the drying process. The specimens were sputter-coated with a 500-Å gold thin film and examined using FEI Quanta 200 ESEM (FEI Co., Hillsboro, OR, USA).

Results and discussion

Flexible silk-CNT scaffold

The MWCNT solution exhibits a homogeneous distribution in 2 wt.% of silk fibroin solution (Figure 1a). Silk-CNT scaffolding was prepared as described, and the silk fibroin film can be peeled from the glass substrate after desiccation. Compared to the CNT embedded in fibroin matrix, CNTs deposited along the glass surface resulted in aggregated clusters in the cell culture medium (Figure 1b,c).

CNTs have been demonstrated to stimulate neuronal differentiation [6, 8]; however, CNTs are easily disintegrated without supporting matrices and require delicate handling and intensive labor. Here, we used fibroin to provide mechanical and structural support for CNT-based scaffolds (Figure 1b). The amphiphilic properties of natural silk fibroin protein can not only disperse CNTs, but also form a polymer matrix to hold CNTs within its polymer network. In comparison to other hydrogels used in tissue engineering, the fibroin matrix can provide sufficient mechanical strength for transplant applications [28].

hESCs grown on silk-CNT scaffold

In our study, a neuronal marker, β-III tubulin, was used to label differentiated neural cells from hESCs cultured on silk-CNT scaffolds, silk scaffolds, and PLO substrates [29]. Distinct neuron somas and axon shootings on silk-CNT substrates were observed (Figure 2c). Cells on silk scaffolds exhibited limited neuronal differentiation. The standard substrate for neuronal differentiation, PLO, supported moderate neuronal differentiation compared to silk-CNT scaffolds. Longer axons with higher density were found on silk-CNT composite scaffolds compared with those on the silk substrate or PLO coating (Figure 2a).

Neuronal differentiation efficiency with image analysis

Two neuronal markers (β-III tubulin and nestin) were used to further determine the hESC differentiation efficiency. Here, β-III tubulin was used to represent the mature differentiated neurons, and nestin represented the neuron precursors [29, 30]. The image analysis results showed that the expression level of β-III tubulin and nestin was highly upregulated in hESCs grown on the silk-CNT substrate ($P < 0.001$, compared to the expression level of cells grown on the PLO substrate, Figure 3). However, fewer neuron cell bodies and little to no axon shootings were found on substrates derived from silk alone compared to cells on the silk-CNT substrate. The axonal lengths of neurons grown on different substrates were measured using the image analysis software as described. Results demonstrated that there is no significant difference between the axon length of cells grown on silk-CNT and PLO substrates ($P = 0.08$), but significantly shorter axons were associated with cells on the silk substrate (Figure 4).

Cell morphology and silk-CNT substrate degradation

We used SEM to investigate the cell morphology on different culturing substrates. Stem cells were grown on various substrates for 7 days with the neuron-inducing medium before fixation. Obvious axon extensions were observed with attached differentiated neuronal cells (Figure 5a,b,c). In comparison to the cells cultured on silk-CNT scaffolds, most of the cells exhibited a flatter morphology with axonal connections limited to two dimensions. Although cells cultured on the PLO-coated glass exhibited long axonal extensions, the spatial density distribution of axonal networks was lower than that on silk-CNT. Cells grown on the silk substrate exhibited three-dimensional [3-D] morphology; however, the cells demonstrated limited axonal extensions along with unstable adhesion to the scaffold. In the case of the cells cultured on silk-CNT scaffolds, dense complex three-dimensional axonal bundle networks were observed. The SEM images further confirmed the results of the image analysis.

Both silk and silk-CNT substrates began to degrade and became more brittle during incubation. After 7 days of incubation with hESCs, fibroin fragments were present under light microscopy. We further investigated the substrate degradation with SEM. In contrast to the flat surface properties shown in both PLO and silk substrates, spherical silk-CNT aggregations were found in the silk-CNT composite (Figure 6C). Those silk-CNT microaggregates ranged from a few microns to tens of microns. After 7 days incubation, three-dimensional porous structures were observed on silk-CNT matrices. There were no distinguished microstructures found on either PLO or silk only substrates. Those porous structures of silk-CNT substrates may provide a higher surface area for cell-substrate interactions and sufficient space for neuron axon extension. Results showed that long axons from the soma extended into the space between silk-CNT fragments. In SEM images, we also noticed that some neuronal cells may migrate into the degraded parts of silk-CNT scaffolds (Figure 5 and 6). The degradation of fibroin-based scaffolds could contribute to the infiltration of cells into three-dimensional matrices (Figure 5 and 6). Confocal laser scanning microscopy was used to confirm the three-dimensional cell growths. Differentiated neuronal cells were labeled with β-III tubulin and scanned with optical sectioning (thickness, 0.44 μm) (Figure 7). 3-D reconstructed images indicated that the cells can grow into the silk-CNT matrices for more than 50 μm. This natural biodegradation feature of the silk-CNT substrates promotes the 3-D cell growth, which resembled the more physiological environment than a two-dimensional [2-D] substrate. As a potential vehicle for neural implantations, the biodegradation of silk-CNT substrates also provides additional benefits to minimize unnecessary removal by surgical intervention.

Conclusions

In this study, our results demonstrated the potential of the silk-CNT composite as scaffolds to support neuronal differentiation for regenerative medicine (Figures 1,2,3,4). The silk-CNT composite scaffold hybridizes advantages from both naturally derived and synthetic materials; fibroin provides a mechanically robust matrix and biodegradable properties for tissue transplantation vehicles [8, 13, 15, 17]. Amphiphilic silk protein here not only provides biodegradable matrices to physically incorporate CNTs in the scaffold, but also acts as an effective dispersant to distribute CNTs homogeneously within the matrix, which is a major limitation for CNT

applications within hydrophilic networks. Additionally, CNTs embedded in the silk matrix may promote electron signal transmissions between neurons [10]. In comparison to 2-D PLO substrates, the silk-CNT composite increases neuronal differentiation and provides three-dimensional matrices for cell growth. Further observation showed that hESCs cultured on the silk-CNT scaffold exhibited higher maturity along with dense axonal projections. Our results support silk-CNT scaffolds as one viable candidate for nerve repair treatments of patients suffering from SCI or MS.

Competing interests

The authors declare that they have no competing interests.

Authors' contributions

CSC, EYTC, and WCC designed the research. CSC, SS, CL, and MB performed the research. CSC, SS, CL, EF, and MB analyzed the data, and CSC, SS, MB, EYTC, EF, and WCC wrote the paper. All authors read and approved the final manuscript.

Acknowledgments

This study was supported by a grant from the Muscular Dystrophy Association (MDA). EYC, MB, and CSC were supported by the UC Merced GRC summer fellowships, California Sea Grant traineeship, John Isaac summer scholarship, Center of Excellence on Health Disparities (1P20MD005049-01 from the National Center on Minority Health and Health Disparities), and Jane Vilas Stem Cell Fellowship.

References

1. Rolls A, Shechter R, Schwartz M: **The bright side of the glial scar in CNS repair.** *Nat Rev Neurosci* 2009, **10:**235-241.

2. Ronsyn MW, Berneman ZN, Van Tendeloo VFI, Jorens PG, Ponsaerts P: **Can cell therapy heal a spinal cord injury?** *Spinal Cord* 2008, **46:**532-539.

3. Zhang SC, Wernig M, Duncan ID, Brustle O, Thomson JA: **In vitro differentiation of transplantable neural precursors from human embryonic stem cells.** *Nat Biotechnol* 2001, **19:**1129-1133.

4. Lutolf MP, Hubbell JA: **Synthetic biomaterials as instructive extracellular microenvironments for morphogenesis in tissue engineering.** *Nature Biotechnol* 2005, **23:**47-55.

5. Silva GA, Czeisler C, Niece KL, Beniash E, Harrington DA, Kessler JA, Stupp SI: **Selective differentiation of neural progenitor cells by high-epitope density nanofibers.** *Science* 2004, **303:**1352-1355.

6. Wang Z, Ruan J, Cui D: **Advances and prospect of nanotechnology in stem cells.** *Nanoscale Res Lett* 2009, **4**:593-605.

7. Dong L, Witkowski CM, Graig MM, Greenwade MM, Joseph KL: **Cytotoxicity effects of different surfactant molecules conjugated to carbon**

nanotubes on human astrocytoma cells. *Nanoscale Res Lett* 2009, **4**:1517-1523.

8. Zhang X, Tsukada M, Morikawa H, Aojima K, Zhang G, Miura M: **Production of silk sericin/silk fibroin blend nanofibers.** *Nanoscale Res Lett* 2011, **6**:510.

9. Yu Y, Zhang Q, Mu Q, Zhang B, Yan B: **Exploring the immunotoxicity of carbon nanotubes.** *Nanoscale Res Lett* 2008, **3**:271-277.
10. Jan E, Kotov NA: **Successful differentiation of mouse neural stem cells on layer-by-layer assembled single-walled carbon nanotube composite.** *Nano Lett* 2007, **7:**1123-1128.

11. Ni Y, Hu H, Malarkey EB, Zhao B, Montana V, Haddon RC, Parpura V: **Chemically functionalized water soluble single-walled carbon nanotubes modulate neurite outgrowth.** *J Nanosci Nanotechnol* 2005, **5:**1707-1712.

12. Mazzatenta A, Giugliano M, Campidelli S, Gambazzi L, Businaro L, Markram H, Prato M, Ballerini L: **Interfacing neurons with carbon nanotubes: electrical signal transfer and synaptic stimulation in cultured brain circuits.** *J Neurosci* 2007, **27:**6931-6936.

13. Horan RL, Antle K, Collette AL, Wang Y, Huang J, Moreau JE, Volloch V, Kaplan DL, Altman GH: **In vitro degradation of silk fibroin.** *Biomaterials* 2005, **26:**3385-3393.

14. Sashina E, Bochek A, Novoselov N, Kirichenko D: **Structure and solubility of natural silk fibroin.** *Russ J Appl Chem* 2006, **79:**869-876.

15. Altman GH, Diaz F, Jakuba C, Calabro T, Horan RL, Chen J, Lu H, Richmond J, Kaplan DL: **Silk-based biomaterials.** *Biomaterials* 2003, **24:**401-416.

16. Kim UJ, Park J, Kim HJ, Wada M, Kaplan DL: **Three-dimensional aqueous-derived biomaterial scaffolds from silk fibroin.** *Biomaterials* 2005, **26:**2775-2785.

17. Wang Y, Kim HJ, Vunjak-Novakovic G, Kaplan DL: **Stem cell-based tissue engineering with silk biomaterials.** *Biomaterials* 2006, **27:**6064-6082.

18. Kim D-H, Kim Y-S, Amsden J, Panilaitis B, Kaplan DL, Omenetto FG, Zakin MR, Rogers JA: **Silicon electronics on silk as a path to bioresorbable, implantable devices.** *Appl Phys Lett* 2009, **95:**133701

19. Wang Y, Kim U-J, Blasioli DJ, Kim H-J, Kaplan DL: **In vitro cartilage tissue engineering with 3D porous aqueous-derived silk scaffolds and mesenchymal stem cells.** *Biomaterials* 2005, **26:**7082-7094.

20. Kim D-H, Viventi J, Amsden JJ, Xiao J, Vigeland L, Kim Y-S, Blanco JA, Panilaitis B, Frechette ES, Contreras D, Kaplan DL, Omenetto FG, Huang Y,

Hwang KC, Zakin MR, Litt B, Rogers JA.: **Dissolvable films of silk fibroin for ultrathin conformal bio-integrated electronics.** *Nat Mater* 2010, **9:**511-517.

21. Zheng M, Jagota A, Semke ED, Diner BA, McLean RS, Lustig SR, Richardson RE, Tassi NG: **DNA-assisted dispersion and separation of carbon nanotubes.** *Nat Mater* 2003, **2:**338-342.

22. Vaisman L, Wagner HD, Marom G: **The role of surfactants in dispersion of carbon nanotubes.** *Adv Colloid and Interface Sci* 2006, **128-130:**37-46.

23. Jiang L, Gao L, Sun J: **Production of aqueous colloidal dispersions of carbon nanotubes.** *J Colloid Interface Sci* 2003, **260:**89-94.

24. Kim H-S, Yoon SH, Kwon S-M, Jin H-J: **pH-sensitive multiwalled carbon nanotube dispersion with silk fibroins.** *Biomacromolecules* 2009, **10:**82-86.

25. Lawrence BD, Marchant JK, Pindrus MA, Omenetto FG, Kaplan DL: **Silk film biomaterials for cornea tissue engineering.** *Biomaterials* 2009, **30:**1299-1308.

26. Chen J, Altman GH, Karageorgiou V, Horan R, Collette A, Volloch V, Colabro T, Kaplan DL: **Human bone marrow stromal cell and ligament fibroblast responses on RGD-modified silk fibers.** *J Biomed Mater Res Part A* 2003, **67A:**559-570.

27. Hu B-Y, Du Z-W, Zhang S-C: **Differentiation of human oligodendrocytes from pluripotent stem cells.** *Nat Protocols* 2009, **4:**1614-1622.

28. Rockwood DN, Preda RC, Yucel T, Wang X, Lovett ML, Kaplan DL: **Materials fabrication from *Bombyx mori* silk fibroin.** *Nat Protocols* 2011, **6:**1612-1631.

29. Gage FH: **Mammalian neural stem cells.** *Science* 2000, **287:**1433-1438.

30. Barberi T, Klivenyi P, Calingasan NY, Lee H, Kawamata H, Loonam K, Perrier AL, Bruses J, Rubio ME, Topf N, Tabar V, Harrison NL, Beal MF, Moore MA, Studer L: **Neural subtype specification of fertilization and nuclear transfer embryonic stem cells and application in parkinsonian mice.** *Nature Biotechnol* 2003, **21:**1200-1207.

Figure 1. Silk dispersion and silk-CNT scaffolding. (**a**) The MWCNT dispersions in DI water (left) and silk fibroin solution (right). MWCNTs form a homogeneous and stable solution without sedimentation in silk fibroin solutions (right); on the contrary, they aggregate into large clusters in water (left). (**b**) Silk fibroin provides stable matrices to hold the CNTs in aqueous environments. (**c**) MWCNTs form large aggregates in aqueous solution (stem cell culture media).

Figure 2. Neuronal marker expression. Neuronal marker, β-tubulin III, expression of hESC cultured on (**a**) PLO exhibiting long two-dimensional axonal development with lower density, (**b**) silk scaffolds exhibiting some cell migration along with negligible axonal projections, and (**c**) silk-CNT scaffolds demonstrating three-dimensional axonal elongation as well as cell migration. Scale bar, 200 μm.

Figure 3. Expression level of β-III tubulin and nestin on PLO, silk, and silk-CNT composite substrates. Expression intensity of β-III tubulin and nestin observed with fluorescence microscopy. Silk-CNT scaffolds exhibited maximum β-III tubulin expression, while nestin expression exhibited a similar trend. Single asterisk represents $P < 0.01$, and double asterisks represent $P < 0.001$.

Figure 4. Axonal length on PLO, silk, and silk-CNT composite substrates. Axonal length measurements with β-III tubulin fluorescence images. PLO and silk-CNT substrates demonstrated similar axonal length; however, silk scaffolds induce very limited axonal length growth. Double asterisks, $P < 0.001$; NS, no statistical significance.

Figure 5. SEM images of hESCs on various substrates. SEM images of (**a**) cells cultured on PLO exhibiting a flat morphology and two-dimensional axonal connections, (**b**) cells cultured on silk scaffolds demonstrating three-dimensional structures and cell migration, and (**c**) cells cultured on silk-CNT scaffolds demonstrating three-dimenstional axonal connections and silk-CNT matrix degradation.

Figure 6. SEM image of silk-CNT composite. SEM images of PLO, silk, and silk-CNT substrates before cell seeding (**A**, **B**, **C**, respectively) and after incubating with hESCs for 7 days (**D**, **E**, **F**, respectively). On the silk-CNT surface, there were some micro silk-CNT aggregates distributed within silk matrices (C). After 7 days, the silk-CNT substrate became porous. Some neuronal axons were found to extend into those concaves on the substrate (F). Scale bar, 20 μm.

Figure 7. hESCs on 3D silk-CNT matrix. Confocal microscopy image of hESC cultured on a silk-CNT scaffold showing β-III tubulin expression in axonal shooting into three-dimensional scaffold matrices. Scale bar, 200 μm.

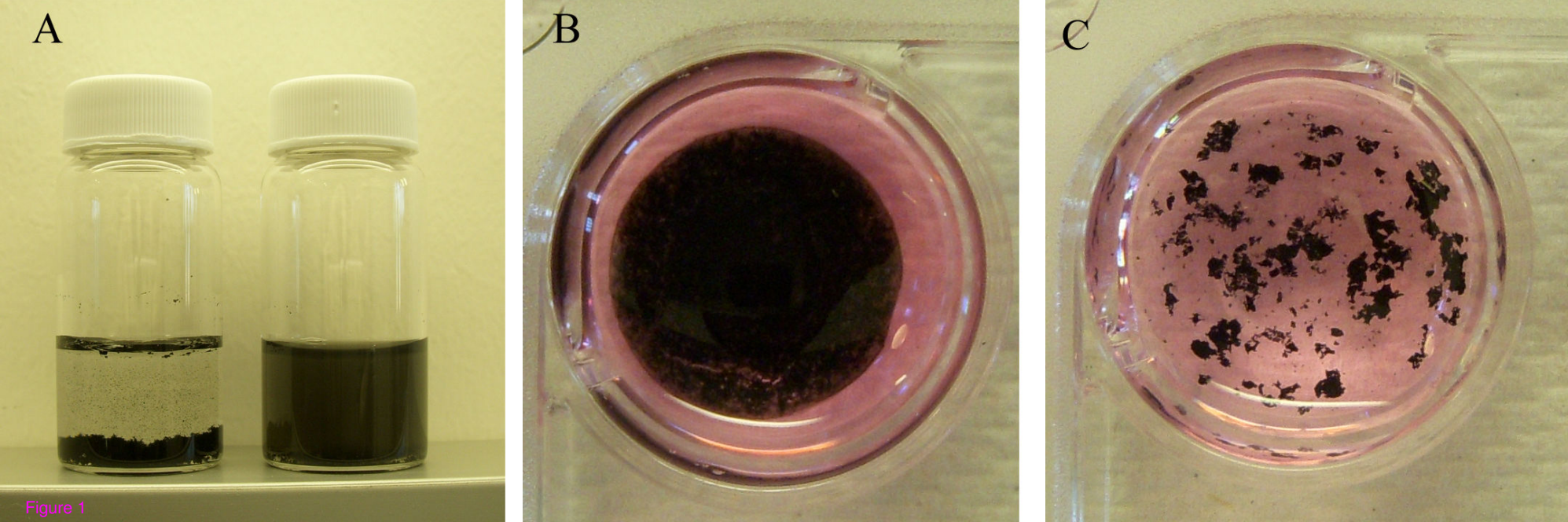

Figure 1

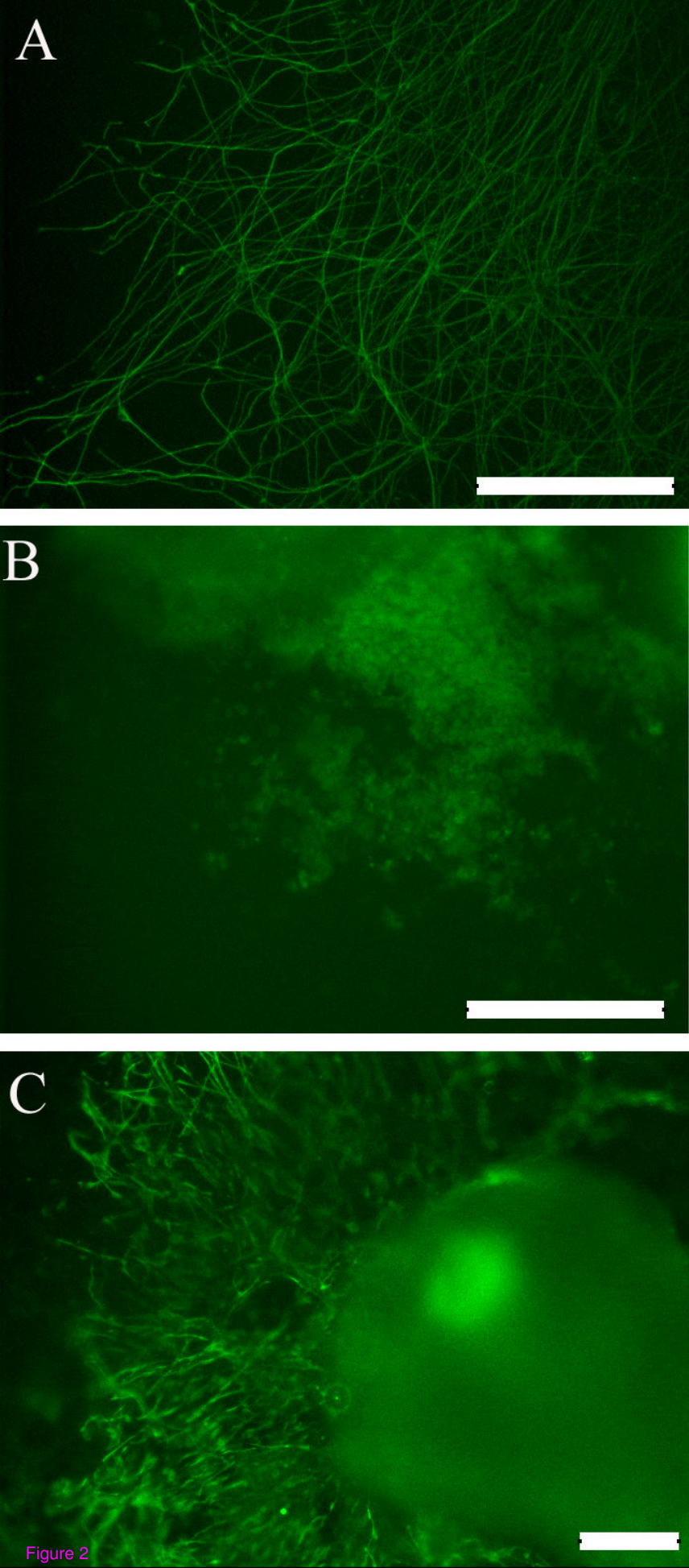

Figure 2

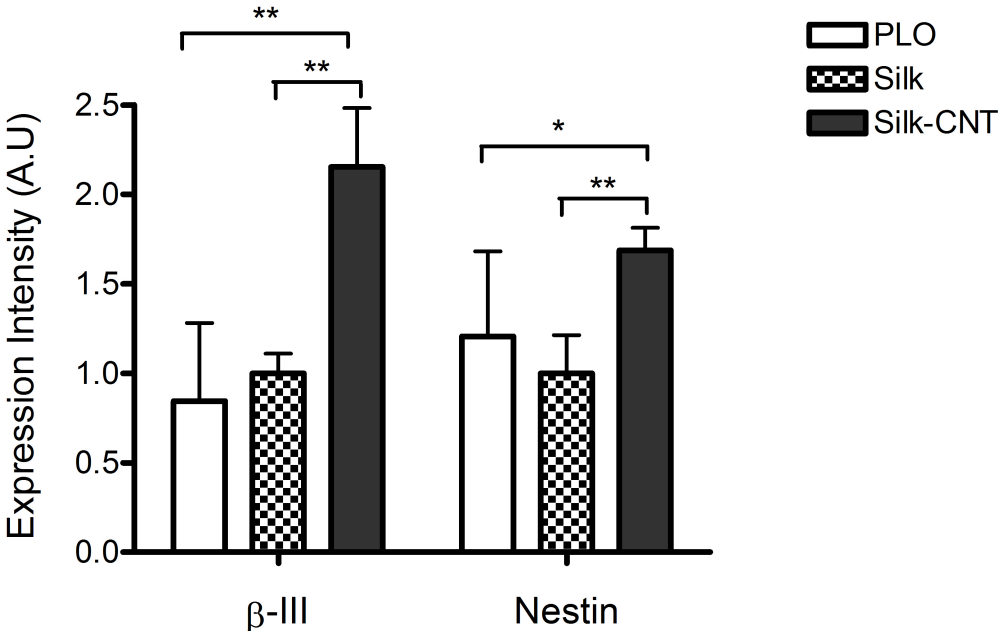
**
**
*
**
PLO
Silk
Silk-CNT
Expression Intensity (A.U)
2.5
2.0
1.5
1.0
0.5
0.0
β-III
Nestin

Figure 3

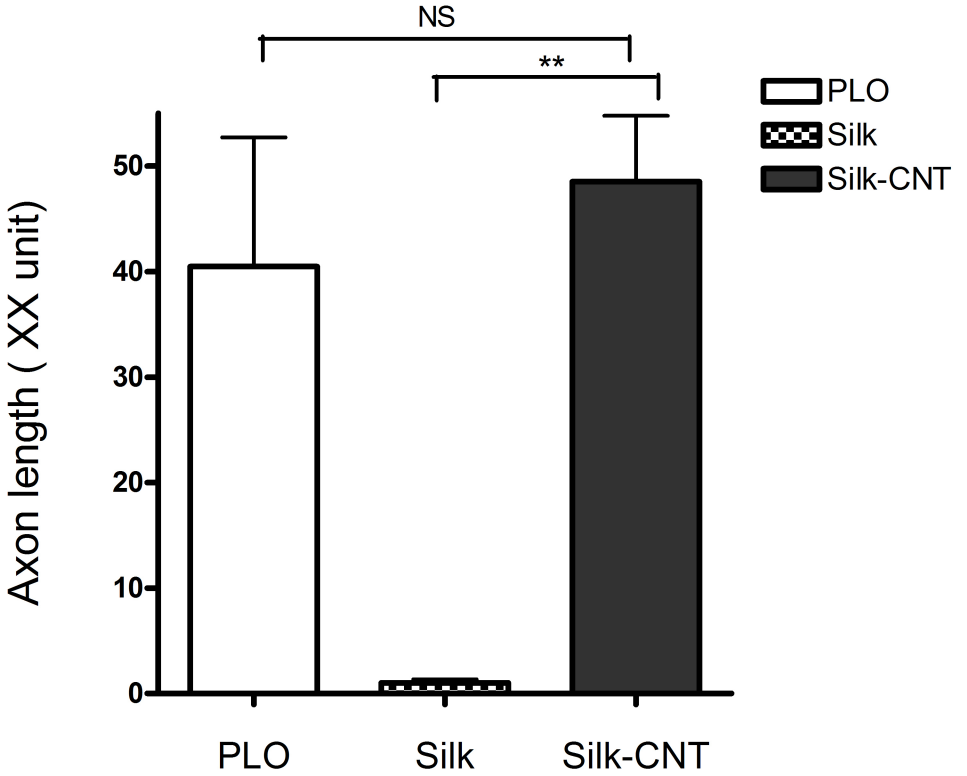
NS
**
PLO
Silk
Silk-CNT
Axon length (XX unit)
50
40
30
20
10
0
PLO
Silk
Silk-CNT

Figure 4

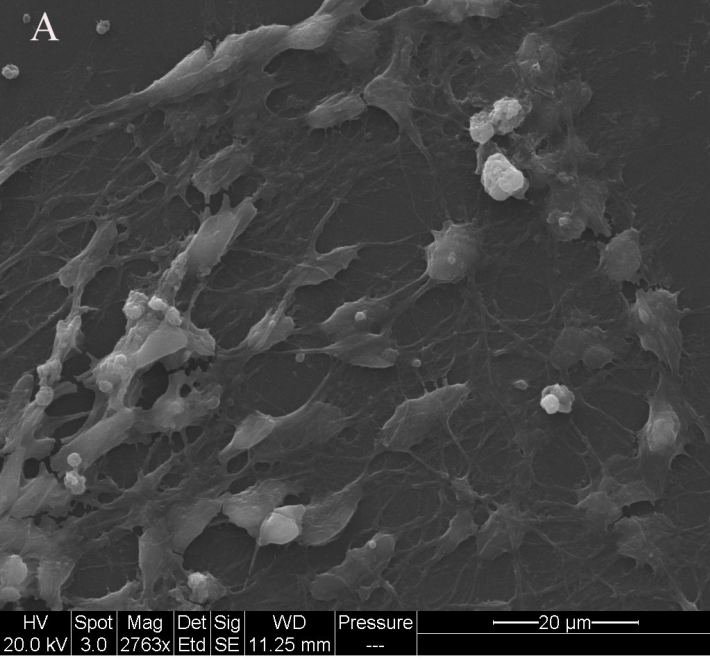
A
HV
20.0 kV
Spot
3.0
Mag
2763x
Det
Etd
Sig
SE
WD
11.25 mm
Pressure
---
20 µm

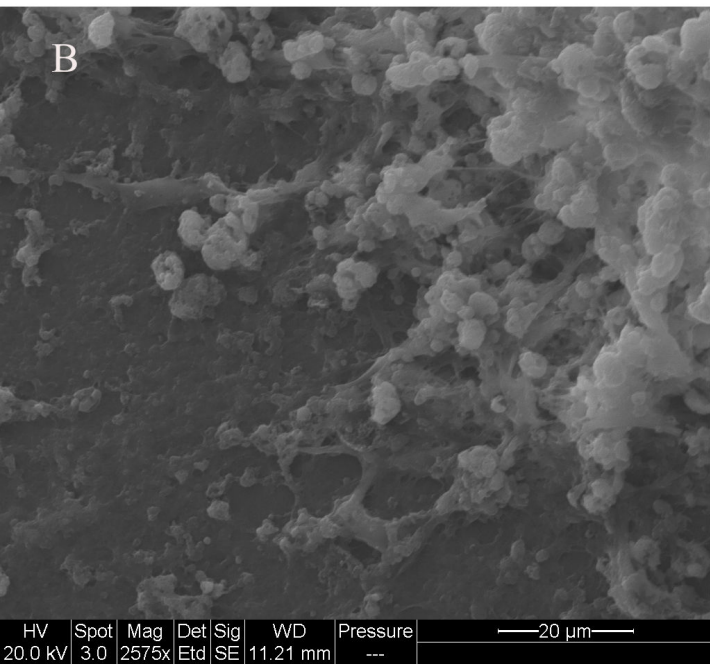
B
HV
20.0 kV
Spot
3.0
Mag
2575x
Det
Etd
Sig
SE
WD
11.21 mm
Pressure
---
20 µm

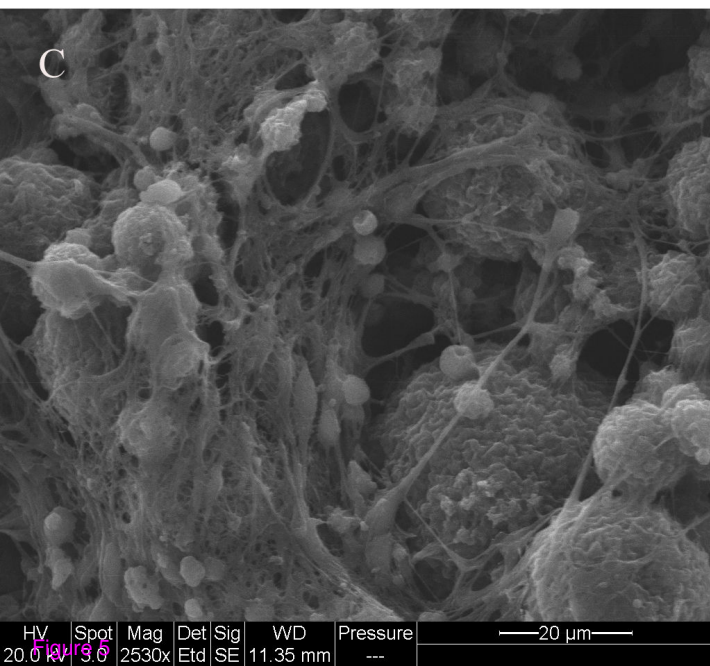
C
HV
20.0 kV
Spot
3.0
Mag
2530x
Det
Etd
Sig
SE
WD
11.35 mm
Pressure
---
20 µm

Figure 5

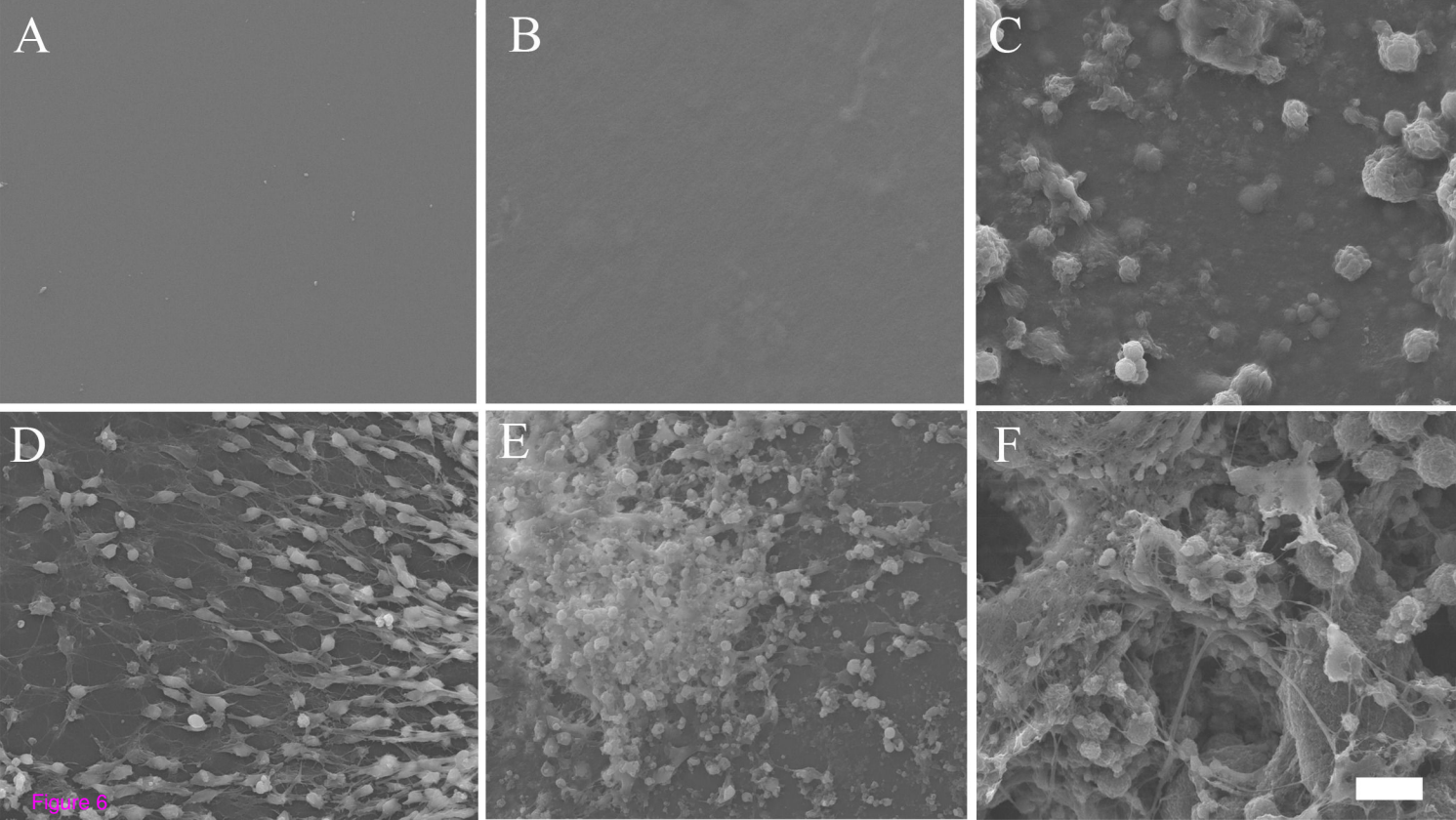

Figure 6

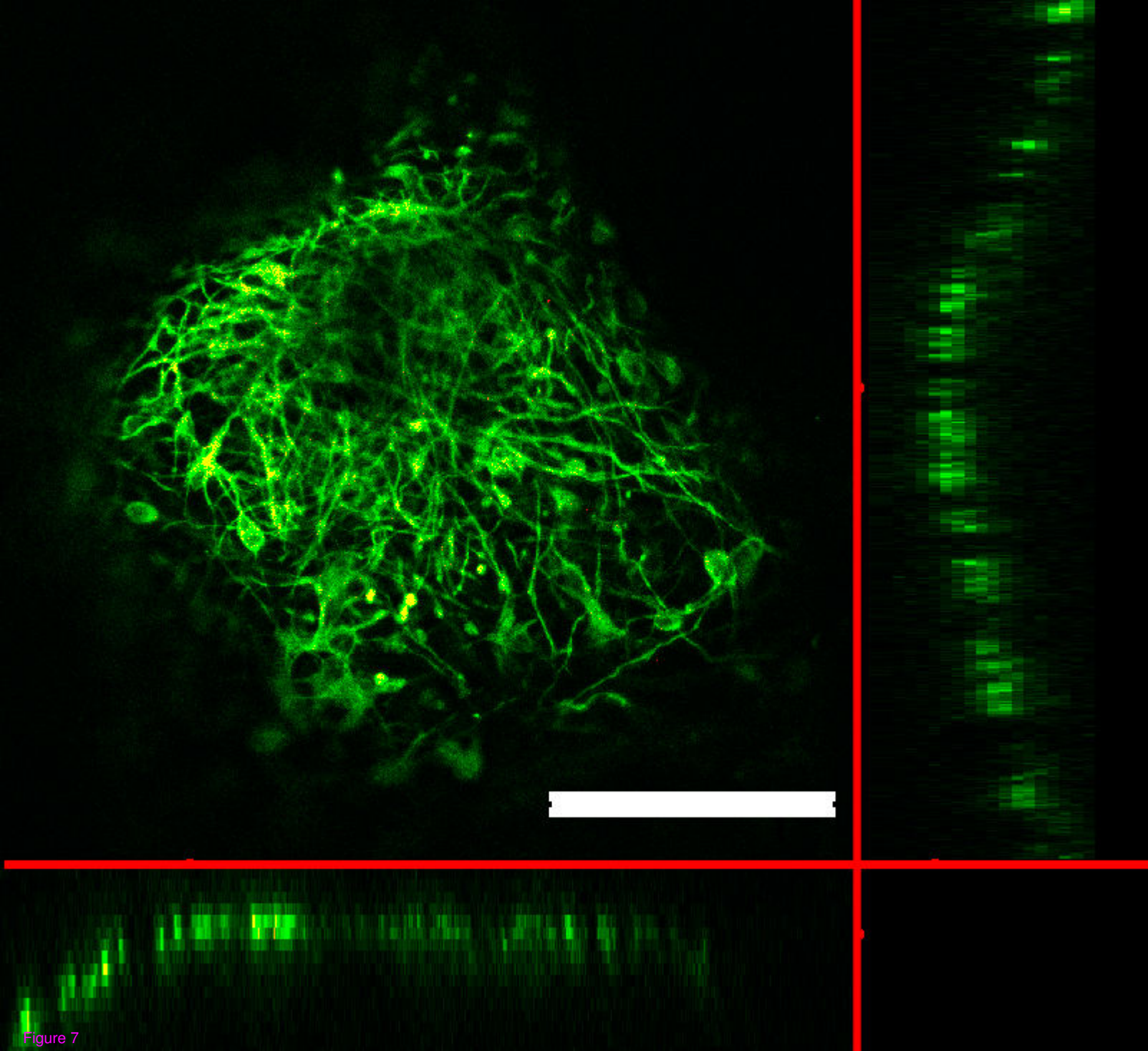

Figure 7